

2015-05-13

Pore Structure and Petrophysical Characterization of Hamelin Pool Stromatolites and Pavements, Shark Bay, Western Australia

Ergin Karaca

University of Miami, erginkrc@hotmail.com

Follow this and additional works at: https://scholarlyrepository.miami.edu/oa_theses

Recommended Citation

Karaca, Ergin, "Pore Structure and Petrophysical Characterization of Hamelin Pool Stromatolites and Pavements, Shark Bay, Western Australia" (2015). *Open Access Theses*. 567.

https://scholarlyrepository.miami.edu/oa_theses/567

This Embargoed is brought to you for free and open access by the Electronic Theses and Dissertations at Scholarly Repository. It has been accepted for inclusion in Open Access Theses by an authorized administrator of Scholarly Repository. For more information, please contact repository.library@miami.edu.

UNIVERSITY OF MIAMI

PORE STRUCTURE AND PETROPHYSICAL CHARACTERIZATION OF
HAMELIN POOL STROMATOLITES AND PAVEMENTS, SHARK BAY,
WESTERN AUSTRALIA

By

Ergin Karaca

A THESIS

Submitted to the Faculty
of the University of Miami
in partial fulfillment of the requirements for
the degree of Master of Science

Coral Gables, Florida

May 2015

UNIVERSITY OF MIAMI

A thesis submitted in partial fulfillment of
the requirements for the degree of
Master of Science

PORE STRUCTURE AND PETROPHYSICAL CHARACTERIZATION OF
HAMELIN POOL STROMATOLITES AND PAVEMENTS, SHARK BAY,
WESTERN AUSTRALIA

Ergin Karaca

Approved:

Gregor P Eberli, Ph.D.
Professor of Marine Geology
and Geophysics

R. Pamela Reid, Ph.D.
Professor of Marine Geology
and Geophysics

Ralf J. Weger, Ph.D.
Associate Scientist of Marine Geology
and Geophysics

M. Brian Blake, Ph.D.
Dean of the Graduate School

James S. Klaus, Ph.D.
Associate Professor of
Geological Sciences

KARACA, ERGIN
Pore Structure and Petrophysical
Characterization of Hamelin Pool Stromatolites
and Pavements, Shark Bay, Western Australia

(M.S., Marine Geology and Geophysics)
(May 2015)

Abstract of a thesis at the University of Miami.

Thesis supervised by Professor Gregor Eberli.
No. of pages in text. (124)

Stromatolites are organosedimentary, lithified structures showing layered growth via trapping and binding of sediments with calcium carbonate precipitation through microbial activity. The age of the oldest stromatolites from the Pilbara Block of Western Australia has been determined to be 3.4 – 3.5 Byr. As such they are the most ancient record of life and they provide 80% of the fossil record of Earth history. Hamelin Pool, Shark Bay, Western Australia is an internationally distinguished area known for hosting the most abundant and diverse modern marine stromatolites in the world. This study focuses on the petrophysical properties of Hamelin Pool stromatolites and associated pavement facies by interrelating porosity, permeability, sonic velocity, resistivity and pore geometry through Digital Image Analysis (DIA).

The microcrystalline carbonate precipitation 'micrite' generates a rigid framework with a wide range of porosities and pore sizes that influence the ultrasonic velocity, permeability and resistivity in stromatolites. A helium pycnometer which measures the true volume and calculates the density was used for porosity determination; and permeability was measured using steady-state air permeability. Digital Image Analysis results show that stromatolites

generally have simple and large pore structures and impressive high permeability values. In the 84 core plugs that were used in this study, the permeability values of the Hamelin Pool stromatolites and pavements range from 8 mD to 9000 mD, while porosity ranges from 16% to 46%.

Ultrasonic velocity, measured under dry and saturated conditions, is generally high with a large scatter at any given porosity. For example, at 29% porosity, velocity ranges from 3611 m/s to 5384 m/s. Similarly at a velocity of 4403 m/s the porosity ranges from 23% to 46%. Digital image analysis indicates that the main control on the variations is the pore complexity and size. Larger pores produce higher velocities at equal porosity. In brine (35 ppt) saturated core plugs compressional velocities increase up to 686m/s. In contrast, shear velocities show both a decrease (up to 578 m/s) and an increase (up to 597 m/s) in shear velocity (V_s) with saturation. These changes in V_s indicate that the shear modulus of stromatolites changes with saturation resulting in both shear weakening and shear strengthening and thus violating the assumption by Gassmann. The large range of porosities at a given velocity, however, makes porosity estimates from seismic inversion a challenge, and similarly, the shear moduli changes and the resultant shear strengthening and weakening add uncertainties to AVO analysis in microbialite strata.

The presence of quartz, which is diagenetically inert, precludes significant dissolution and reprecipitation, and results in lower seismic velocities of these carbonate rocks. The quartz percentage in each specimen was related to

velocities and pore structures and confirms the effect of mineral variability on ultrasonic velocities.

The cementation factor “m” (from Archie’s equation, $F = \phi^{-m}$) determined from electrical resistivity varies from 2.0 to 3.7 in stromatolites and from 2.0 to 3.1 in pavements. The cementation factors are much narrower with respect to other carbonates, which can decrease the uncertainties when making the hydrocarbon/water saturation estimations in stromatolites and pavements.

Porosity, permeability, ultrasonic velocity and resistivity were investigated in different meso/microfabrics and showed that different internal structures of stromatolites do not have a distinctive effect on petrophysical properties.

Acknowledgements

First and foremost, I would like to thank and express my gratitude to my advisor Dr. Gregor Eberli for his invaluable support, suggestions and time that he spent on my project in the period of my graduate studies at the University of Miami. Being a geophysicist, I was thrilled with how his superb skills of teaching strengthened my knowledge in geology. I am indebted to Dr. Ralf Weger for enlightening me in any aspect of academic research which helped me succeed. I would like to thank Dr. Pamela Reid and Erica Suosaari for their decisions to open a petrophysics position, hire me into the project and give me the opportunity to work on stromatolites in their home, Hamelin Pool. I send my regards and thanks to Dr. James Klaus for being a part of my committee and his inestimable suggestions on my research. I am thankful to Dr. Phillip Playford for his guidance during the time that he was in Hamelin Pool. I send my thanks to Dr. Greta MacKenzie for helping me with my thin sections and giving remarkable ideas for my research. I am also sending my deepest regards and thanks to Dr. Donald McNeill for his help.

I would like to express my gratitude to the Turkish Petroleum Corporation who sponsored me in the pursuit of my master's degree. Furthermore, the opportunity to be a part of the Division of Marine Geology and Geophysics provided me with a priceless experience and valuable knowledge in my field. I also want to thank the CSL - Center for Carbonate Research - for their financial help throughout my project.

I would like to send my thanks to all MGG community and my Turkish friends ,who never cut off their support towards my project and who always made me feel like I have a family in Miami. I also would like to thank my lovely friends Anna Ling, Kimberly Galvez, Leticia Rodriguez, and Yusuf Secerdin for their invaluable support and friendship.

Last but not least, I want to thank my mother, my father and my brother who were always supporting and motivating me in this challenging process. I am very proud of my little nephew who was born in Miami and motivated me each time I see his growth.

Table of Contents

LIST OF FIGURES	viii
LIST OF TABLES	xii
CHAPTER 1. INTRODUCTION	1
1.1. Scope of Thesis.....	1
1.1.1 Research Objectives	3
1.2. Background	5
1.2.1. Study Area	5
1.2.1.1. Regional Geology of Shark Bay	5
1.2.1.2. Regional Settings of Shark Bay	6
1.2.1.3. Common Components of the Depositional Environment.....	8
1.2.1.4. The Hamelin Pool Coquina	9
1.2.1.5. Origin of the Term “Stromatolite” and Definition	11
1.2.1.6. Modern Stromatolites	11
1.2.2. Hamelin Pool Stromatolites	12
1.2.2.1. Background	12
1.2.2.2. Internal Structure of Stromatolites	14
1.2.3. Hamelin Pool Carbonate Pavement	22
1.3. Outline of Research-Approach	23
1.4. Outline of Thesis	24
CHAPTER 2. DATA SET	26
2.1. Stromatolite Heads and Pavement.....	26
2.1.1. Textural Classification of Carbonates.....	27
2.1.1.1. Background	27
2.1.1.2. Hamelin Pool Stromatolites and Pavements	29
CHAPTER 3. METHODS	31
3.1. Digital Image Analysis (DIA).....	31

3.2. Porosity and Permeability.....	32
3.2.1. Porosity	32
3.2.2. Permeability	32
3.3. Ultrasonic Velocity.....	34
3.3.1. The NER AutoLab 1000 System	34
3.3.2. Lab Analysis.....	36
3.4. Electrical Resistivity.....	38
3.5. Mineralogy Determination	39
CHAPTER 4. PORE STRUCTURE AND PETROPHYSICAL CHARACTERIZATION	41
4.1. Pore Structure Characterization using Digital Image Analysis (DIA)	41
4.1.1. Pore Structures of the Hamelin Pool Stromatolites and Pavements ..	41
4.2. Porosity and Permeability.....	43
4.3. Ultrasonic Velocity.....	50
4.3.1. Velocity versus Porosity	51
4.3.2. Velocity versus Pore Structure.....	56
4.3.3. Velocity versus Pressure.....	61
4.3.4. Velocity Development under Saturation	62
4.3.5. Mineralogy and Quartz Percentage	65
4.3.6. Summary.....	74
4.3.7. Implications for Fluid Substitution and Seismic Inversion.....	76
4.4. Electrical Resistivity.....	77
4.4.1. Background.....	77
4.4.2. Resistivity of Hamelin Pool Stromatolites and Pavements	79
4.4.3. Summary.....	85
CHAPTER 5. DISCUSSION AND COMPARISON.....	87
5.1. Background	87
5.1.1. Background of Bahamian Stromatolites	87
5.1.2. Tongue of The Ocean Hardgrounds	89
5.2. Pore Structure of the Bahamian Microbialites	90
5.3. Porosity and Permeability.....	92

5.4. Ultrasonic Velocity	95
5.5. Electrical Resistivity.....	99
CHAPTER 6. CONCLUSIONS	103
References	106
APPENDIX 1. Data used in this petrophysical reseach	116
APPENDIX 2. Data used in this petrophysical reseach	119
APPENDIX 3. Data used in this petrophysical reseach	122

LIST OF FIGURES

Figure 1.1 – The map of Hamelin Pool, Shark Bay Western Australia.....	2
Figure 1.2 – Data set consisting of stromatolites and pavements.....	4
Figure 1.3 – Geological map of Shark Bay.....	6
Figure 1.4 – Hamelin Pool map with transect locations.....	7
Figure 1.5 – Common components of the depositional environment.....	9
Figure 1.6 – Hamelin Pool coquina ridges.....	10
Figure 1.7 – Stromatolites in the intertidal zone at Flagpole Landing area.....	12
Figure 1.8 – The first stromatolite distribution model of Hamelin Pool.....	14
Figure 1.9 – The classic growth model of Hamelin Pool stromatolites.....	15
Figure 1.10 – Stromatolite distribution by Jahnert and Collins, (2012).....	16
Figure 1.11 – Schematic diagram of internal microbial fabrics.....	17
Figure 1.12 – Color guide of meso/microfabrics.....	18
Figure 1.13 – Slabbed vertical sections.....	19
Figure 1.14 – Slabbed vertical sections.....	20
Figure 1.15 – Stromatolite distribution with respect to internal fabrics.....	21
Figure 1.16 – Microbial pavements in Hamelin Pool.....	22
Figure 2.1 – Vertical and Horizontal core-plug acquisition.....	27
Figure 2.2 – Dunham, Embry and Klován rock texture classification.....	29
Figure 2.3 – Thin section images of Hamelin Pool stromatolites and pavements.....	30
Figure 3.1 – The DIA document of a quantified section.....	31
Figure 3.2 – Schematic diagram of steady state air permeability.....	33
Figure 3.3 – The NER AutoLab 1000 complete setup.....	35
Figure 3.4 – The core holder and transducers of the system.....	35

Figure 3.5 – An example of acquired wave forms.....	37
Figure 3.6 – A general sketch of NER AutoLab system.....	39
Figure 3.7 – Two XRD results showing the undissolved material.....	40
Figure 4.1 – DomSize versus PoA cross-plot.....	42
Figure 4.2 – DomSize versus PoA cross-plot with internal fabrics.....	43
Figure 4.3 – Permeability versus porosity cross-plot.....	45
Figure 4.4 – DomSize versus PoA cross-plot with permeability.....	47
Figure 4.5 – Permeability versus porosity cross-plot with distance from Shore...48	
Figure 4.6 – Permeability versus porosity cross-plot with water depth.....	48
Figure 4.7 – Permeability versus porosity cross-plot with tidal zone.....	49
Figure 4.8 – Permeability versus porosity cross-plot with Internal fabrics.....	50
Figure 4.9 – Compressional velocity versus porosity with Wyllie Time Average.....	53
Figure 4.10 – Shear velocity versus porosity cross-plot.....	54
Figure 4.11 – Vp/Vs ratios with compressional velocity cross-plot.....	55
Figure 4.12 – Vp/Vs ratio versus porosity cross-plot.....	56
Figure 4.13 – DomSize versus PoA cross-plot with compressional velocity.....	58
Figure 4.14 – Thin section photos and their corresponding velocity values.....	59
Figure 4.15 – Compressional velocity versus porosity with DomSize and PoA..	60
Figure 4.16 – Compressional velocity versus porosity with internal structure.....	60
Figure 4.17 – Compressional velocity versus effective pressure.....	62
Figure 4.18 – Cross-plots of Vp wet vs. Vp dry and Vs wet vs. Vs dry.....	63
Figure 4.19 – μ_{wet}/μ_{dry} versus Vp/Vgassmann ratio cross-plot.....	64
Figure 4.20 – Hamelin Pool map with quartz distribution in stromatolites.....	66
Figure 4.21 – Vp versus porosity with quartz percentages.....	67

Figure 4.22 – DomSize versus PoA cross-plot with quartz and Vp velocity.....	68
Figure 4.23 – Correlation of quartz by using pore structure parameters.....	70
Figure 4.24 – Correlation of quartz by using pore structure parameters.....	71
Figure 4.25 – Correlation of quartz by using pore structure parameters.....	72
Figure 4.26 – Correlation of quartz by using pore structure parameters.....	73
Figure 4.27 – The velocity gradient with respect to quartz.....	74
Figure 4.28 – Formation factor versus porosity introductory cross-plot.....	78
Figure 4.29 – DomSize versus PoA with Formation factor introductory plot.....	79
Figure 4.30 – The minimum and maximum cementation factors of stromatolites and pavements.....	80
Figure 4.31 – DomSize versus PoA with Formation factor	81
Figure 4.32 – DomSize versus PoA with cementation factor.....	82
Figure 4.33 – Permeability versus porosity with cementation factor introductory plot.....	83
Figure 4.34 – Permeability versus porosity with cementation factor	84
Figure 4.35 – Formation factor versus porosity with internal fabrics.....	85
Figure 5.1– Distribution of stromatolites in Exuma Cays.....	88
Figure 5.2 – Giant stromatolites in Exuma sound, Bahamas.....	89
Figure 5.3 – The map of Bahamas and Tongue of the Ocean.....	90
Figure 5.4 – DomSize versus PoA comparison	91
Figure 5.5 – Permeability versus porosity comparison.....	93
Figure 5.6 – DomSize versus PoA with permeability comparison.....	93
Figure 5.7 – Thin section images of stromatolites and hardgrounds of Bahamian samples.....	94
Figure 5.8 – Compressional velocity versus effective pressure comparison.....	96
Figure 5.9 – Compressional velocity versus porosity comparison.....	97

Figure 5.10 – DomSize versus PoA with compressional velocity comparison....98

Figure 5.11 – Formation factor versus porosity comparison.....100

Figure 5.12 – DomSize versus PoA with cementation factor comparison.....101

Figure 5.13 – Permeability versus porosity with cementation factor comparison
.....102

LIST OF TABLES

Table 1.1 – List of researchers and their work on stromatolites.....	16
Table 4.1 – Vertically and horizontally drilled core-plugs and their porosity and permeability values.....	46

CHAPTER 1. INTRODUCTION

1.1. Scope of Thesis

Stromatolites are organosedimentary, lithified and laminated structures that are also the most ancient fossil record on Earth. The oldest stromatolites are approximately 3.5 billion years old (Hofmann et al., 1999; Altermann & Kazmierczak, 2003; Allwood et al., 2006). Although stromatolites were abundant in the Neo-Proterozoic and the Precambrian, modern stromatolites are rare. Modern stromatolites occur in the Shark Bay area of Western Australia in the hypersaline Hamelin Pool and in the high-energy, normal marine waters of the Exumas, Bahamas (Playford et al., 1976; Dravis 1983, Dill et al., 1986).

Carbonates have very complex porous media because of their variable pore sizes with their cooperated pore types. Therefore, their petrophysical responses are difficult to predict with classic theoretical approaches. Eberli et al (2003), Weger et al (2009) and Verwer et al (2011) carried out several studies with respect to acoustic velocity and electrical resistivity in carbonates consisting of various textures and pore structures. The data sets that they used were all carbonates containing the textural elements in Dunham (1962) classification and pore types in Choquette and Pray (1970) classification. Stromatolites which grow by trapping, binding and microbial precipitation are expected to develop a unique fabric and pore structure. Thus, they are expected to have a unique petrophysical signature. The wide variety of stromatolites and associated cemented facies in Hamelin Pool, hereafter called “pavements”, offer the unique opportunity to study organosedimentary carbonate rocks in regards to their petrophysical response.

Hamelin Pool, Shark Bay, Western Australia (Figure 1.1) is an internationally distinguished area that is known for hosting the most abundant and diverse modern marine stromatolites and coquina in the world (Playford et al., 1976; Jahnert and Collins, 2013). Hamelin Pool is located at $25^{\circ} 30' - 26^{\circ} 30' S$ & $113^{\circ} 53' - 114^{\circ} 15' E$ (Figure 1.2). The pool covers an area of 1238 square kilometer with a maximum water depth of 10 meters (Logan and Cebulski, 1970a; Burne and Johnson, 2012).

Hamelin Pool became an isolated bay when the Faure Sill formed approximately 4000 years ago in the northernmost part of the bay. The sill started to restrict water interchange and created a hyper-saline marine environment (Playford et al., 1990). Hamelin Pool's salinity ranges from 55 ppt to 70 ppt throughout the year (Logan and Cebulski, 1970a; Playford, 1979; Jahnert and Collins, 2011; Burne and Johnson, 2012).

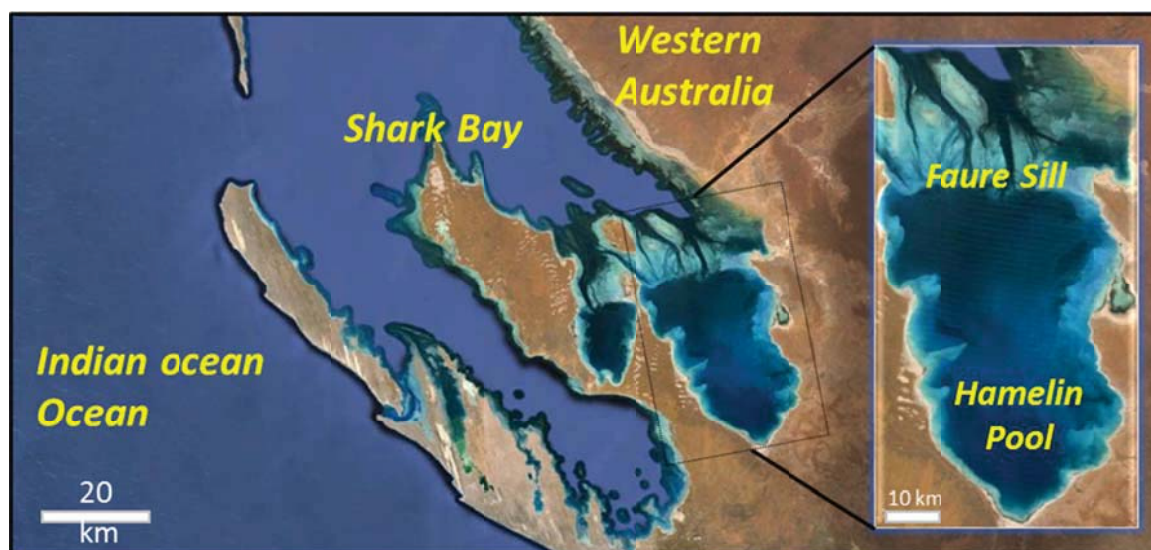


Figure 1.1: Hamelin Pool, Shark Bay, Western Australia. The Bay covers an area of ~13000 square kilometers with a maximum depth of 10 meters. The image is adapted from Google Earth, 2014 and modified.

1.1.1 Research Objectives

This project is part of a multi-disciplinary research effort in the Hamelin Pool by students, faculty of the University of Miami, RSMAS with collaboration with researchers from Stanford University, Duquesne University, University of Florida and, National Aeronautics and Space Administration (NASA). The objective of this component of the research program is to conduct a petrophysical study on stromatolites and associated facies in Hamelin Pool by measuring the porosity, permeability, sonic velocity and resistivity. To obtain this objective, the petrophysical properties will be correlated to pore structure parameters using Digital Image Analysis (DIA) of the analyzed samples for the assessment of the influence of the microbially generated pore structure on the petrophysical properties. The petrophysical characteristics of the stromatolites and pavements from Hamelin Pool (Figure 1.2) will be then compared to a data set of other microbialites, (i.e, Bahamian stromatolites) and Tongue of the Ocean hardground samples that were investigated in another study by Dr. Gregor Eberli. These combined data sets will help refine the petrophysical characteristics of microbialites.

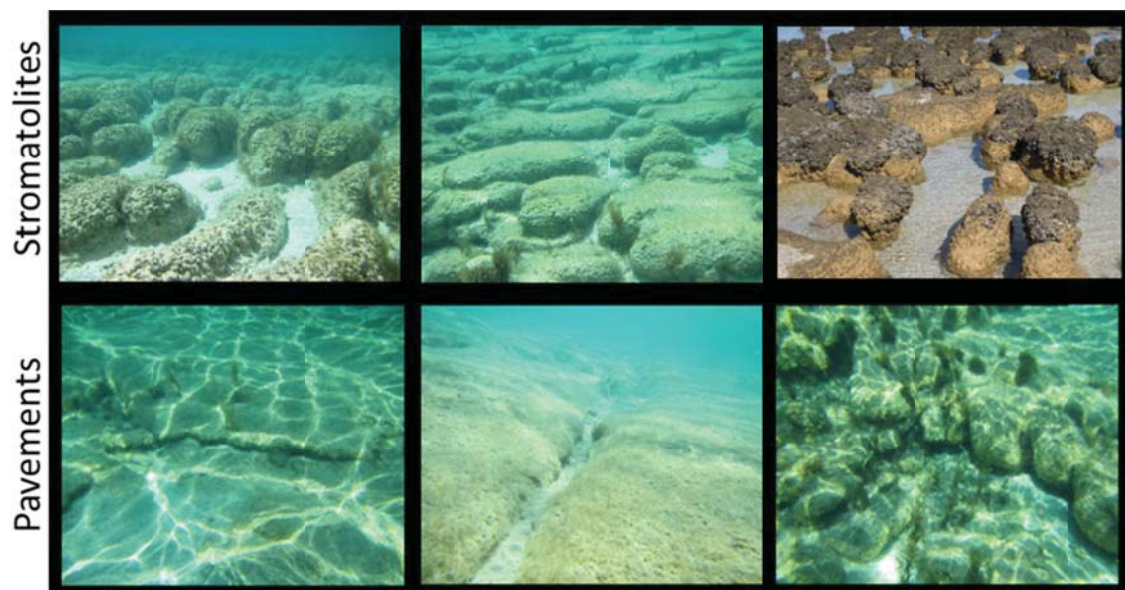


Figure 1.2: The Hamelin Pool data set consists of samples from the stromatolites of the subtidal to intertidal zones and pavements forming in the pool.

The specific objectives of this study are:

1. Document the petrophysical properties of microbialite types forming in Hamelin Pool.
2. Determine what effect the internal structure of stromatolites has on petrophysical properties.
3. Analyze the petrophysical properties of the cemented “pavement” facies, formed in association with Hamelin Pool stromatolites.
4. Correlate the data set of this study to data from other microbialites to assess if Hamelin Pool stromatolites are distinct from other data sets.

1.2. Background

1.2.1. Study Area

1.2.1.1. Regional Geology of Shark Bay

Shark Bay is formed by the islands and ridges of Edel Land, the Bernier-Dorre Island chain and Dirk Hartog Island which overlie Tertiary anticlines in the Indian Ocean (Figure 1.3). The exposed rocks that envelop the bay are Tertiary and Pleistocene marine and terrestrial limestones and sandstones (Playford, 1990), Holocene sands, beach ridges, and stromatolites veneer these older deposits. Neogene and Cretaceous sandstone and limestone are exposed to the east of Hamelin Pool (Butcher et al., 1984; Jahnert and Collins, 2012; Playford et al., 2013). There are massive Pleistocene eolian limestones along the west coast. A quartz-rich eolian dune shelters a large part of Hamelin Pool along the Western side (Jahnert and Collins, 2012).

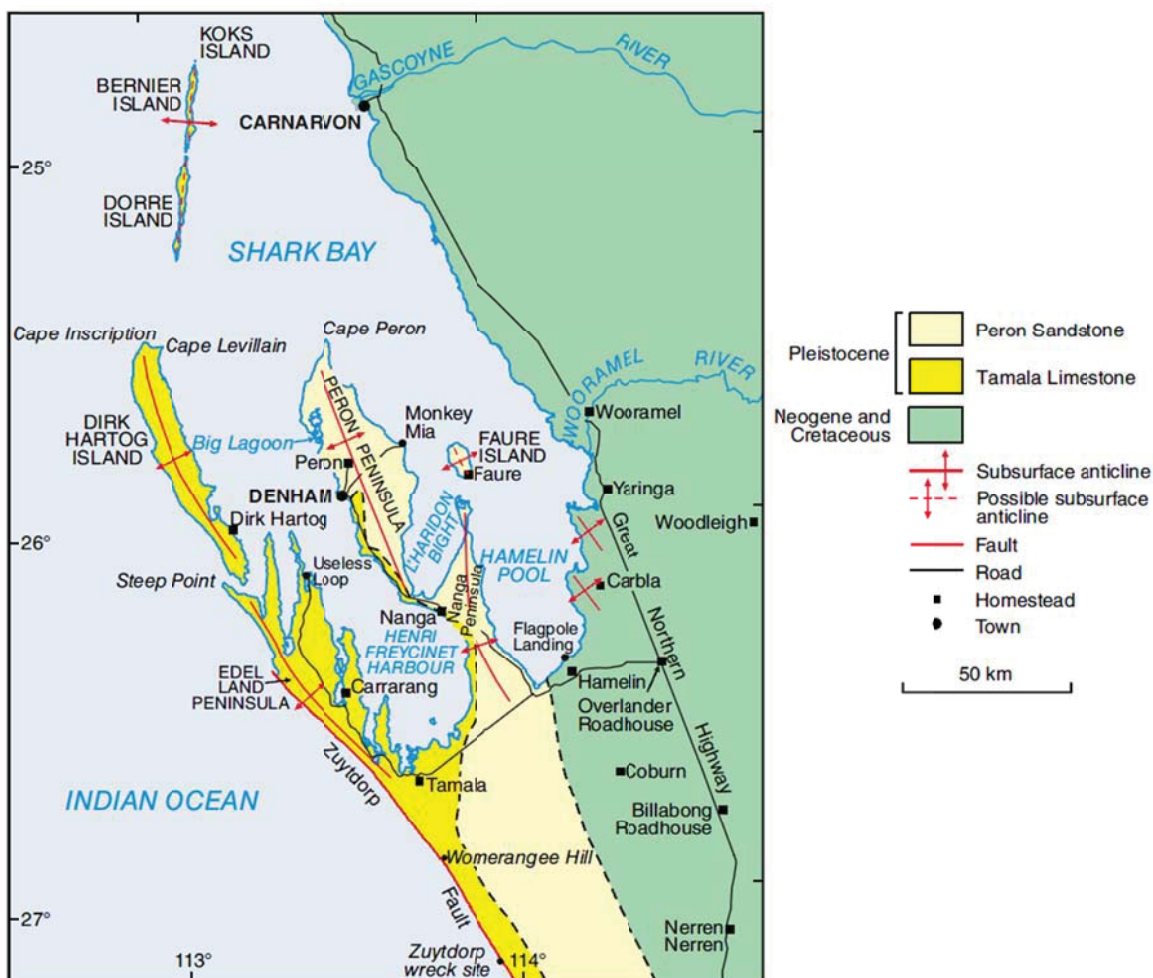


Figure 1.3: Geological map of Shark Bay, Western Australia (Playford et al., 2013)

1.2.1.2. Regional Settings of Shark Bay

Hamelin Pool, Shark Bay, Western Australia is located at $25^{\circ} 30' 26^{\circ} 30'S$ & $113^{\circ}53' - 114^{\circ} 15'E$ (Figure 1.4). Hamelin Pool is well-known for its enlarged coquina ridges, seagrasses at Faure Sill and deposits made through bacterial activity (Jahnert and Collins, 2011). The bay covers an area of ~13000 square kilometers with a maximum water depth of 10 meters (Logan and Cebulski, 1970a; Burne and Johnson, 2012).



Figure 1.4: Transect location map in Hamelin Pool, Shark Bay, Western Australia. The image is adapted from Google Earth, 2014 and modified.

Hamelin Pool is separated from Shark Bay by the Faure Sill which is located in the northernmost point of the U-shaped embayment. The Faure Sill has an average depth of 1-2 meters, but the depth variation can extent to 5-6 meters in some narrow channels (Burling et al. 2003). Therefore, the water circulation into Hamelin Pool is restricted by the Faure Sill. The low exchange of normal seawater across the Sill combined with evaporation makes Hamelin Pool

hypersaline with a salinity range of 55 ppt to 70 ppt throughout the year (Playford, 1979; Jahnert and Collins, 2011).

The annual evaporation is approximately 2200 mm while the average annual precipitation is 210 mm (Playford and Cockbain, 1976). The extreme environmental conditions in Hamelin Pool generate an environment for microbial mat development, the existence of stromatolites, and the small bivalve *Fragum erugatum*. The dead shells of *Fragum erugatum* pile up and cover a large area on the shores of Hamelin Pool, referred to as the Hamelin Coquina (Playford, 1990). The microbial deposits surrounding Hamelin Pool cover approximately 300 km² of the 1400 km² Holocene deposits (Jahnert and Collins, 2012).

1.2.1.3. Common Components of the Depositional Environment

The majority of sediments in Shark Bay, Western Australia consist of biogenetic carbonate sediments. Terrigenous quartz grains enter the pool from the weathering of the Peron Sandstone which is located (Figure 1.3) between Hamelin Pool and Henri Freycinet Harbour (Davies, 1970b). The sediment composition of Shark Bay was first reported by Davies (1970b) and Read (1974) (Figure 1.5).

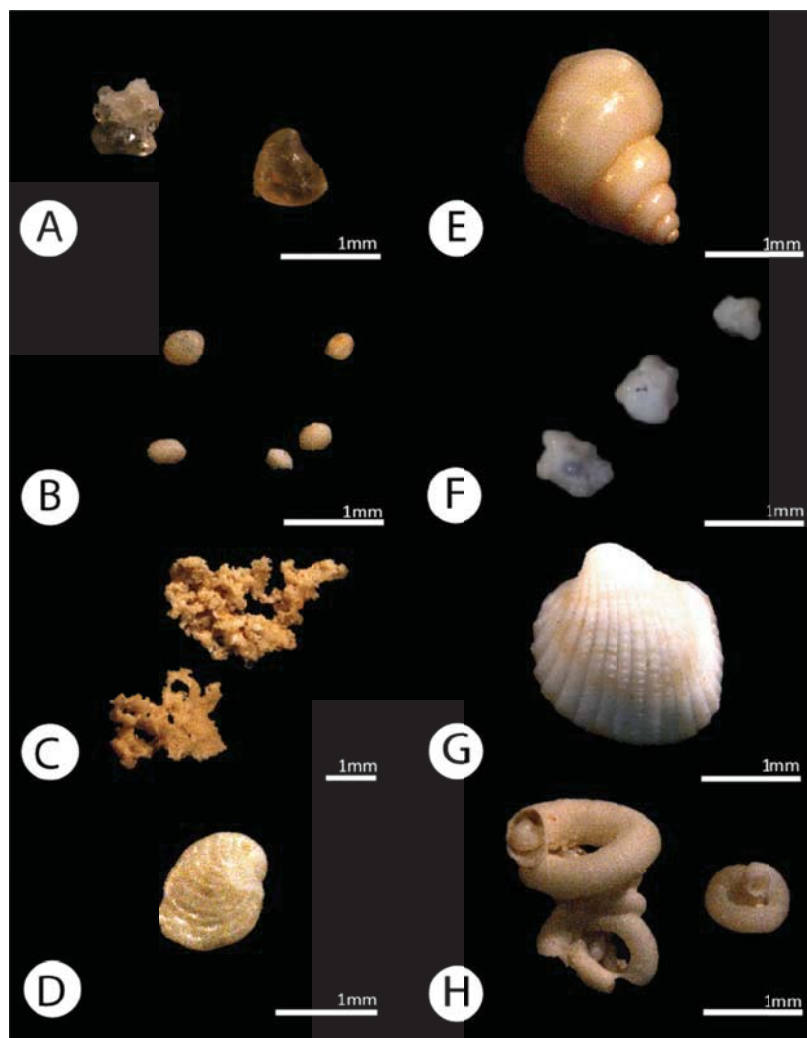


Figure 1.5: Common components of the sediment of Hamelin Pool, Shark Bay. A) quartz grains. B) carbonate peloids. C) irregular micritic grains. D) foraminifera tests. E) mollusk shells. F) grapestones. G) *Fragum erugatum* bivalve shells. and H) serpulid tubes (from Giusfredi, 2014).

1.2.1.4. The Hamelin Pool Coquina

High salinity in Hamelin Pool provides conditions favorable to the bivalve *Fragum erugatum*. The hypersaline waters also limit competing organisms (Jahnert et al., 2012). This combination produces an abundance of these bivalves and accumulation of these shells. The *Fragum erugatum* bivalves in the hypersaline waters of Hamelin Pool Hamelin Pool are smaller than those in the

open ocean, which tend to be three times bigger. Bivalve shells are deposited in the basin but are also washed ashore to form the Hamelin Pool coquina (Figure 1.6) (Playford et al., 2013). These Holocene coquina deposits form a sequence of supratidal beach ridges with a maximum thickness of 3 meters (Logan et al., 1974; Butcher, 1981; Playford 1990; Jahnert and Collins, 2012). In the last 6000 years, a regional sea level fall of about 2.5 meters (Jahnert and Collins, 2012) may have contributed to a seaward-prograding ridge system. These coquina ridges occupy an approximately $\sim 54 \text{ km}^2$ area along the margin of Hamelin Pool. Some of the larger and higher beach ridges are thought to be the result of massive cyclones (storm surge) while smaller storms might have formed the small beach ridges (Jahnert and Collins, 2012; Playford et al., 2013).



Figure 1.6: Coquina ridges dipping west towards to shores in Hamelin Pool near Flagpole Landing area.

1.2.1.5. Origin of the Term “Stromatolite” and Definition

“Stromatolith” is a German term and it was coined by Ernst Kalkowsky (1908) (Figure 1.8). The reason behind this naming was laminated structures of problematical origin found in the Triassic Buntsandstein of northern Germany. The original term was replaced by the term “stromatolite” (Kalkowsky, 1908; Logan and Ginsburg, 1964; Hofmann, 1969). Stromatolites are organosedimentary, lithified structures that show layered growth via trapping and binding of sediments with calcium carbonate precipitation through microbial activity (Walter, 1972; Awramik and Margulis, 1974; Schopf, 1983; Krumbein, 1983; Burne and Moore, 1987; Grotzinger and Knoll, 1999; Altermann & Kazmierczak, 2003; Dupraz and Visscher, 2005; Reid, 2013). The age of the oldest stromatolites from the Pilbara Block of Western Australia have been determined to be 3.4 – 3.5 Byr old (Walter et al., 1980). As such, they are the most ancient record of life on Earth.

1.2.1.6. Modern Stromatolites

Today, modern marine stromatolites form in two well-known locations; 1- The margin of Exuma Sound, Bahamas where they form in an open marine environment (Dravis, 1983; Dill et al. 1986; Reid et al., 2000) and 2- in Hamelin Pool, Shark Bay, Australia (Figure 1.7), where they thrive in an estuarine marine environment (Logan and Cebulski, 1970; Playford, 1990; Jahnert and Collins, 2012). Stromatolites are also found in freshwater. Laguna Bacalar in Mexico, Chetumal Bay in Belize, Lake Salda and Lake Van in Turkey, Pavilion and Kelly Lakes in Canada are some of the places where modern fresh water stromatolites

are forming today (Rasmussen et. al, 1993; Braithwaite et al.,1996; Ferris et al.,1997; Gischler et al.,2008).



Figure 1.7: Stromatolites in the intertidal zone at Flagpole Landing area in Hamelin Pool, Western Australia.

1.2.2. Hamelin Pool Stromatolites

1.2.2.1. Background

Hamelin Pool area has been studied in many aspects by many scientists. Hamelin Pool stromatolites were discovered by D. Johnstone, P.E. Playford and R.L. Chase when the West Australian Petroleum Company (WAPET) was doing

an investigation of the Hamelin Pool area (Playford et al., 2013). Originally, these structures were thought to be algal mounds forming via blue-green algae. In 1955, David Churchill from the University of Western Australia Botany Department analyzed one of the samples collected by Playford and confirmed the presence of cyanobacteria (Playford et al., 2013). The first paper on Hamelin Pool stromatolites was published by B. Logan in 1961. Logan (1961 and 1964) suggested that stromatolites form in the intertidal zone and the supra-tidal zone shelters the eroded structures (Figure 1.8). However, Fisher (1965), Monty (1965) and Playford (1972) pointed out that stromatolites are also present in the sub-tidal zone. Hoffman (1976) documented that living stromatolites with a colloform mat form in up to 2 meters of water depth in Hamelin Pool. Reid et al. (2003) analyzed Bahamian stromatolites and concluded that microbes precipitate the microcrystalline carbonate “micrite” which provides a rigid framework and cement. Accretion of the stromatolites forming in the sub-tidal zone is predominantly caused by microbial precipitation while trapping and binding of sediments are the primary mode of accretion for inter-tidal zone stromatolites (Reid et al., 2003).

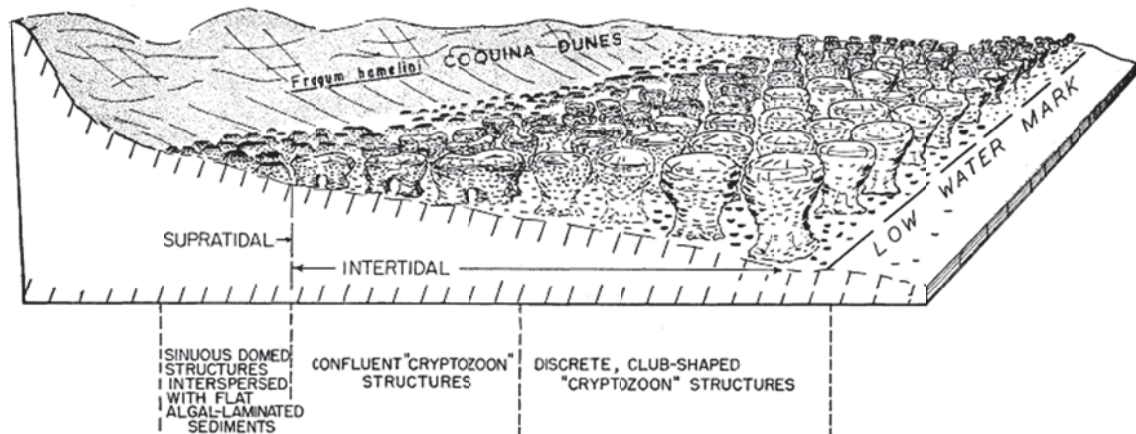


Figure 1.8: The first model that showed the stromatolite distribution at Flint Cliff, Hamelin Pool, Western Australia (Logan, 1961).

1.2.2.2. Internal Structure of Stromatolites

Stromatolites have distinct internal fabrics. Trapping and binding of sediments, distribution of macropores, type of organic matter, carbonate precipitation, existing voids and bioturbation are some of the causes of the internal structural differences in stromatolites (Jahnert and Collins, 2011). Laminated internal microstructures correspond to previous surface mat type (Reid et al., 2000). Thus, these fabrics can be correlated with different kinds of mats formed by microbial communities (Reid et al., 2003; Jahnert and Collins, 2011). There are nine different types of microbial mats in Hamelin Pool (Bauld, 1984; Golubic, 1985). However, just three of them are recognized as forming columnar and mound-shaped stromatolites in Hamelin Pool (Figure 1.9). Pustular mat in the intertidal zone generates an unlaminated internal fabric. Smooth mat stromatolites are located in the lower intertidal to shallowest intertidal zones forming a laminated fabric. In the subtidal environments, the colloform mat type is

shown to possess weak lamination (Playford, 1990). There are different models suggested by researchers working on Hamelin Pool stromatolites and their growth for different tidal environments and their corresponded mat types (Table 1.1).

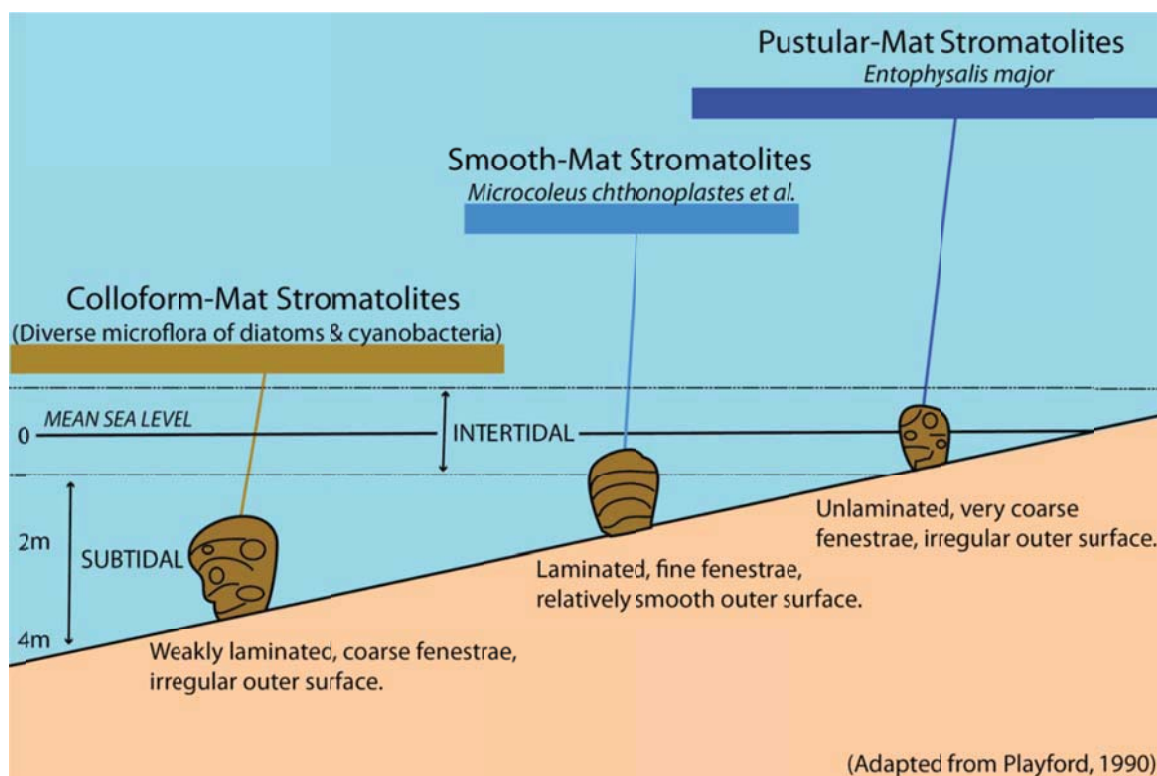


Figure 1.9: The classic growth model of Hamelin Pools stromatolites (Playford, 1990).

Jahnert and Collins (2011) proposed a new depositional model for Hamelin Pool showing different tidal environments, corresponding mat types and deposits (Figure 1.10). They also describe a new stromatolite type “Cerebroid” in sub-tidal areas with an unlaminated internal structure. Jahnert and Collins (2012) correlate the growth structure of stromatolites with water depth (Figure 1.11).

Table 1.1: Researchers working on Hamelin Pool stromatolites and their various approaches to intertidal and subtidal stromatolite types (Jahnert and Collins, 2012).

Littoral zone	Intertidal	Subtidal	
Authors			
Logan et al., 1974	Pustular, smooth	Colloform	Microbial type
Playford, 1990	Pustular	Smooth, colloform	
Reid et al., 2003	Intertidal Calcarenite Stromatolites	Subtidal Micritic Stromatolites	
This paper (Jahnert and Collins, 2012)	Pustular	Smooth*, colloform*, cerebroid*, pavement* (*10× area of intertidal)	

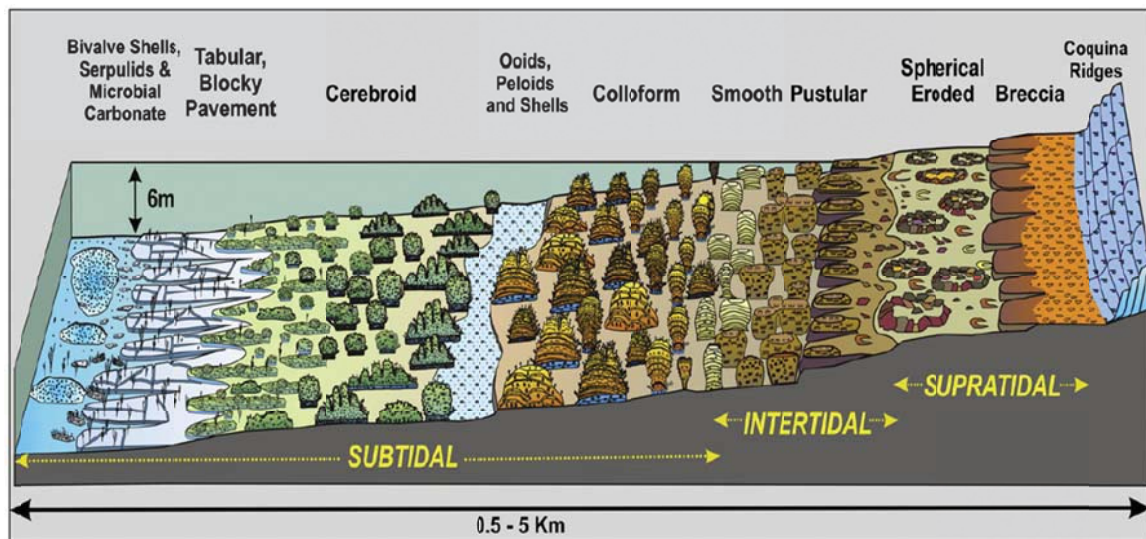


Figure 1.10: Stromatolite distribution with extensive sub-tidal deposits in Shark Bay/Hamelin Pool (Jahnert and Collins, 2011).

Microbial precipitation of microcrystalline carbonate (micrite) is highly significant for petrophysical properties of stromatolites as it provides a rigid framework and cement (Reid et al, 2003). Rocks with intergranular porosity are generally regarded as weak and they tend to have low acoustic velocities.

However, Intergranular porosity in microbialites generates a significant stiffness resulting in petrophysically high velocity and porosity values (Eberli et al, 2012).

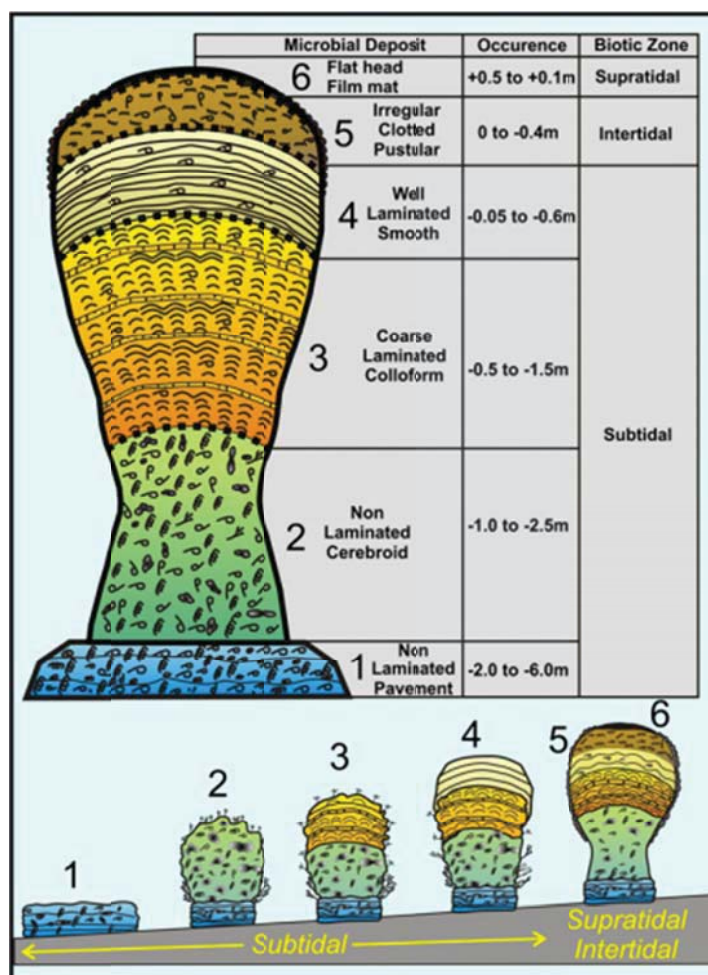


Figure 1.11: Schematic diagram of internal microbial fabrics of stromatolites within Hamelin Pool relative to water depth (Jahnert and Collins, 2012).

As part of the ongoing study Paul Hagan and Erica Parke (University of Miami) classified the internal structure of Hamelin Pool stromatolites by considering meso/microstructures recorded on vertical slabs of stromatolite heads. The various meso/microfabrics are color-coded in order to define the distribution of internal structures around the pool (Figure 1.12). Figures 1.13 and

1.14 display the different meso-scale fabrics defined by Parke. These micro/mesostructures will be correlated to the petrophysical properties. If a correlation exists, petrophysical properties such as permeability and sonic velocity can be estimated from the visual inspection of stromatolites.

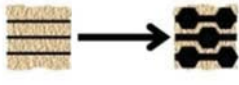
Mesofabric	Microfabric	Micrite A	Micrite B
Unlaminated	Massive	1 Army Green	
	Clotted	3A Gray	3B Gray
	Massive + Sediment	4A Dark Blue	4B Dark Blue
Laminated	Very Fine	2 Light Green	
	Very Fine	5A Pink	5B Pink
	Fine	6 Red	9 Light Purple 10 Dark Purple
	Medium		13 Turquoise
	Coarse	8 Yellow	7 Orange
Diagenetic			11 Brown 12 Light Blue

Fig. 6 - Matrix of Microfabrics as generated by the RSMAS Shark Bay Research Team, 2014

Figure 1.12: Color guide of meso/microfabric of Hamelin Stromatolites (adapted from Hagan, 2015).

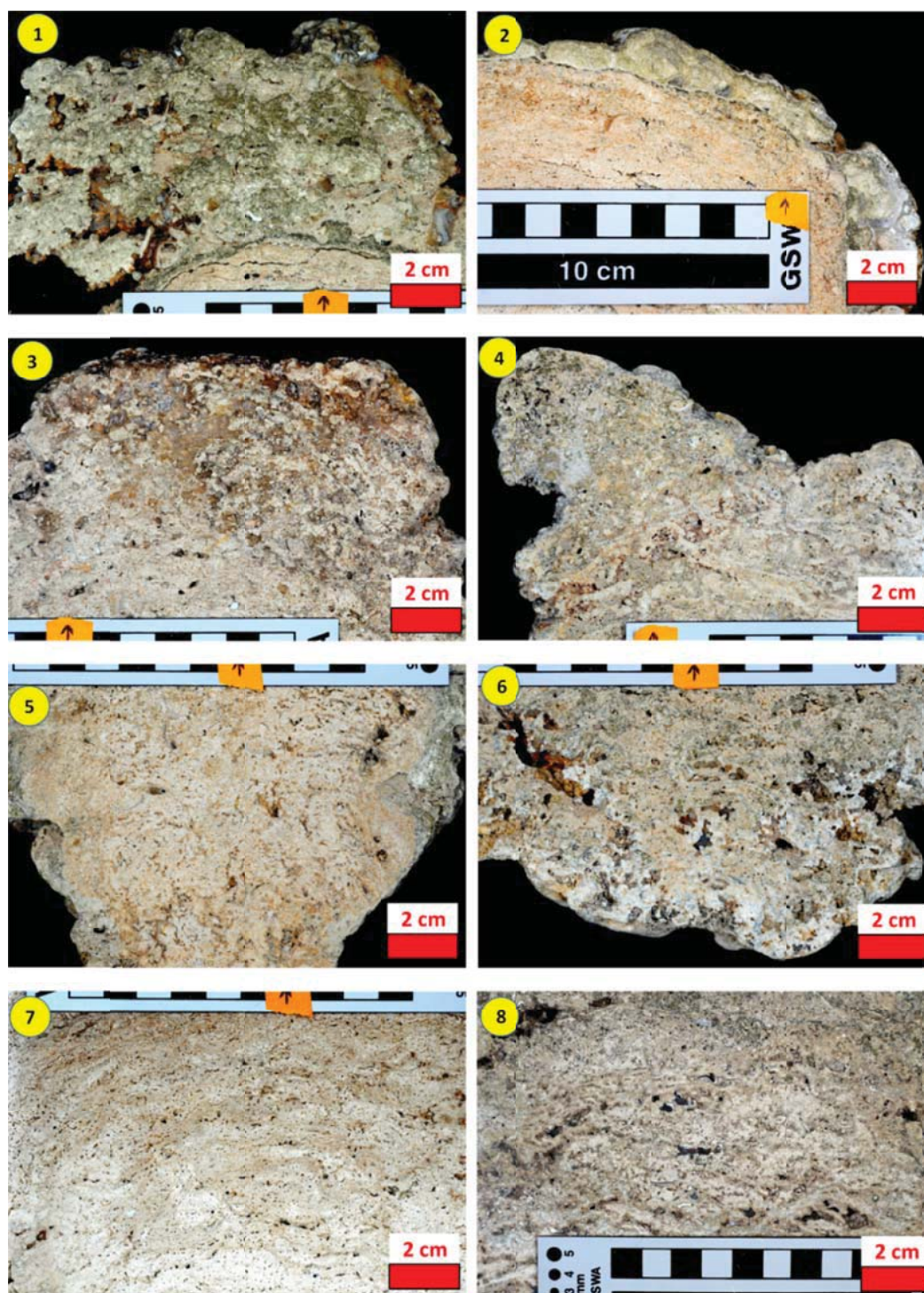


Figure 1.13: Slabbed vertical sections; 1) army-green (cauliflower-like), 2) light-green (laminated micrite fabric), 3) gray A (unlaminated clotted fabric), 4) gray B (unlaminated clotted fabric), 5) dark-blue A (the massive micrite and sediment fabric), 6) dark-blue B (the massive micrite and sediment fabric), 7) pink A (very finely laminated fabric), 8) pink B (very finely laminated fabric), adapted from Hagan (2015).

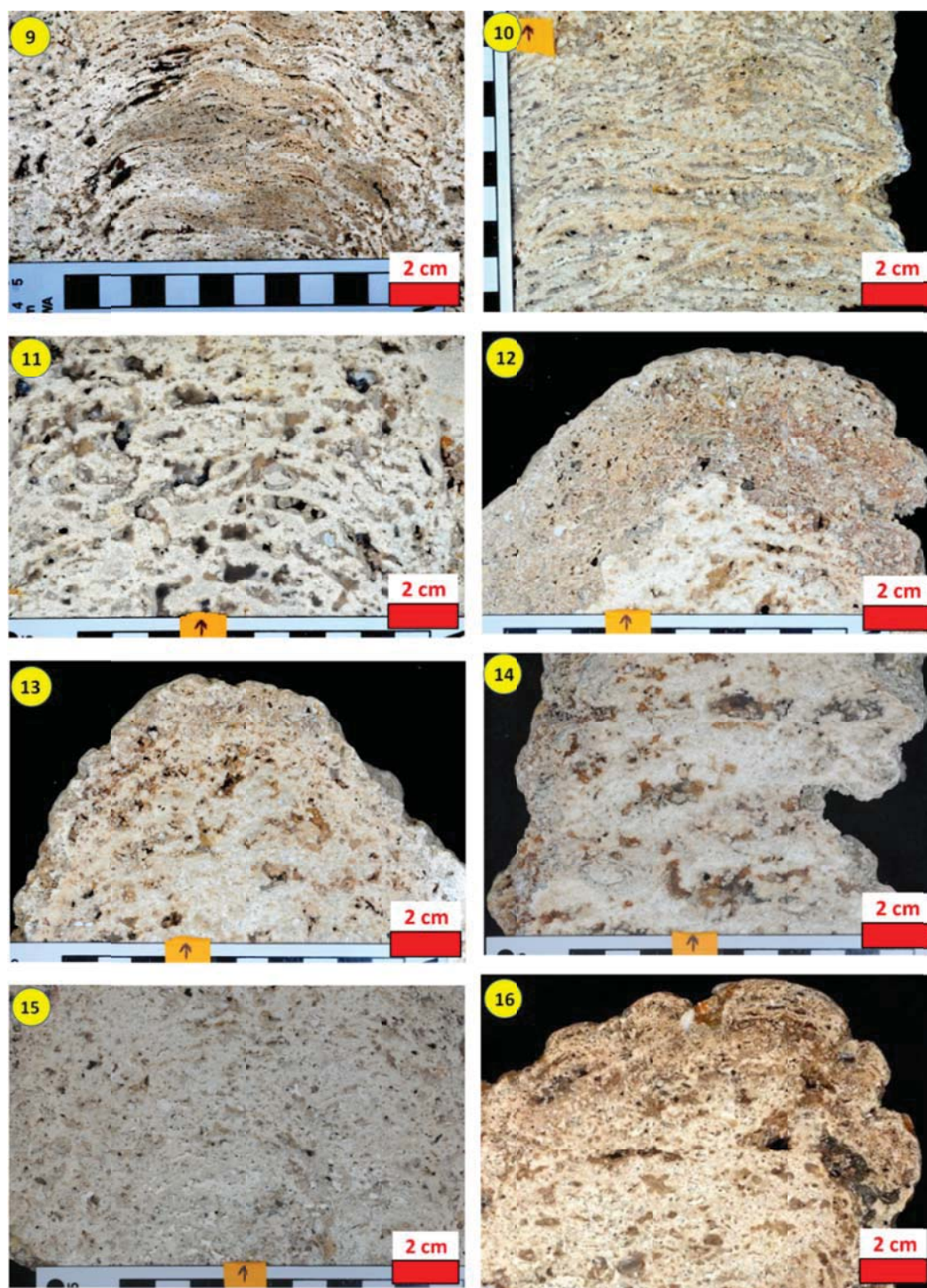


Figure 1.14: Slabbed vertical sections; 9) red (finely laminated with fabric), 10) orange (medium laminated fabric), 11) yellow (coarsely laminated fabric), 12) light-purple (very fine laminated microfabric), 13) dark-purple A (very finely laminated fabric), 14) brown (very coarsely layered fabric), 15) light-blue (network of dense carbonate with fine to medium irregular voids), 16) turquoise, adapted from Hagan (2015).

The distribution of the micro/mesostructures in the stromatolites at different transects in Hamelin Pool visualized by the colors of the classification (Figure 1.15). No clear pattern exists in the pool, indicating that internal structure of the stromatolites is diverse throughout basin.

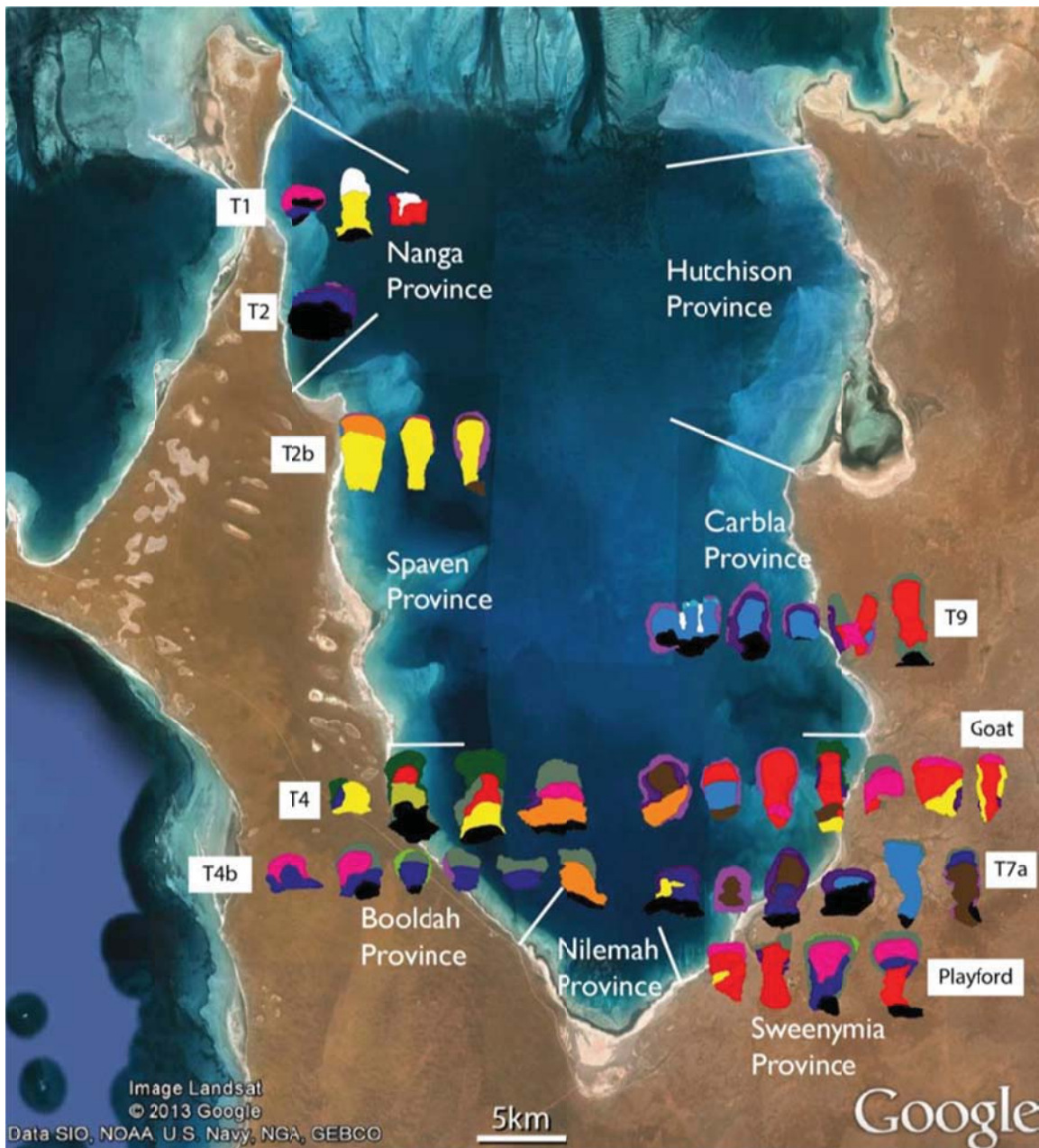


Figure 1.15 Microfabric distribution of stromatolite heads in Hamelin Pool (adapted from Hagan, 2015).

1.2.3. Hamelin Pool Carbonate Pavement

Large areas of subtidal carbonate deposits within Hamelin Pool are cemented by microbial activity to form what several researchers call pavements (Figure 1.16). The pavements encompass approximately 220 km² and their formation extends to 5-6 meters water depth. The pavement deposits with a tabular and blocky structure, are 10 times greater in spatial extent than the stromatolite deposits of intertidal areas (Jahnert and Collins, 2012; Playford et al., 2013). The pavements consist of sands on the sea floor that are cemented by microbial aragonite precipitation (Jahnert and Collins, 2012; Playford et al., 2013). Stromatolites that extend to approximately 4 meters of water depth in Hamelin Pool have formed on these microbial induced pavements (Jahnert and Collins, 2013).

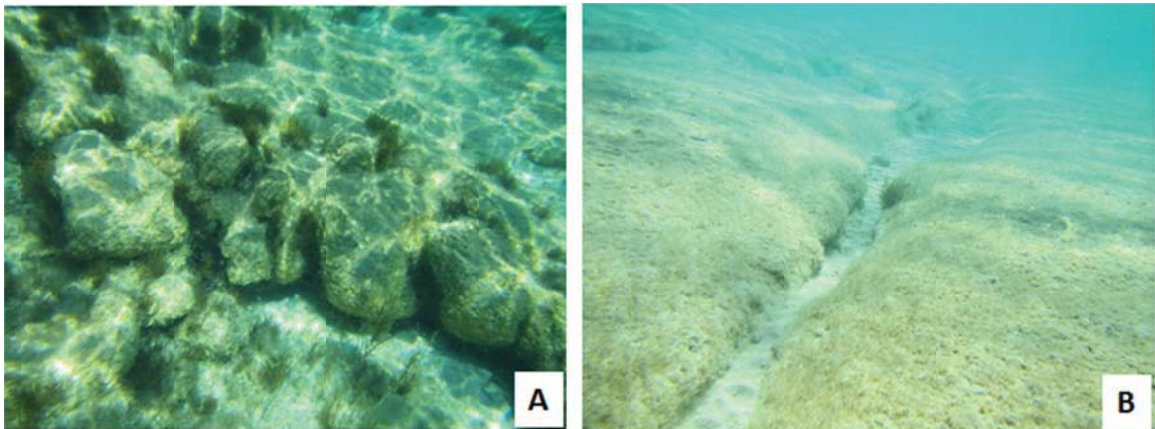


Figure 1.16: (A) Microbial pavements in 2-3 meters of water depth in Hamelin Pool, (B) Microbial limestone pavements covered by thin growths of green algae in Hamelin Pool.

The surficial microbial communities on pavements (and colloform structures) coexist with the other organisms that contribute to the composition. In

addition to the abundant *Fragum erugatum* shells, the pavements host serpulids, diatoms, green alga (*Acetabularia*), crustaceans, foraminifera and micro-gastropods (Jahnert and Collins, 2013).

1.3. Outline of Research-Approach

This thesis applies the following approaches and methods to fulfill the objectives:

1. Four different petrophysical properties were measured on the stromatolites and the pavements of Hamelin Pool. The samples were chosen from all types of tidal environments and mat types and their corresponding internal fabrics. The porosity values of vertical and horizontal core-plugs were measured in a helium pycnometer. Dry and saturated acoustic velocity measurements and electrical resistivity measurements were performed in the NER AutoLab 1000 system in the Petrophysics Laboratory at the University of Miami, RSMAS.
2. Thin sections of core-plugs were obtained for petrographic analysis. Digital image analysis (DIA) of these thin sections quantifies the following pore structure parameters; Dominant Pore Size (DomSize) and Perimeter Over Area (PoA).
3. A data set of Bahamian stromatolites and hardgrounds was used to make a petrophysical comparison to Hamelin Pools stromatolites and pavements.

1.4. Outline of Thesis

Chapter 1: Introduction and Background – This chapter gives the background information on Hamelin Pool and stromatolite formation. In addition, the significance of a petrophysical study on modern stromatolites is highlighted.

Chapter 2: Data Set – The data set that is being investigated is introduced and a petrographic description of stromatolites and pavement is given.

Chapter 3: Methods – Detailed description of the methodology is given with regards to sample acquisition, preparation, X-ray diffraction and petrophysical measurements of porosity, permeability, acoustic velocity, electrical resistivity and DIA (Digital Image Analysis).

Chapter 4: Pore Structure and Petrophysical Characterization – This chapter presents permeability and porosity results and the two petrophysical measurements of acoustic velocity and electrical resistivity. Samples collected from pavements and stromatolite heads is examined and the results are plotted and interpreted. The petrophysical data of horizontally and vertically drilled plugs is correlated to evaluate if internal fabric anisotropy has any effect on petrophysical properties. Thin sections are analyzed by using DIA, which quantifies the pore structures. The parameters provided by DIA is correlated with the measured petrophysical data.

Chapter 5: Discussion and Comparison – The results from Hamelin Pool stromatolites and pavements are compared with a data set that includes samples

from the modern stromatolites in the Bahamas and Tongue of The Ocean hardgrounds.

Chapter 6: Conclusions – This section gives a summary of the petrophysical properties of stromatolites heads and pavement samples from Hamelin Pool and the comparison with the comprehensive data set.

CHAPTER 2. DATA SET

2.1. Stromatolite Heads and Pavement

Eighty-four 3.81cm diameter core-plugs were acquired from thirty-six heads and pavements in selected locations and transitions at Hamelin Pool, Shark Bay, Western Australia. Vertical and horizontal core plugs were drilled to assess anisotropy in the samples (Figure 2.1). Sixty-one of the ninety-three core-plugs were obtained from stromatolite heads whereas the other twenty-three are pavement samples.

The core plugs drilled from heads and pavements were measured for permeability, porosity, sonic velocity, resistivity and Digital Image Analysis (DIA) measurements. The goal of this study is to help improve the understanding of the petrophysical properties and pore characterization of microbialites, especially the stromatolites of the Hamelin Pool. Moreover, correlating sonic velocity results with porosity and permeability on cross-plots using the pore geometry data will give a better understanding of the structure of these relatively complex, heterogeneous pore systems.

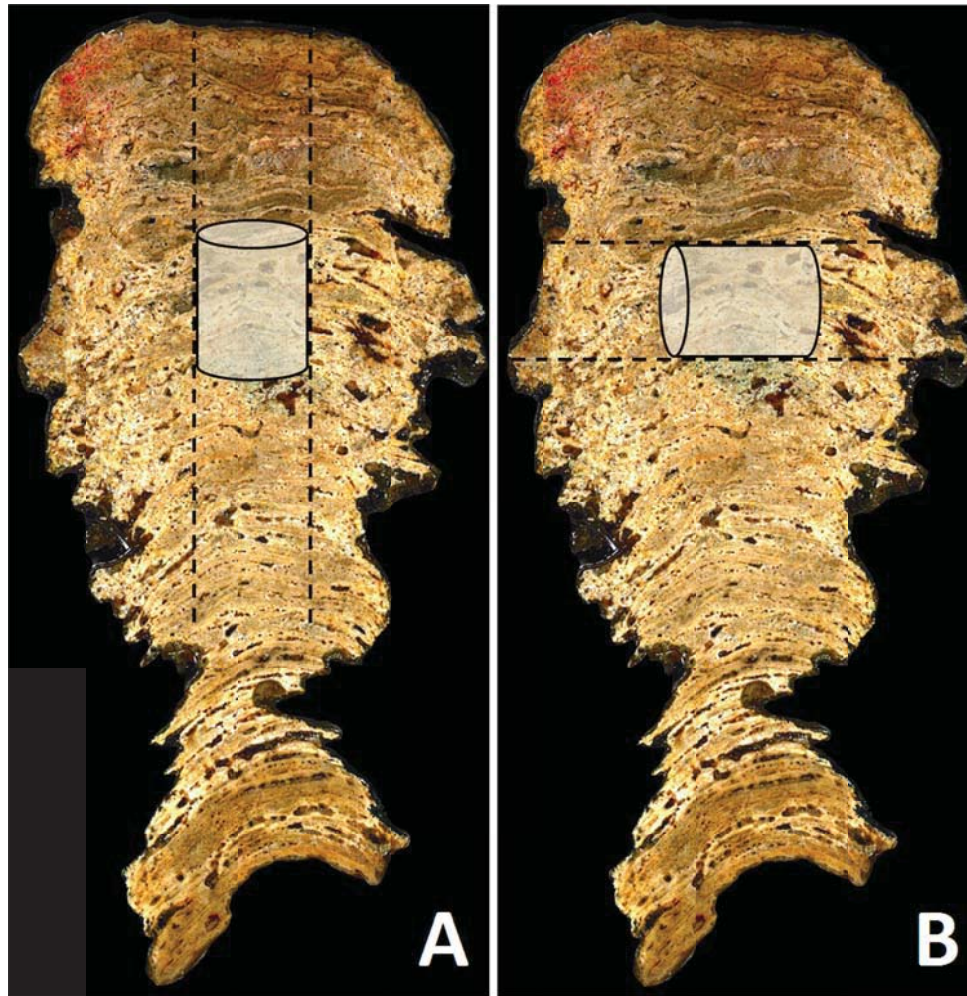


Figure 2.1: Illustration of vertical (A) and horizontal (B) core-plug acquisition in a stromatolite of Hamelin Pool.

2.1.1. Textural Classification of Carbonates

2.1.1.1. Background

More than twenty different methods to classify carbonates have been generated since 1960. Archie (1952), Folk (1959 and 1962), Dunham (1962), Todd (1966), Choquette and Pray (1970), Embry and Klovan (1971), James (1984), Lucia (1995), Scholle and Ulmer-Scholle (2003), and Kendall, (2005)

have either originated their own classification schemes or made modifications from an existing schemes. Here, the Embry and Klovan (1971) carbonate texture classification scheme, which is a modified version of (Dunham, 1962), is used to classify the thin sections of Hamelin Pool stromatolites and pavements (Figure 2.2)

The original Dunham classification focuses upon depositional textures to classify carbonates. Rocks that consists of carbonate mud with less than 10 percent carbonate grains describe *mudstone* and with more than 10 percent carbonate grains describe *wackestone*. Grain-supported limestones with some amount of mud are *packstone* while the absence of mud makes them *grainstone*. *Boundstone* is distinguished if binding is presence during deposition. Lastly, samples with almost no sign of their original depositional textures are called *crystalline* carbonates in the scheme (Dunham, 1962). In 1972, five additional groups were added to the Dunham classification by Embry and Klovan (1972). According to Embry and Klovan, Dunham classification was deficient in respect to its size variation definitions. If there are more than 10% of components which are larger than 2mm, the modified classification calls them '*Floatstone*' and '*Rudstone*'. While the particles of >2mm make up the framework of *rudstone*, those particles float in a fine-grained matrix which makes the framework of *floatstone*. *Boundstone* is split into three categories as *framestone*, which builds a rigid framework, *bindstone* which forms by encrusting and binding and lastly *bafflestone*, (Klement, 1967) which forms by baffling (Embry and Klovan, 1971).

Allochthonous limestone original components not organically bound during deposition					Autochthonous limestone original components organically bound during deposition				
Less than 10% >2 mm components				Greater than 10% >2 mm components		Boundstone			
Contains lime mud (<0.02 mm)			No lime mud		Matrix supported	>2 mm component supported	By organisms which act as barriers	By organisms which encrust and bind	By organisms which build a rigid framework
Mud supported		Grain supported							
Less than 10% grains (>0.02 mm to <2 mm)	Greater than 10% grains								
Mudstone	Wackestone	Packstone	Grainstone	Floatstone	Rudstone	Bafflestone	Bindstone	Framestone	

Figure 2.2: Dunham rock texture classification and modified by (Embry and Klovan, 1971).

2.1.1.2. Hamelin Pool Stromatolites and Pavements

Stromatolites that were organically bound during accumulation are generally recognized as boundstones (Judd and Hovland, 2007). The thin section images in Figure 2.3 show that most of the stromatolites are *bindstones* (images a, b, and, c) and some of them are *grainstones* (image d). In pavements, the grains are larger than 2 mm and apparently those grains are not the framework of the samples. In this case, the *floatstone* description of (Embry and Klovan, 1971) carbonate texture can be applied for most of them (images e,f and, g). There are also some *grainstone* in the pavements (image h).

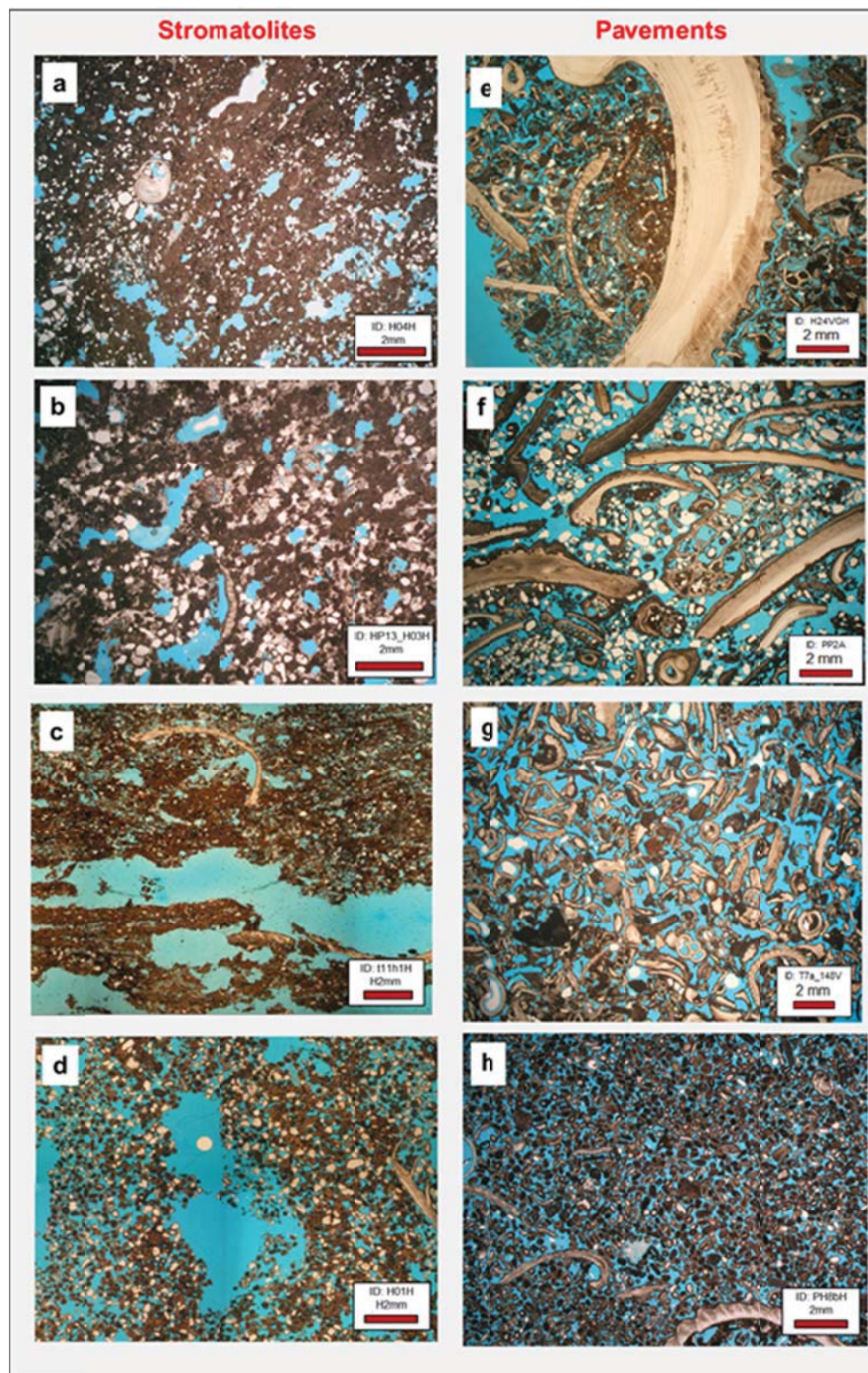


Figure 2.3: Hamelin Pool stromatolites (on the right) and the pavements (on the left). Thin sections of a,b,c,d are floatstone and e,f,g,h are grainstone according to the classification of Embry and Klovan (1971) modified from Dunham (1962).

CHAPTER 3. METHODS

3.1. Digital Image Analysis (DIA)

Digital image analysis (DIA) is performed on thin sections of a 0.5 cm thick sub-sample from the edge of each core plug. Acquisition, segmentation and pores structure analysis is performed according to the workflow described by Weger et al. (2009). In this workflow, thin sections are photographed under cross-polarization light through an Olympus BH2 petrographic microscope at ~6 micron/pixel resolution. Then the images are segmented and pore shape parameters are calculated using a MATLAB script created by Weger et al. (2009) (Figure 3.1). The DIA provides 37 different parameters for an individual thin section. Four of these parameters are used for correlation to the physical properties. These four are Dominant Pore Size (DomSize), Roundness (g), Aspect Ratio (AR), and Perimeter over Area (PoA).

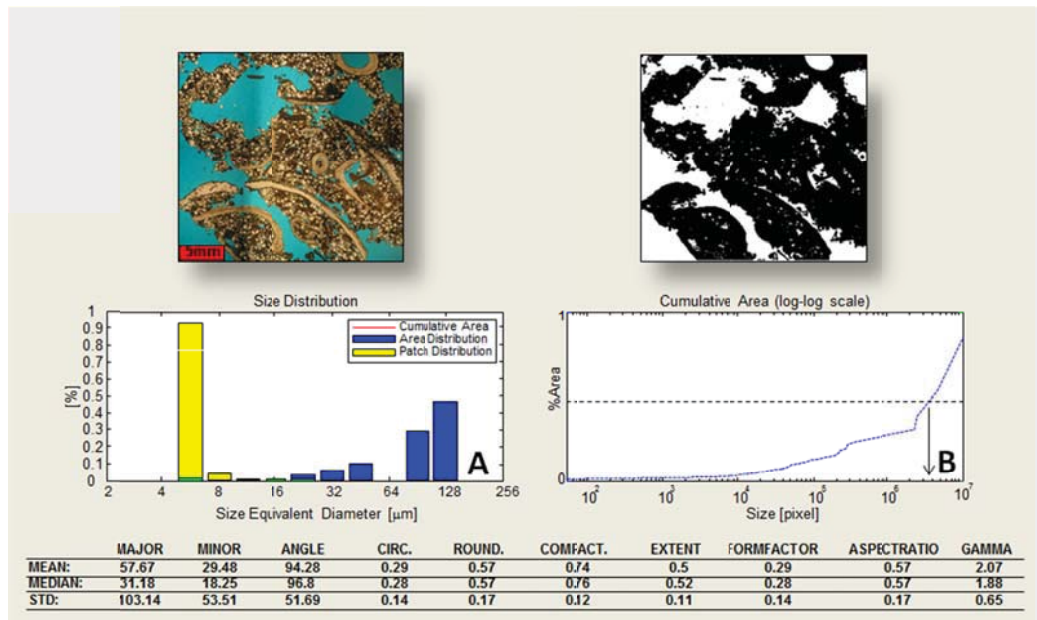


Figure 3.1: An example of DIA document of a quantified thin section with cross-plots and variables. (A) Pore size distribution and (B) Cumulative pore area.

3.2. Porosity and Permeability

3.2.1. Porosity

Bulk volume of each plug sample is obtained by measuring their diameter and lengths. Fractional porosity (ϕ) is measured by obtaining the grain volume from a helium pycnometer (Keng, 1969). Subtracting the grain volume from the bulk volume of the plugs gives the fractional porosity.

$$\text{Total Porosity:} \quad V_{Pt} = V_B - V_g \quad (1)$$

Where;

V_B = Bulk volume
 V_g = Grain volume
 V_{Pt} = Total porosity

$$\text{Percentage Porosity:} \quad \% \text{ Porosity} = \phi = (V_{Pt}/V_B) \times 100\% \quad (2)$$

3.2.2. Permeability

Permeability measurements (performed by Schlumberger) are steady-state air permeability with Nitrogen gas (Figure 3.2). Polished and dried core-plugs are placed in a core holder with a rubber sleeve, which seals the core-plugs. Air is injected at a constant pressure until the stabilization takes place. For each sample, the single flow rate of nitrogen gas is measured up to 1cc/sec with a net confining pressure of 400psi. The flow rate and difference between each end of the plug samples are analyzed by using the integrated form of Darcy's law for a compressible fluid (Ohen and Kersey, 1993). After application of different gas

flow rates, the slope of the cross-plot of V_a versus $(\rho_1^2 + \rho_2^2) / L$ provides the air permeability.

$$k_a = \frac{2000\rho_a\mu q_a L}{(\rho_1^2 + \rho_2^2)A} \quad (3)$$

Where;

k_a = air permeability, md
 ρ_a = atmospheric pressure, atm
 μ = air viscosity, cP
 q_a = gas flow rate at atmospheric pressure, cm³/sec
 L = Length, cm
 A = cross-sectional area, cm²
 ρ_1 = upstream pressure, atm
 ρ_2 = outlet pressure, atm

And where;

$$V_a = q_a / A \text{ cm/sec} \quad (4)$$

V_a ; (Calculated gas flow rate considering the selected cross-sectional area)

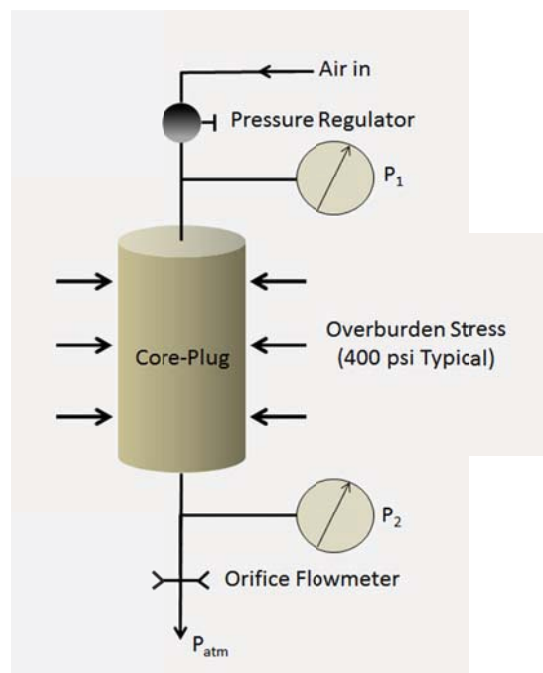


Figure 3.2: A schematic diagram of steady-state air pressure permeability modified from Ohen and Kersey (1993).

After application of different gas flow rates, the slope of the cross-plot of V_a versus $(\rho_1^2 + \rho_2^2) / L$ provides the air permeability.

3.3. Ultrasonic Velocity

3.3.1. The NER AutoLab 1000 System

Sonic velocities were performed on a NER AutoLab 1000 system (Figure 3.3) designed and fabricated by New England Research, Inc. The system has a core holder (Figure 3.4) and a multifunctioning pressure vessel which produces confining pressures up to 100 MPa (15,000 psi) and transducers for different measurement options such as sonic velocities (V_p – compressional wave velocity and V_s – shear wave velocity), electrical resistivity, pore volume and linear compressibility, steady state permeability and transient permeability. The external furnace system heats the system to imitate desired reservoir conditions. The ultrasonic transducers measure one compressional and two orthogonally polarized shear waves at selected confining pressures and temperatures.



Figure 3.3: The NER AutoLab 1000 complete setup.

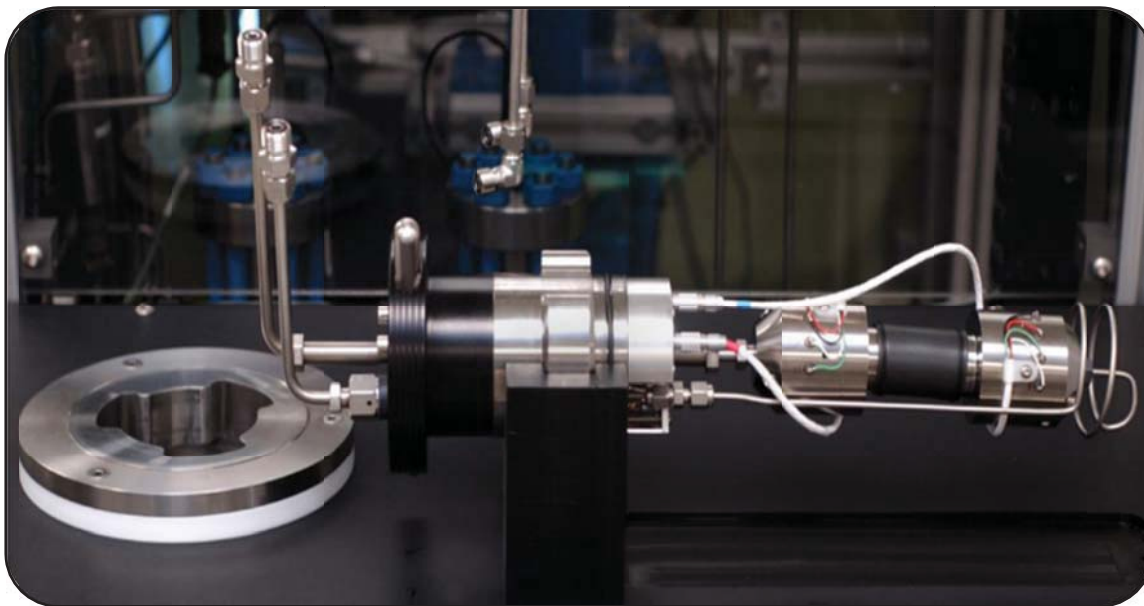


Figure 3.4: The core holder and the transducers of the NER AutoLab 1000 system.

3.3.2. Lab Analysis

In order to perform ultrasonic measurements, the initial process of sample preparation is completed for porosity and permeability measurements. Plugs (3.81 cm diameter) are cut and polished with the goal to obtain flat surfaces that increase contact to the transducers in order to produce more accurate sonic velocity measurements. The cylindrical core-plugs are dried at 60°C for two days and put in a desiccator to remove all moisture in the pore spaces. Rubber sleeves are used to seal each specimen from the confining oil in the pressure vessel. In ultrasonic measurements, compressional and shear waves undergo attenuations related to the physical state of materials (Toksoz et al., 1979). Throughout the ultrasonic measurements with the given frequency of 1MHz and actual center frequency of the received signal of approximately 800-900 KHz, one compressional (V_p) and two orthogonally polarized shear waves (V_{S1} and V_{S2}) are acquired at each given confining and pore pressures combination used. For this study, the maximum applied pressure was chosen as 20 MPa which can simulate common reservoir conditions. Samples were measured in two different conditions. For the dry core-plugs, confining pressure steps were set in a sequence from 3 MPa to 20 MPa. After the dry measurements, the core-plugs are saturated in brine containing of 35ppt of sodium chloride and placed into a vacuum pump to ensure that the brine penetrate fully into the pore system. For the saturated core-plugs, confining pressure steps are set in sequence from 6 MPa to 23 MPa while the pore-fluid pressure is kept at 3 MPa. As a result,

effective pressure conditions during the saturated measurements match the effective pressure conditions of the dry measurements.

3.3.3 Data Processing and Quality Control

Each ultrasonic measurement is recorded on a data sheet by the NER AutoLab 1000 system. Compressional and shear velocities are determined by picking the first arrival of each waveform (Figure 3.5). For consistency, a script programmed by Dr. Ralf Weger was used. The velocity is calculated by using the formula of Galileo Galilei “distance = velocity x time” with the appropriate correction for the travel time through the transducer assembly.

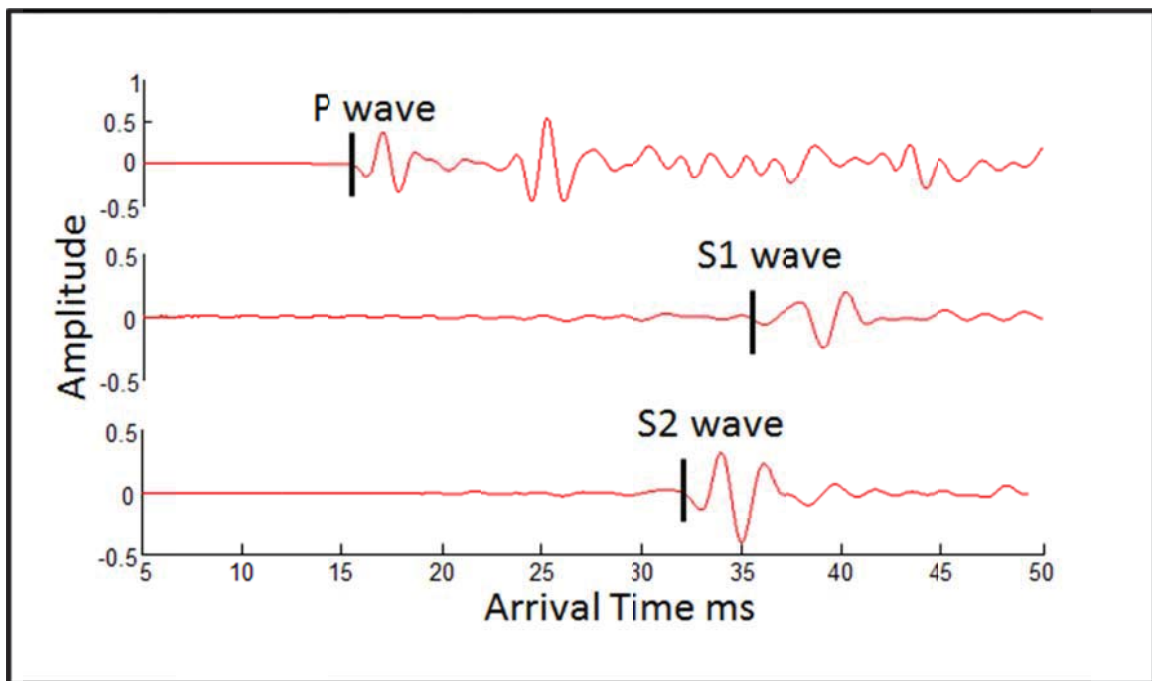


Figure 3.5: An illustration of waveforms and first arrival picking. Black line gives the position of the first arrival.

Quality control of the data is completed based on several factors such as V_p/V_s ratios and the consistency of velocity versus porosity or permeability. Due to the fact that stromatolites and pavements tend to have large V_p/V_s ranges, the samples which have V_p/V_s ratios of lower than 1.5 or higher than 2.0 were eliminated. The known scattering windows of carbonates with respect to velocity, porosity and pore types help to eliminate the defective data in our data set.

3.4. Electrical Resistivity

Complex electrical resistivity of 35ppt brine saturated samples is measured using a four-electrode technique with a frequency range from 0.01 Hz to 100 KHz created by a function generator (Figure 3.6). The transmitter produces a square wave constant-current source signal. Resistivity is measured at the same effective pressure steps as the ultrasonic measurements (from 3 MPa to 20 MPa). An automatic correction is made for temperature variations to 25 °C for each measurement. A resistor of known electrical resistivity helps measure the resistance of the samples by measuring the voltage over both. After amplification of the signal, it is transferred to a digital oscilloscope. The frequency used to determine the cementation factor is 720 Hz. The Cementation Factor 'm' of each specimen was calculated from the measured Formation Factor 'F' using Archie's equation, $F = \varphi^{-m}$ (where φ is porosity).

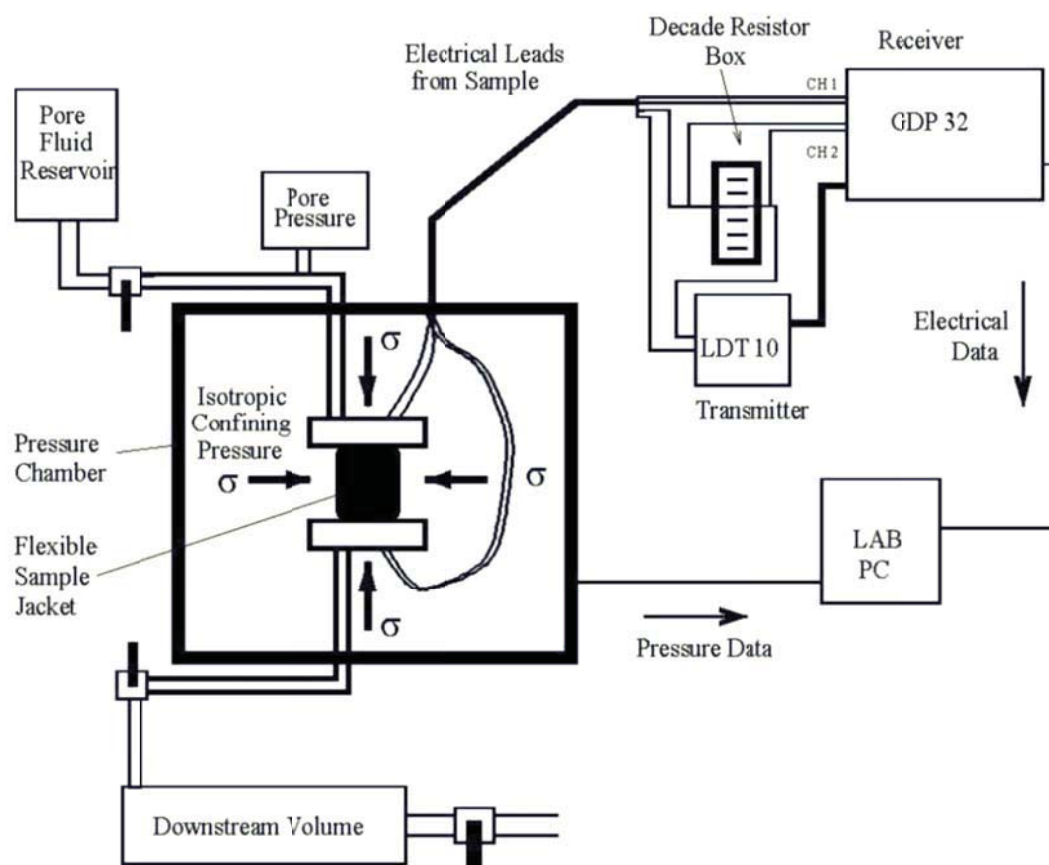


Figure 3.6: A general sketch of the laboratory equipment of NER AutoLab system (Seabrook, 2001) with the pressurizing system, processor, receiver and transmitter for the geophysical data and the PC for data processing.

3.5. Mineralogy Determination

The PANalytical X'PertPRO X-ray Diffractometer is used to determine the mineralogical composition of the samples based on aragonite and low-Mg or high-Mg calcite (Figure 3.7). The data is processed by using High Score Plus software. The first XRD analysis showed that stromatolites in Hamelin Pool consist of an average high-Mg calcite content of 10.8% while there is no low-Mg calcite present. In order to obtain the exact percentage of quartz mineral in

stromatolites and pavements all carbonate is dissolved with hydrochloric acid solution (10%) and organic carbon is removed with bleach in 100 milligrams of ground samples. Beakers were weighted before and after the experiment to obtain the amount of undissolved material. Finally, a second XRD analysis was performed to make sure that the remaining material is only quartz.

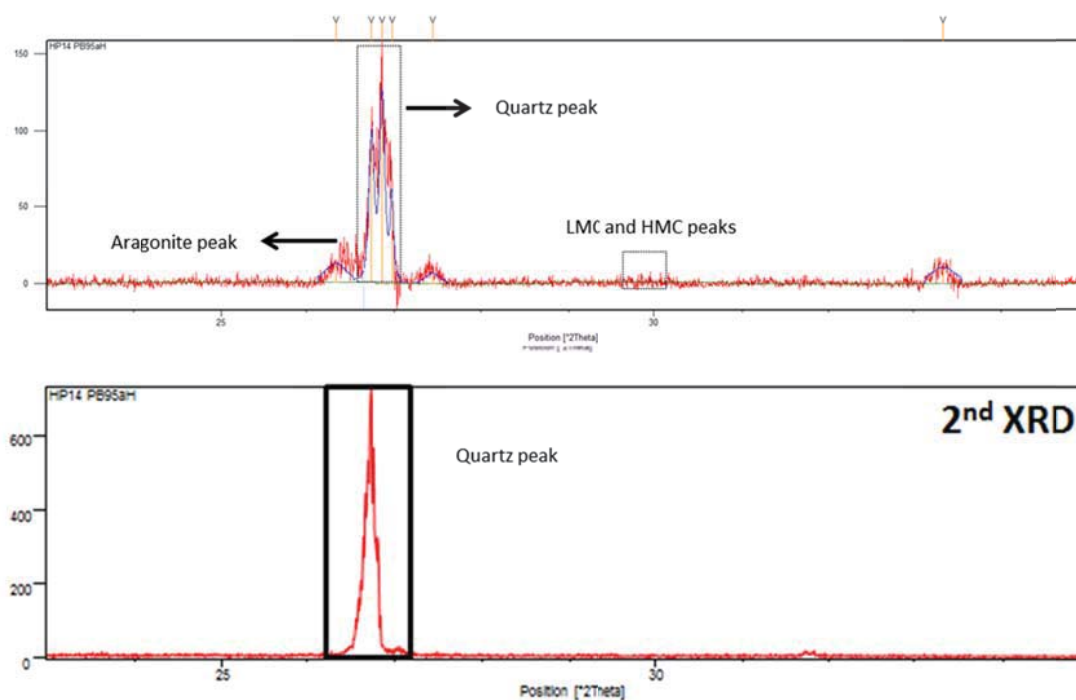


Figure 3.7: First XRD shows the mineral composition of the sample. Second XRD shows the quartz peak after dissolving the organic and the inorganic carbons in the samples.

CHAPTER 4. PORE STRUCTURE AND PETROPHYSICAL CHARACTERIZATION

4.1. Pore Structure Characterization Using Digital Image Analysis (DIA)

In this study the Dominant Pore Size (DomSize) and Perimeter over Area (PoA) are used to assess the pore structure and complexity of the stromatolite heads and pavement samples. Perimeter over Area (PoA) is the ratio of total pore-space area to the total perimeter of the pore space on a thin section. PoA describes the complexity of the pore system. Smaller values of PoA indicate a less complex pore structure. Dominant Pore Size (DomSize) is measured by considering the upper boundary of the pore sizes comprising 50% percent of porosity on a thin section. Weger et al. (2009) correlated the pore geometry parameters and velocities and found that samples with simple pore structures (small values of PoA) and high values of DomSizes are faster than samples with small complicated pore structure. The reference data from Weger et al. (2009) and Verwer et al. (2011) are used to illustrate the general trend of carbonate rocks in most of the cross-plots throughout this thesis.

4.1.1. Pore Structures of the Hamelin Pool Stromatolites and Pavements

PoA values of the reference data ranges from 20 mm^{-1} to 304 mm^{-1} and DomSize ranges from $14 \text{ }\mu\text{m}$ to $2349 \text{ }\mu\text{m}$. PoA values of Hamelin Pool stromatolites and pavements range from 9.3 mm^{-1} to 70 mm^{-1} and DomSize values range from $140 \text{ }\mu\text{m}$ to $3193 \text{ }\mu\text{m}$. Comparison of PoA and DomSize between reference data and the data from Hamelin Pool show that Hamelin Pool stromatolites and pavements have overall simple pores with variable sizes (Figure 4.1). Because stromatolites are layered structures, vertical and horizontal

core-plugs were analyzed to assess the degree of anisotropy present in the samples. No considerable anisotropy is found in either the stromatolites or the pavements.

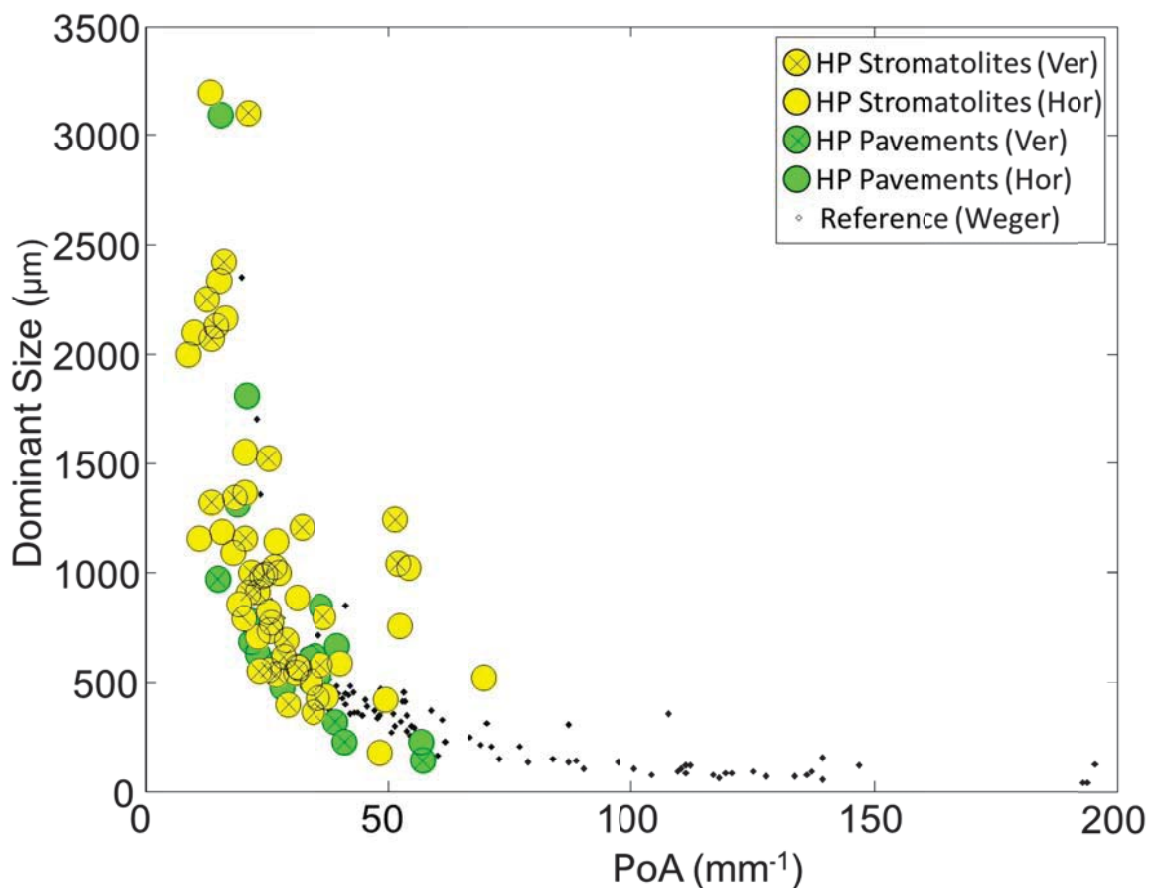


Figure 4.1: Dominant pore size versus perimeter over area cross-plot shows the pore structure and complexity.

Hagan (2014) described and classified the meso/microfabric of the stromatolites using the polished samples, thin sections, and SEM images. Using his classification for the stromatolite samples and comparing it to the DIA pore structure parameters reveals no correlation between the fabric of the internal structure and pore structure (Figure 4.2). However, fine to medium or coarse

samples display slightly simpler and bigger pores relative to the fine and very fine samples.

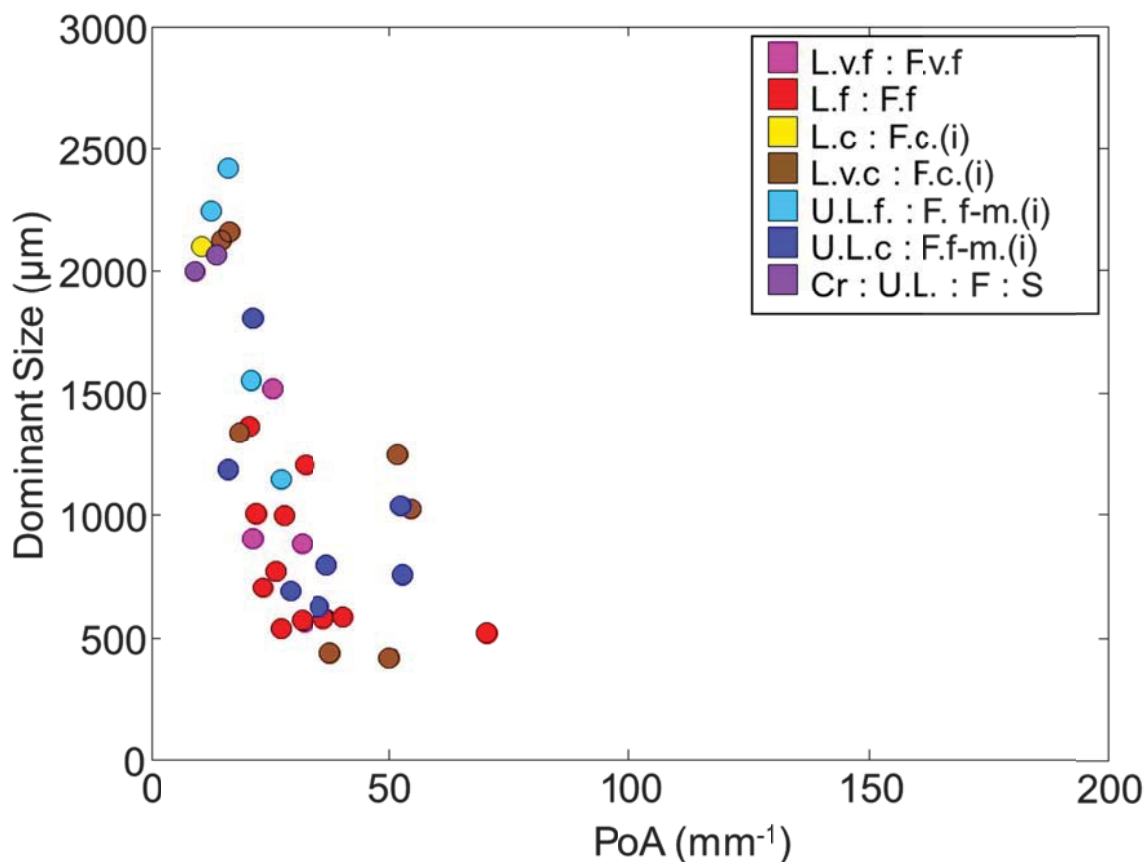


Figure 4.2: Dominant pore size versus perimeter over area cross-plot in respect to internal structure classification (L: laminated, F: fenestrae, U: unlaminated, C: crust, S: serpulid, i: irregular, f: fine, v.f: very fine, f-m: fine to medium, c: coarse and Cr: Crust).

4.2. Porosity and Permeability

Carbonate rocks have a large range of porosity because of constant cementation and dissolution processes that alter their mineralogy and the pore structure. As a result, porosity can be created or destroyed by these continuous processes and simultaneously they often affect permeability (Eberli et. al., 2013). The Hamelin Pool stromatolites range in porosity from 16% to 46%, while the

pavements range from from 18% to 44%. No anisotropy is observed in vertical versus horizontal plugs (Table 4.1). Permeability values of the Hamelin Pool stromatolites range from 570 mD to 9000 mD, while pavements range from 7 mD to 5140 mD (Figure 4.3). One pavement sample had lower permeability, but all others show high permeability similar to stromatolite samples. As for porosity, no anisotropy is observed. Porosity of the Hamelin Pool samples is high when compared to a representative dataset of various carbonate sample, but it is not unusually high. However, the permeability of the Hamelin Pool stromatolites and pavements is almost a magnitude higher than rocks with similar porosity in the reference data (Figure 4.3). This unusually high permeability is apparently independent of porosity. The stromatolite with the lowest porosity (16%) has 1747 mD of permeability, while the stromatolite with the highest porosity (43%) has a similar permeability of 2100 mD. Likewise, all pavement samples, with one exception display high permeability, and like the stromatolites do not show a correlation between porosity and permeability.

In order to assess whether a relationship exists between pore structure and permeability, the DIA parameters for dominant pore size (DomSize) and PoA of Hamelin Pool stromatolites and pavements are cross-plotted and color-coded with their permeability values (Figure 4.4). No clear trend is observed. However, samples with lower permeability tend to have relatively small DomSize values and high PoA values and the majority of core-plugs with high permeability have relatively large DomSize and small PoA values. In comparison to the reference data set of other carbonates the Hamelin Pool samples lack complicated pore

structures with high PoA but have simple pores of variable sizes. This large and simple pore structure is interpreted to be the reason for the high permeability.

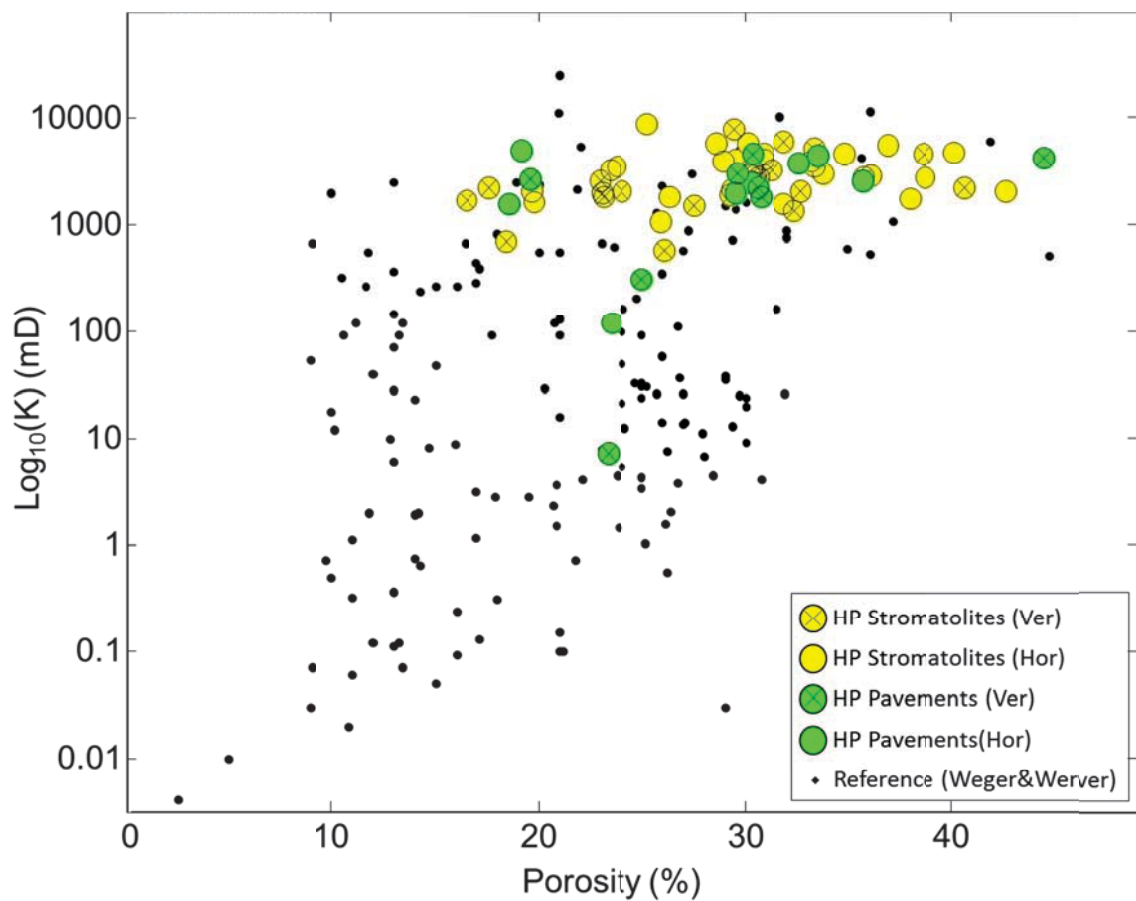


Figure 4.3: Permeability and porosity cross-plot of Hamelin Pool (HP) stromatolites (yellow) and pavements (green). Both sample sets display a high permeability that is independent of porosity. Crosses in circles represent the vertical drilled core plugs.

Table 4.1: Porosity and permeability values of Hamelin Pool stromatolite and pavement samples. The sections are separated with vertical and horizontal samples.

Hamelin Pool Stromatolites					
Sample ID - Vertical	K (mD)	Phi (%)	Sample ID - Horizontal	K (mD)	Phi (%)
H2	1747.1	16.46	H1	8990.65	25.27
H4	2241.21	17.59	H3	1654.25	19.74
H6	1392.56	32.38	H5	2101.11	42.65
H8	1519.84	27.53	H7	1809.51	37.9
H10	577.69	26.09	H9	1086.7	25.96
H13	1876.13	23.08	H11	2113.86	19.62
H15	2113.24	24.03	H12	3405.12	30.28
H16	1922.86	29.27	H14	3620.2	33.32
H18	2128.43	32.66	H17	3272.02	23.39
H19	2274.11	40.59	H20	1613.51	31.84
H21	3298.4	31.27	H22	2183.95	29.31
H23	2502.98	30.37	H24	1886.22	26.37
H25	5367.9	33.33	H26	2978.72	35.98
H28	1990.49	23	H27	4245.32	30.81
H30	2646.08	22.89	H29	2956	30.4
H32	2900.17	35.67	H31	4612.37	30.82
H34	2874.43	30.57	H33	3588.62	23.75
H36	2933.85	30.2	H35	3076.67	33.76
H38	702.4	18.39	H37	4127.82	29.55
H55	4056	33.16	H52	5824	28.57
H56	4720	38.63	H53	4795	40.13
H61	6156	31.85	H54	5760	36.88
H51	8139	29.41	H57	2876	38.73
			H58	4041	28.96
			H59	4702	34.76
			H60	6028	30.06
Hamelin Pool Pavements					
Sample ID - Vertical	K (mD)	Phi (%)	Sample ID - Horizontal	K (mD)	Phi (%)
P1	4745	30.38	P2	3831	32.6
P13	1885	30.75	P3	2573.92	30.23
P14	317	24.98	P11	5142	19.14
P16	2232	30.60	P12	1627	18.60
P17	2791	19.56	P15	4493	33.53
P19	7.46	23.34	P18	1978	29.53
P21	3047	29.62	P20	120	23.53
P22	4420	44.44	P23	2674	35.72

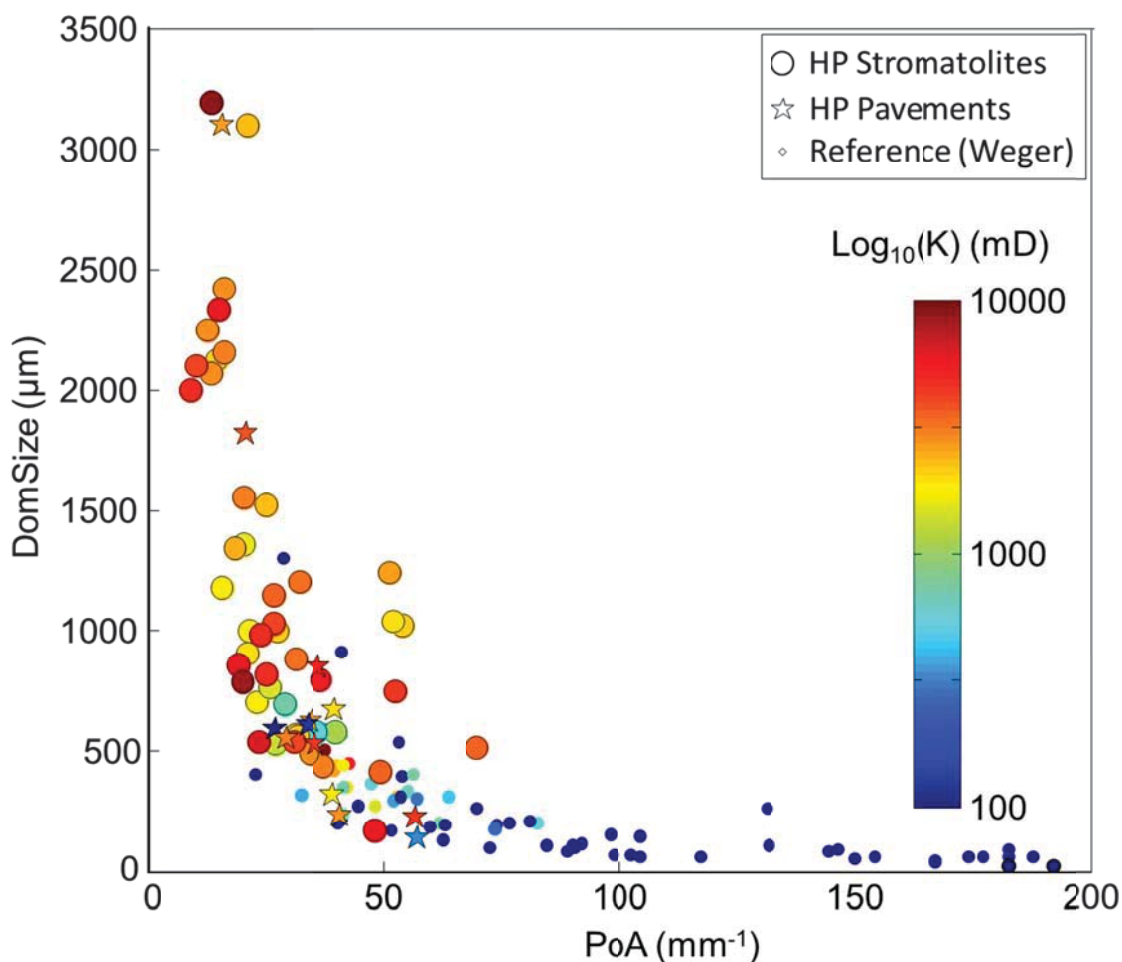


Figure 4.4: Crossplot of the two DIA parameters DomSize and PoA with the permeability data in color bar. Round dots are stromatolites, stars are the pavements and the small dots are carbonates from the data set of Weger et al. (2009). No clear trend is observed.

In order to relate the environmental factors to porosity and permeability, the Hamelin Pool stromatolites and pavements cross-plots are coded for distance from shore, type of head shape, and water depth (Figure 4.5, Figure 4.6, and Figure 4.7). Besides a weak trend of lower porosity with distance from shore (Figure 4.5) no relationship exists between these environmental factors and porosity and permeability.

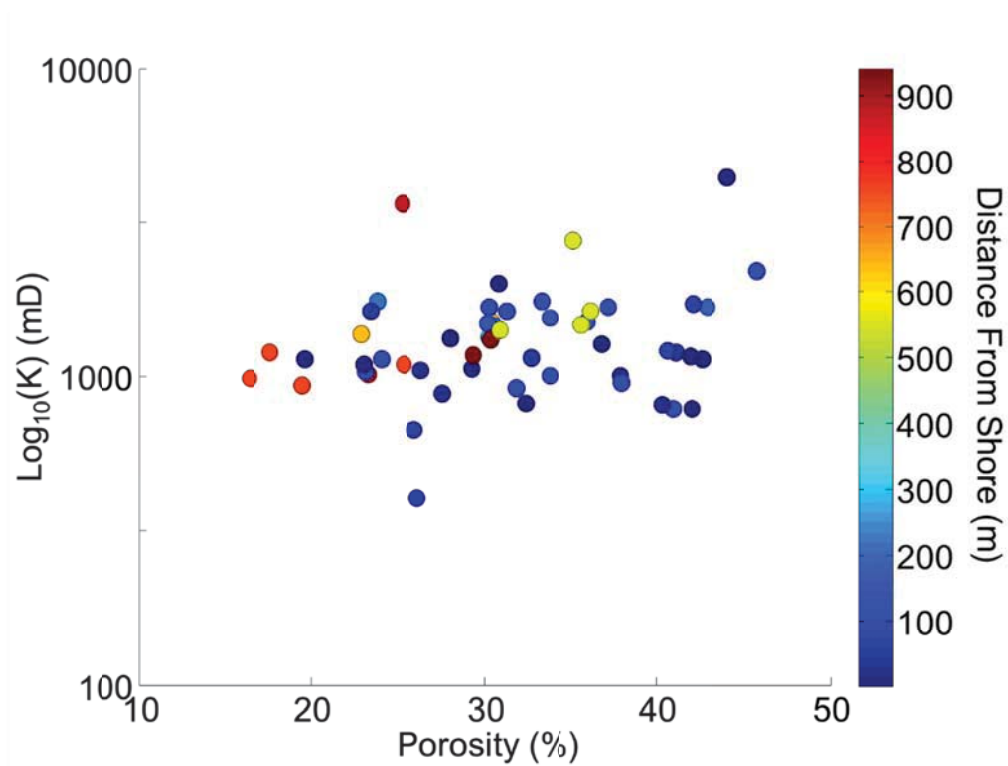


Figure 4.5: Porosity versus permeability data in respect to distance from shore.

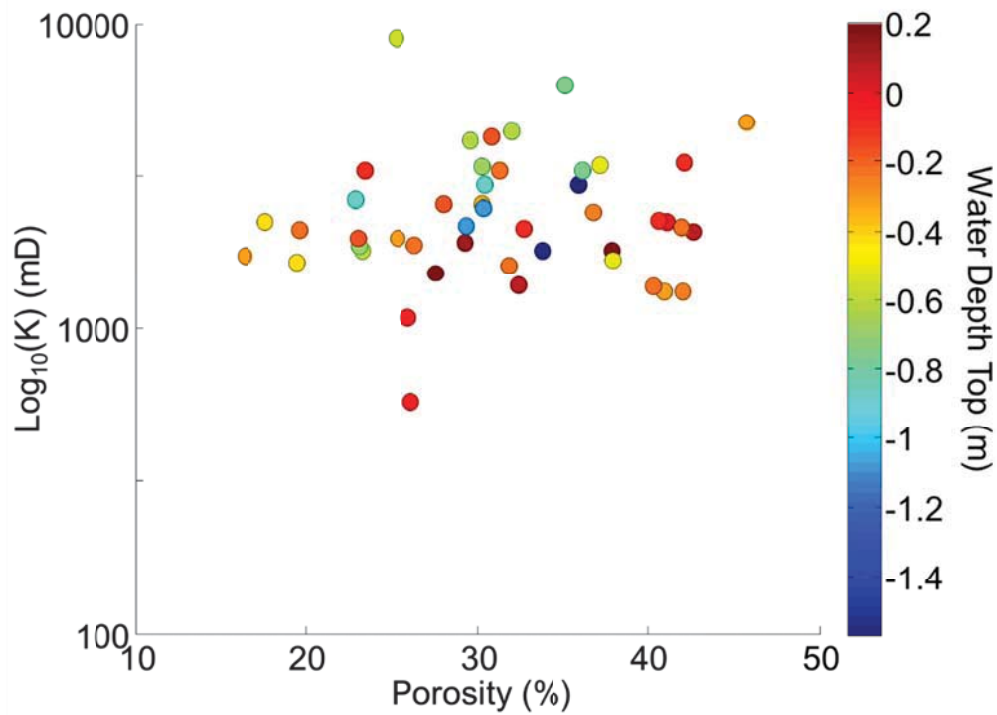


Figure 4.6: Porosity versus permeability data in respect to water depth.

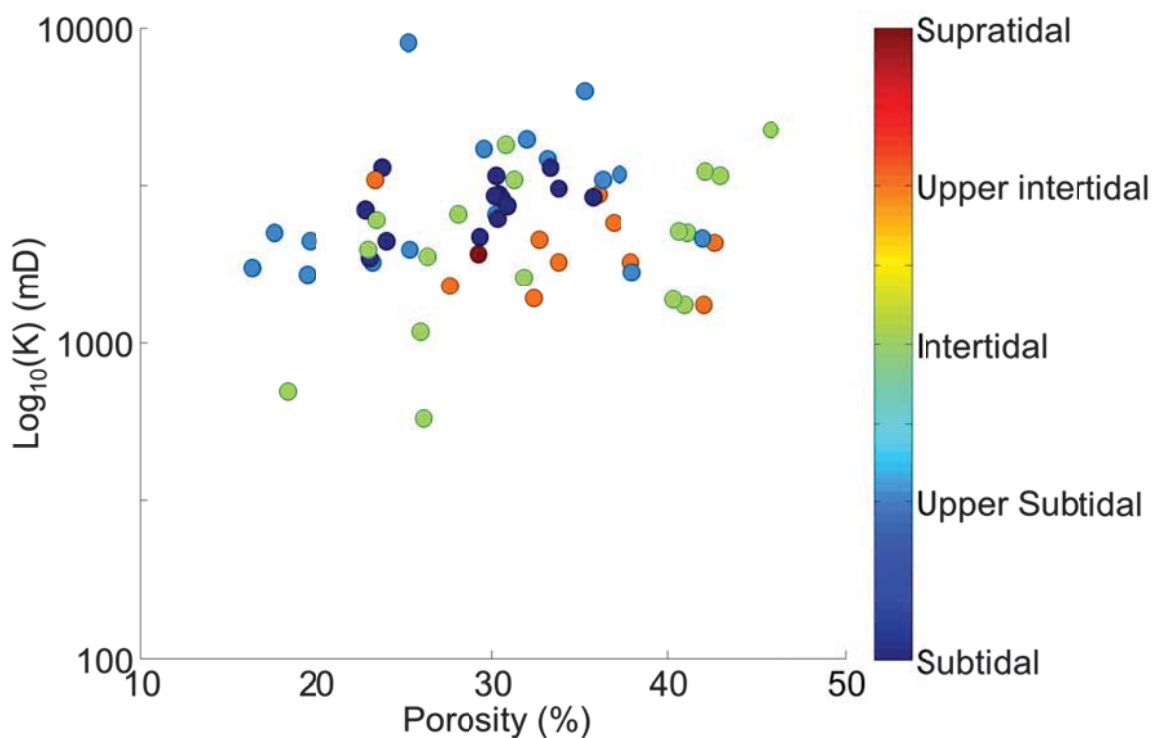


Figure 4.7: Porosity versus permeability data in respect to tidal zones.

Hagan (2015) described the meso- and microfabric of the stromatolites and related them to microbial mat types and their position in a shore to basin profile. In Figure 4.8 the meso/microfabric classification of Hagan is used for the color-coding in the porosity and permeability cross-plot. The fabrics are not distinctive enough to create a recognizable pattern with changing porosity. This suggests that there is no apparent relationship between internal structure and both porosity and permeability in Hamelin Pool stromatolites and pavements.

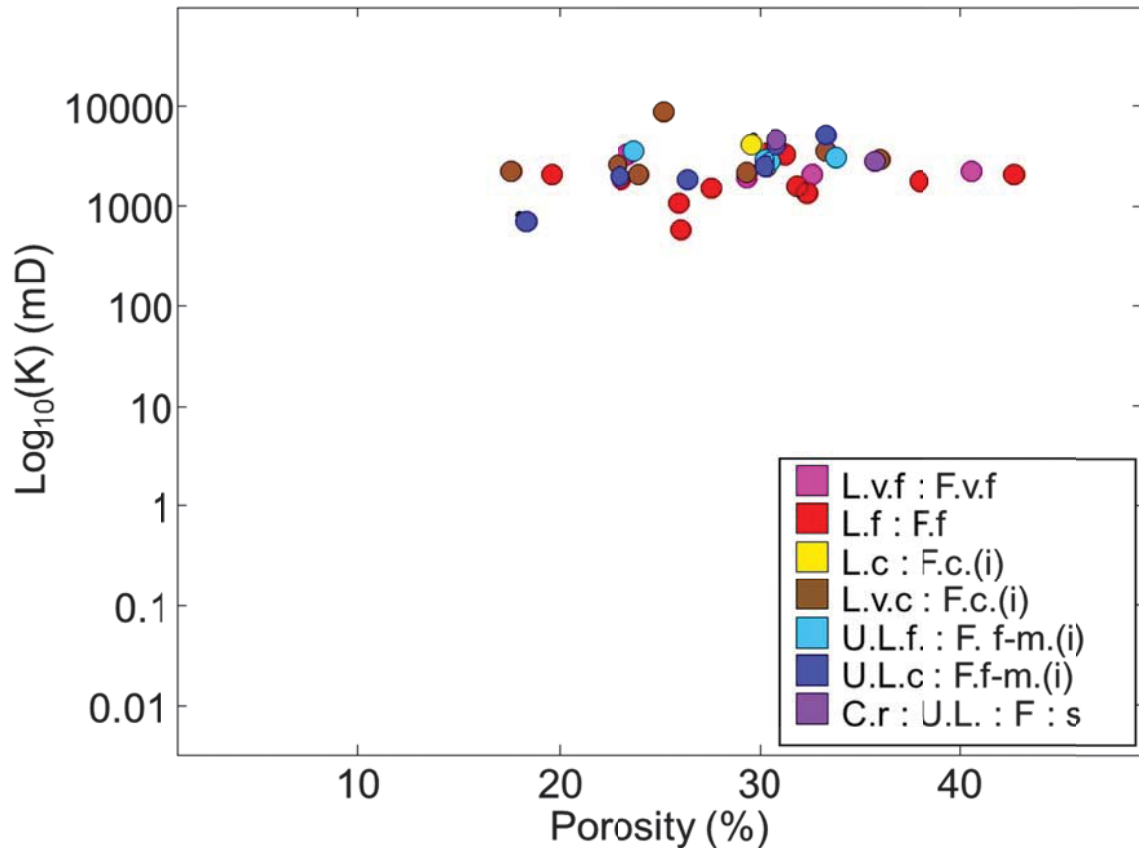


Figure 4.8: Porosity versus permeability data in respect to the internal structure classification of meso/microfabrics by Hagan (2015) (L: laminated, F: fenestrae, U: unlaminated, C: crust, S: serpulid, i: irregular, f: fine, v.f: very fine, f-m: fine to medium, c: coarse, v.c: very coarse).

4.3. Ultrasonic Velocity

Anselmetti and Eberli (1997) analyzed 295 carbonate samples with V_p values ranging from 1700 to 6500 m/s and V_s values ranging from 700 to 3400 m/s. The reason that carbonates have such a wide range of V_p and V_s values is their wide range of porosity and different pore systems. Mineralogy is not a cause of these ranges according to Anselmetti and Eberli (1997). Complex pore systems such as vugs, channels, molds, and fractures are encountered more frequently in carbonates than in siliciclastics (Wang, 1997). Porosity and pore

geometry combined are the main control of acoustic velocities in carbonate rocks (Anselmetti and Eberli, 1993; Eberli et al., 2003). Weger et al. (2008) confirmed this finding by using DIA parameters to quantify the pore structure. His analyses clearly document that samples of uniform mineralogy, large, simple pores result in higher velocity than small, complex pores that are more compliant. His data consists of representative samples covering all of Dunham's textures and all of Choquette and Pray's pore types. Here, the pore structures of the Hamelin Pool stromatolites and pavements are displayed in comparison with this reference data set. In the following paragraphs, the velocity of the Hamelin Pool stromatolites and pavements are first related to porosity. Then, the relation between pore structure and velocity is analyzed. Subsequently, the influence of pressure on their velocity is assessed. Finally, the influence of saturation is analyzed.

4.3.1. Velocity versus Porosity

Wyllie et al. (1958) performed an experimental investigation on siliciclastic and carbonate rocks to determine the probable effect of a porous medium and the interacting fluid on acoustic signals. The "time-average" equation was derived from this empirical data, which relates the measured velocity, the velocity of the saturating fluid and the grain velocity. The "time-average" equation states that

$$\frac{1}{V_M} = \frac{\varphi}{V_F} + \frac{1 - \varphi}{V_R} \quad (5)$$

Where V_M = measured velocity, V_F = velocity of saturating fluid. V_R = velocity of the solid rock and φ = porosity.

The time-average equation was aimed to estimate acoustic velocities from other parameters (V_F , V_R , and ϕ). Wyllie's experiment produces reasonable reliable results for siliciclastic rocks with mostly intergranular pore type. However, in the same paper, Wyllie et al. (1958) document that carbonate rocks show a poor correlation between velocity and porosity. They postulate that the pore structure is responsible for this behavior.

Hamelin Pool stromatolites and pavements have relatively high velocities given their high values of porosity (Figure 4.9). They are all above the Wyllie time-average equation for calcite and they show large variation of velocity at the same porosity. For instance, at 29% porosity, velocities range from 3611 m/s to 5384 m/s. Similarly at a velocity of 4403 m/s the porosities range from 23% to 46%. The sample with the highest porosity of 46% is not only above the Wyllie estimation; it is also above the reference data. This large variation indicates that velocity in the stromatolites and pavements from Hamelin Pool are not porosity dependent. There is a slight anisotropy in the stromatolites and pavements; horizontal core plugs are slightly faster than vertical core plugs (Figure 4.9). This behavior is not unusual in the stromatolite samples that have laminations. Since the laminations show horizontal layering such as in Figure 2.1, horizontally drilled samples have vertical layers which have continuity from the top to the bottom of the core plugs. This provides more contact in between the sediments and can make the velocities faster.

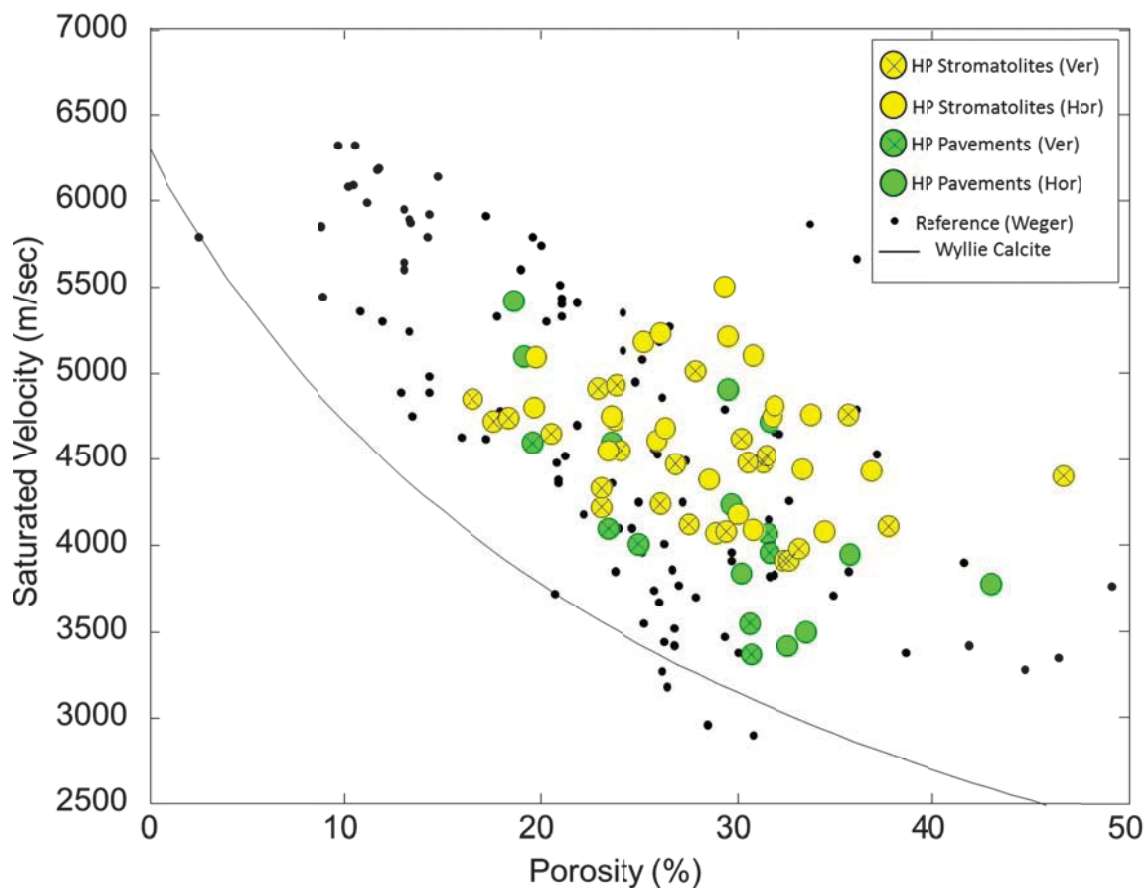


Figure 4.9: Saturated compressional velocities versus Porosity with Wyllie “time-average” for calcite (1958).

The Hamelin Pool stromatolites and pavements display a large range shear velocity with a minimum shear velocity of 1800 m/s at the porosity of 30% and maximum velocity of 3419 at porosity of 18% (Figure 4.10). Similarly as in the compressional wave velocity, there are large variations of shear velocity at any given porosity. For example, at 30% porosity the velocity ranges from 1800 m/s to 3420 m/s.

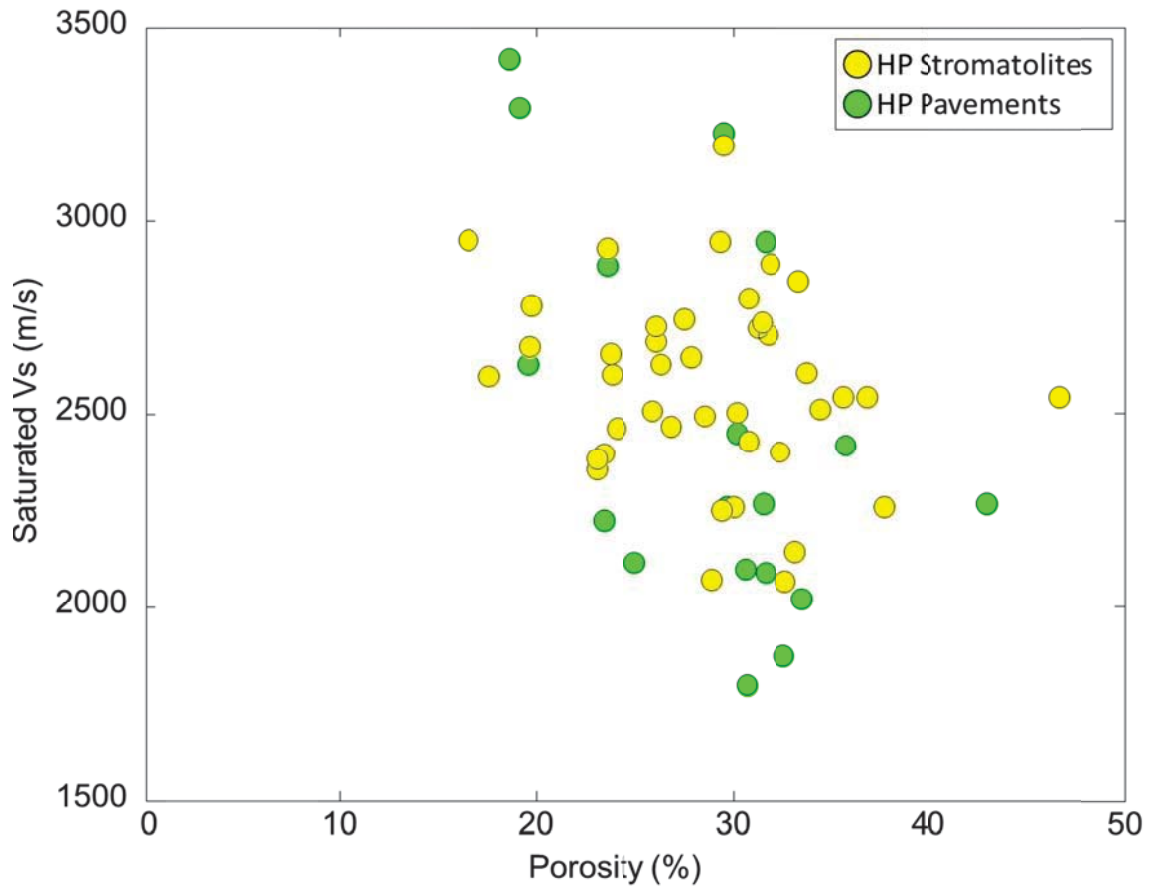


Figure 4.10: Saturated shear velocities versus porosity at 20 MPa effective pressure.

Different ratio of compressional velocity and shear velocity (V_p/V_s) is often characteristic of changes in lithology. Pickett (1963) found that limestones have a V_p/V_s range of about 1.9, dolomites of about 1.8, and sandstones about 1.6. In carbonates, the V_p/V_s ratio is very sensitive to different fluids such as gas, water or brine (King, 1966; Tatham and Stoffa, 1976; Tatham, 1982). Anselmetti and Eberli (1993) used 210 carbonates from different areas consisting of different pore structures and fabrics. Overall, the V_p/V_s ratio of those samples displayed a ratio from 1.8 to 2.

The V_p/V_s ratios of Hamelin Pool stromatolites and pavements show a range from 1.5 to 1.9 (Figure 4.11). The average V_p/V_s ratio of the stromatolites and pavements is 1.76 and 1.72 respectively. However, most of the samples from Hamelin pool show lower V_p/V_s ratios than the carbonates analyzed by Weger et al. (2009).

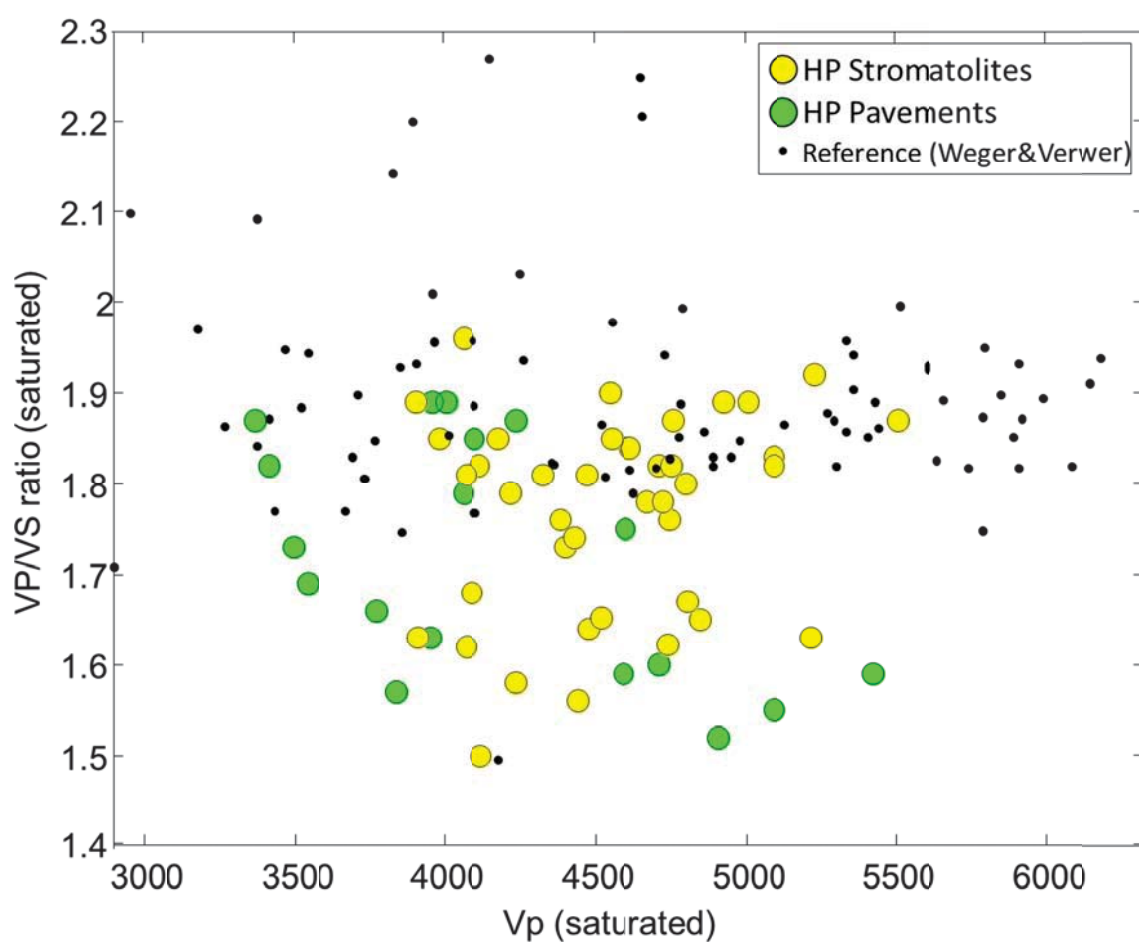


Figure 4.11: V_p/V_s ratios and compressional velocities of Hamelin Pool stromatolites and pavements.

Figure 4.12 shows the V_p/V_s ratios with respect to porosity in Hamelin Pool stromatolites and pavements. Both stromatolites and pavements do not show a clear trend of V_p/V_s ratio with increase or decrease in porosity values.

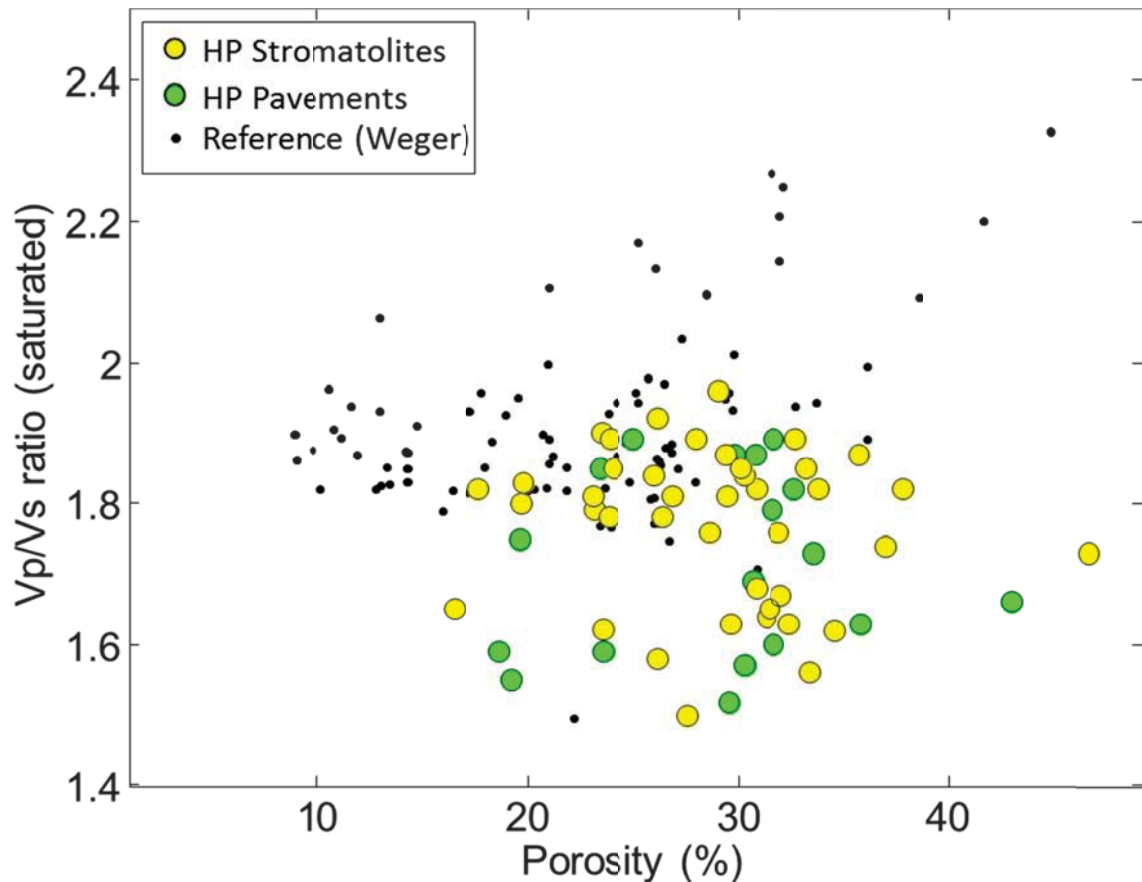


Figure 4.12: V_p/V_s ratios versus porosity of Hamelin Pool stromatolites and pavements. Neither stromatolites nor pavements do not display a clear trend with increase or decrease of porosity values.

4.3.2. Velocity versus Pore Structure

The large variation of velocity at any given porosity indicates that other factors than porosity alone determine the acoustic behavior of the Hamlein Pool stromatolites and pavements. Several studies have shown that the most important parameter besides porosity influencing the velocity in carbonates is

pore structure (Wyllie et al. 1956; Anselmetti and Eberli, 1993; Weger et al., 2008). In order to evaluate the relationship between pore structure and ultrasonic velocities, the DIA parameters DomSize versus PoA are correlated to velocity (Figure 4.13). In a cross plot of the two parameters color-coded with velocity data, there is a slight trend of increasing velocities with increasing DomSize values. Figure 4.14 displays the minimum, median, and maximum velocities in Hamelin Pool. The velocities and the corresponding thin section photos confirm that pore complexity and dominant pore size have an observable effect on ultrasonic velocities corroborating Weger et al., (2009). The observation that an increase of pore size and pore structure simplicity is coupled with an increase in velocity confirms the acoustic behavior -- pore structure relationship found in the reference data from Weger et al., (2009).

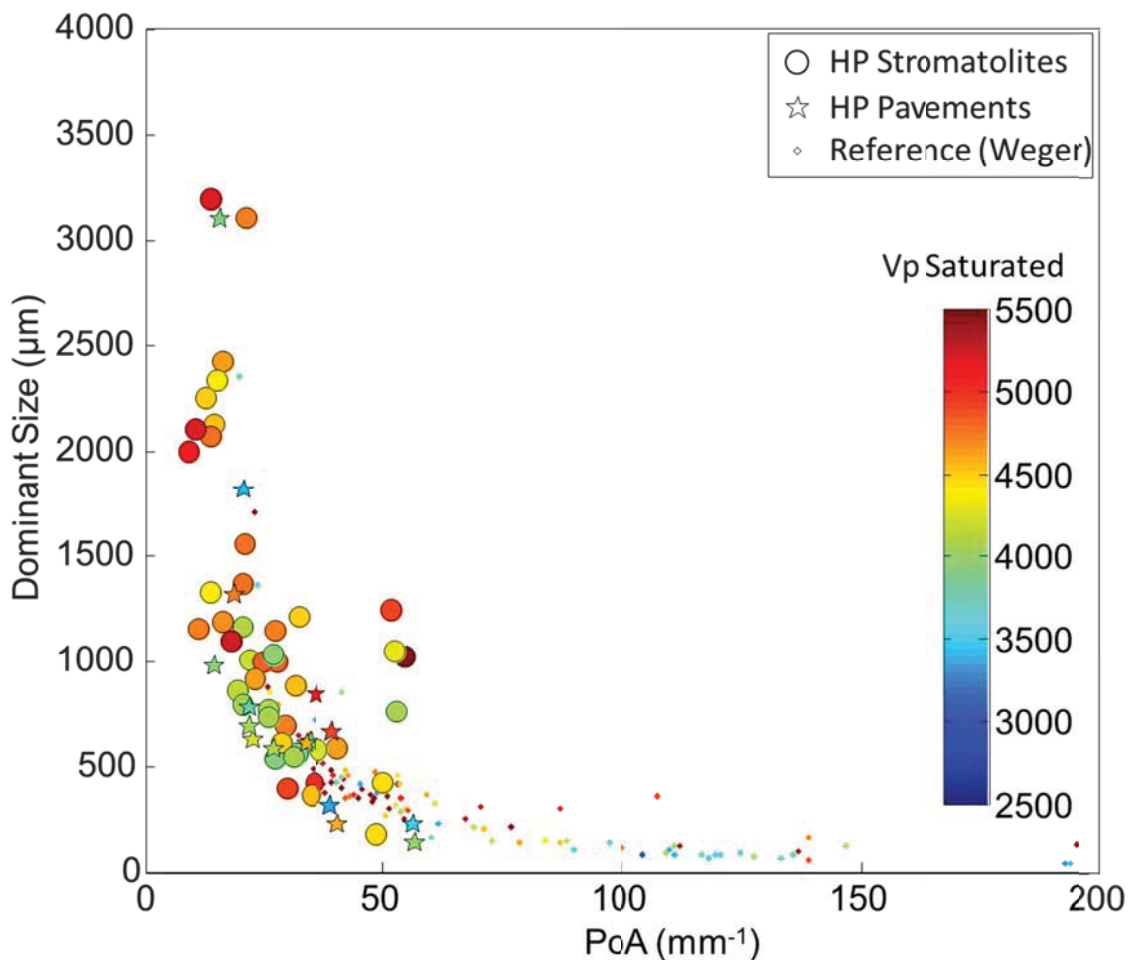


Figure 4.13: Pore structure and velocities of Hamelin Pool data with reference data from Weger et al. (2009).

In the porosity versus velocity cross plot with color-coding of DomSize (left in Figure 4.15) and PoA (right in Figure 4.15), the relationship between pore structure and velocity is best illustrated. There is a general trend of higher velocity with larger DomSize, indicated with warm colors in Figure 4.15. The complexity of the pore system is measured by the DIA parameter PoA. As mentioned earlier the pore structure of the stromatolites and pavements are all relatively simple pores, not exceeding 70 mm⁻¹. Consequently, the PoA does not

show a strong trend in the velocity- porosity cross plot. Yet, the blue colors, indicating simple pore structure are more abundant in the high velocity samples (Figure 4.15).

Saturated Core-plugs	Minimum P velocity	Median	Mximum P velocity
Vertical	3389.05	4474,84	4808.78
Horizontal	3120.01	4747,34	5383,8

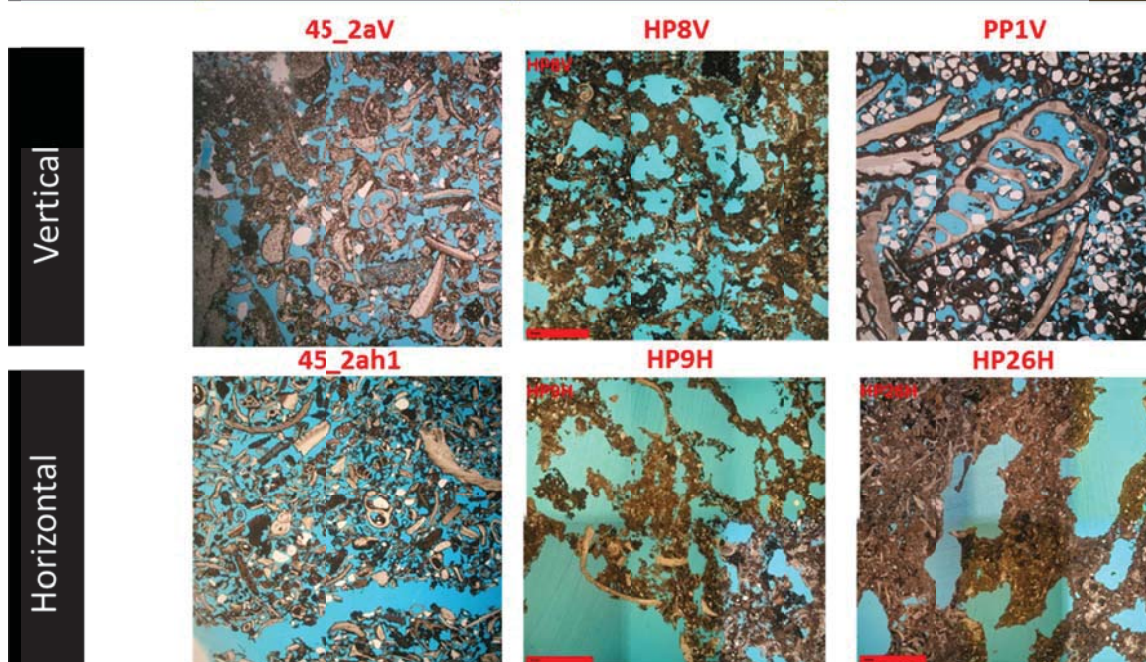


Figure 4.14: Thin section photo micrographs and corresponding minimum, median and maximum compressional velocities of vertical and horizontal core plugs. The pore structures on the thin sections show a correlation with velocity values. Samples with simple and big pores have higher velocity values than the samples with more complex and small pores.

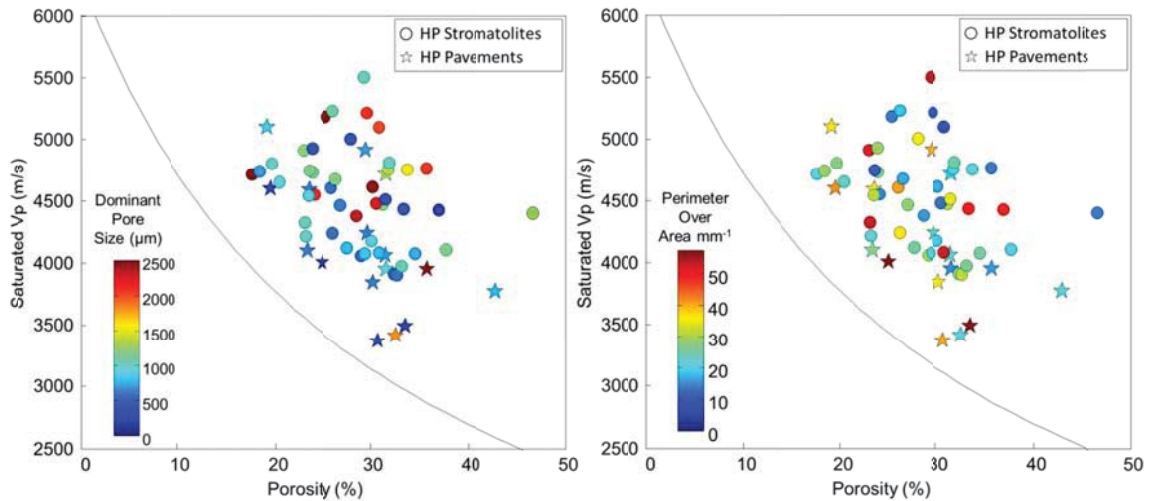


Figure 4.15: Saturated compressional velocity versus porosity cross plot with superimposed DomSize (on the left) and PoA (on the right).

The classification of the meso/microfabrics (from Hagan) and velocity cross-plot of Hamelin Pool stromatolites indicate that the internal structure does not have a distinctive influence on ultrasonic velocities (Figure 4.16)

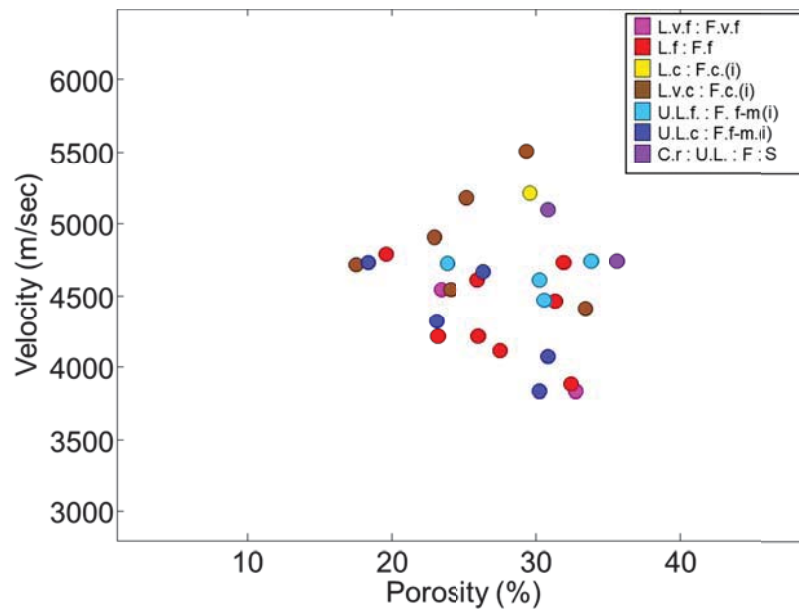


Figure 4.16: Velocity versus porosity in respect to the internal structure classification of meso/microfabrics by Hagan (2015) (L: laminated, F: fenestrae, U: unlaminated, C: crust, S: serpulid, i: irregular, f: fine, v.f: very fine, f-m: fine to medium, c: coarse).

4.3.3. Velocity versus Pressure

The microcrystalline micrite that is precipitated by microbial communities provides a rigid framework in the stromatolites (Reid et al., 2003). Hence, stromatolites potentially can endure high pressures while preserving their physical integrity and primary porosity. This potential pressure resistance is assessed by measuring velocity at 5 pressure steps from 3 – 20 MPa (Figure 4.17). The measured ultrasonic velocities of Hamelin Pool stromatolites and pavements vary widely from 3089 m/s to 5383 m/s at the effective pressure of 20 MPa. Horizontal core-plugs of stromatolites are slightly faster relative to vertical core-plugs and pavements. However, all samples display a similar acoustic behavior with increasing pressure. In all samples, ultrasonic velocities do not change much with increasing effective pressure. For example in stromatolites, the slowest V_p of 3736 m/s at 5 MPa is measured as 3903 m/s at 20 MPa while the fastest V_p of 5235 m/s at 5 MPa is measured as 5504 m/s at 20 MPa. Similarly, in pavements, the slowest V_p of 3184 m/s at 5 MPa is measured as 3369 m/s at 20 MPa while the fastest V_p of 4914 m/s at 5 MPa is measured as 5424 m/s at 20 MPa. This implies that Hamelin Pool stromatolites and pavements are pressure resistant.

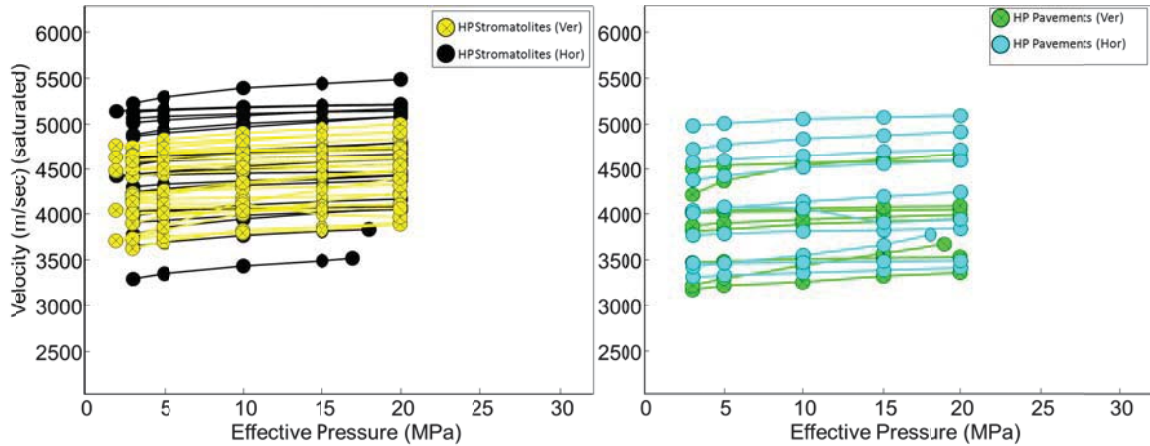


Figure 4.17: Sonic velocities versus effective pressure of Hamelin Pool stromatolites and pavements. Changes in pressure do not change velocities significantly both in stromatolites and pavements. Horizontal core plugs are slightly faster than vertical ones in both Hamelin Pool stromatolites and pavements.

4.3.4. Velocity Development under Saturation

Baechle et al. (2009) analyzed 38 limestone samples to assess the effect of fluid substitution on the acoustic behavior of carbonates. His experiments are also a test of the validity of Gassmann's fluid substitution, which predicts P-wave velocities in carbonates filled with one type of fluid from velocities measured with another type of fluid. Gassmann (1951) main assumption is that shear modulus of rocks do not change with the interaction of fluids. However, carbonates undergo shear weakening and shear strengthening with the interaction of fluids (Beachle et al., 2009).

The fluid substitution states that;

$$V_{P_{Gass}} = \sqrt{\frac{K_{Gass} + (4/3)\mu}{\rho}} \quad (6)$$

where, V_{Pgass} = Gassmann predicted velocities, K_{gass} = bulk moduli calculated by Gassmann, ρ = saturated bulk density and μ = shear moduli.

In the saturation experiments on the Hamelin Pool samples most compressional velocities of brine saturated are, as expected, faster than the velocity of the dry core-plugs. However, the shear wave velocities are also changing, indicating that the shear modulus is not constant as postulated by Gassmann (1951). In saturated core-plugs from Hamelin Pool, compressional velocities increase up to 686 m/s with saturation (Figure 4.18). In contrast, shear wave velocities show both a decrease (up to 578 m/s) and an increase (up to 597 m/s) in velocity (V_s) with saturation. These changes in V_s indicate that the stromatolites do change the shear modulus with saturation resulting in both shear weakening and shear strengthening and thus violating the assumption by Gassmann (1951).

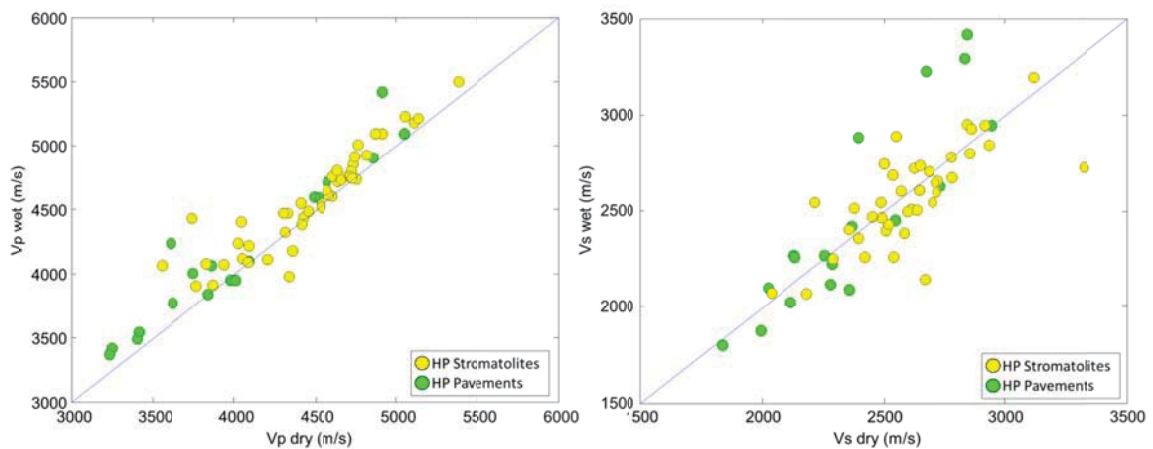


Figure 4.18: Crossplots of V_p and V_s under fully water-saturated and dry conditions at 20 MPa effective pressure. The velocities of compressional waves show an overall increase while shear waves display both decrease and increase.

Figure 4.19 displays the changes of the ratio of wet and dry shear moduli in percentages and the ratio of measured saturated velocity to Gassmann's calculated velocity. In contrast one of the Gassmann's assumptions which state that fluid interaction does not change shear moduli, Hamelin Pool stromatolites and pavements show both shear weakening and shear strengthening. The ratios of V_p measured and V_p calculated from Gassmann equations show that stromatolites and pavements display both Gassmann underestimation and overestimation.

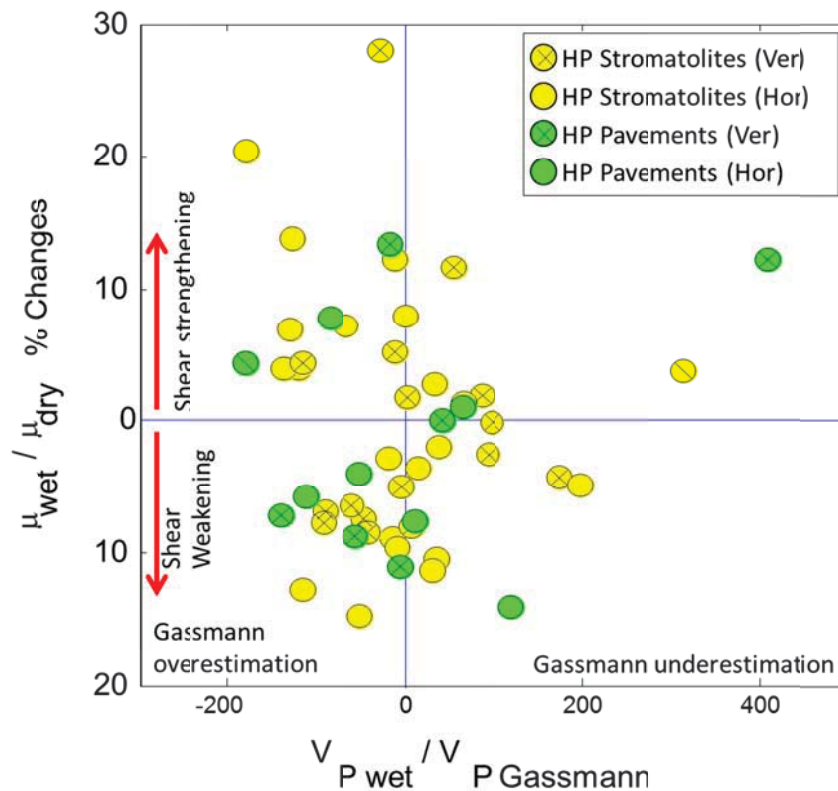


Figure 4.19: The changes in shear modulus and shear velocity with saturation under 20 MPa effective pressure. The cross-plot displays the changes of the ratio of wet and dry shear moduli in percentages and the ratio of measured saturated velocity to Gassmann's calculated velocity. In contrast one of the Gassmann's predictions postulating that fluid interaction does not change shear moduli, Hamelin Pool samples show both shear weakening and shear strengthening.

4.3.5. Mineralogy and Quartz Percentage

Porosity and pore geometry are the main controllers of acoustic velocities in carbonate rocks and there are several other factors such as saturation, fluid type, pressure and burial depth (Wang et al., 2001). Porosity differs with respect to lithology and diagenetic alterations and varies with the pore type (Eberli et al., 2003). However, in mixed systems the amount of quartz and other siliciclastic minerals influence the acoustic velocity (Kenter et al. 2002; Braaksma et al. 2003). The presence of quartz, which is diagenetically inert, precludes significant dissolution and reprecipitation, and results in lower seismic velocities of these carbonate rocks. The quartz percentage in each specimen was related to velocities and pore structures and confirms the effect of mineral variability on ultrasonic velocities (Anselmetti et al., 1997).

Apart from microbial precipitation, stromatolites trap and bind sediments in their depositional environment (Walter, 1972; Awramik and Margulis, 1974; Schopf, 1983; Krumbein, 1983; Burne and Moore, 1987; Grotzinger and Knoll, 1999; Altermann & Kazmierczak, 2003; Dupraz and Visscher, 2005; Reid, 2013). Additionally, stromatolites forming in the areas consisting of siliciclastic deposits trap detrital quartz in their structures (Lynn, 1990).

Along the western shoreline of Shark Bay, including Hamelin Pool, outcrops of the Peron (quartz) Sandstone are found, which overlies a calcilutite (type of limestone consisting of dominantly mud size carbonate grains), dolomite, and limestone. The eolian Peron Sandstone has a maximum thickness of 121 meters. There are red quartz outcrops on the surface while the subsurface

includes red (or red-brown) and yellow quartz (Logan et al., 1970). The subsurface Toolonga Calcilutite, the oldest rock in Shark Bay, is exposed intermittently on the eastern side of the Bay. The surface rocks in this region are white chalk and greenish-white calcareous mudstone, which have mostly recrystallized into calcrete with some flint nodules (Playford et al., 2013).

The quartz mineral distribution of stromatolite head samples is significantly influenced by the location. The stromatolites forming along the western shore of Hamelin Pool show higher percentages of quartz than on the eastern shoreline (Figure 4.20).

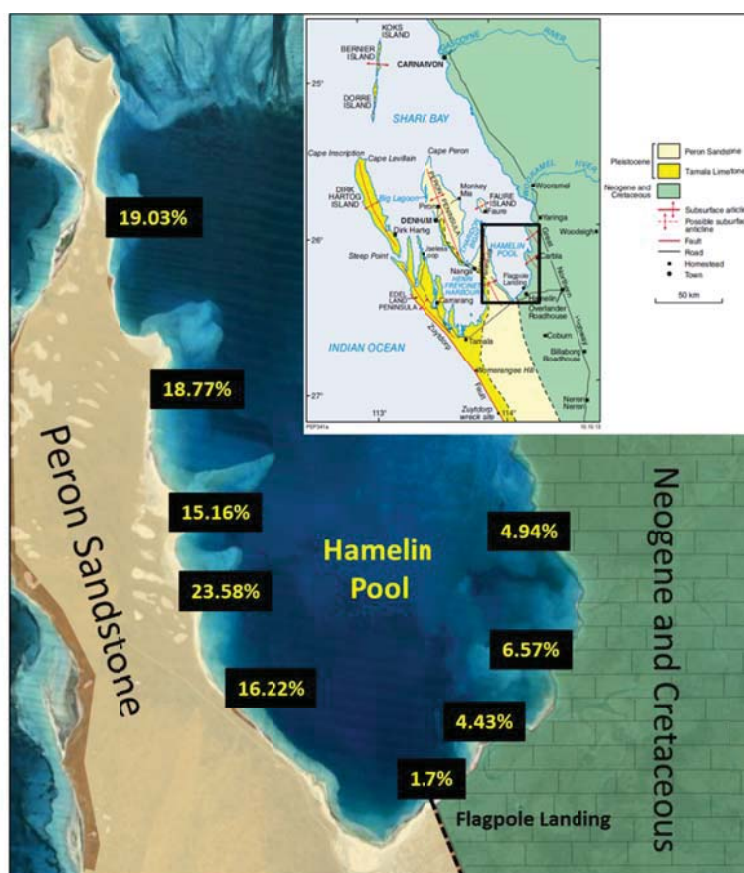


Figure 4.20: Quartz mineral distribution in stromatolite heads in Hamelin Pool, Shark Bay (Maps are adapted from Playford et al., 2013 and Google Earth)

Porosity, pore structure, and velocities are correlated with the quartz mineral percentages of each sample to analyze the effect of quartz on the velocities of the stromatolites and the pavements of Hamelin Pool. Figure 4.21 displays the correlation between porosity, velocity and varying quartz percentages. The cross-plot in Figure 4.20 shows that velocity of Hamelin Pool stromatolites and pavements do not show a clear trend as a function of quartz percentages. In order to evaluate the relationship of quartz and velocity in more detail, they are analyzed in combination with pore structure parameters in the following section.

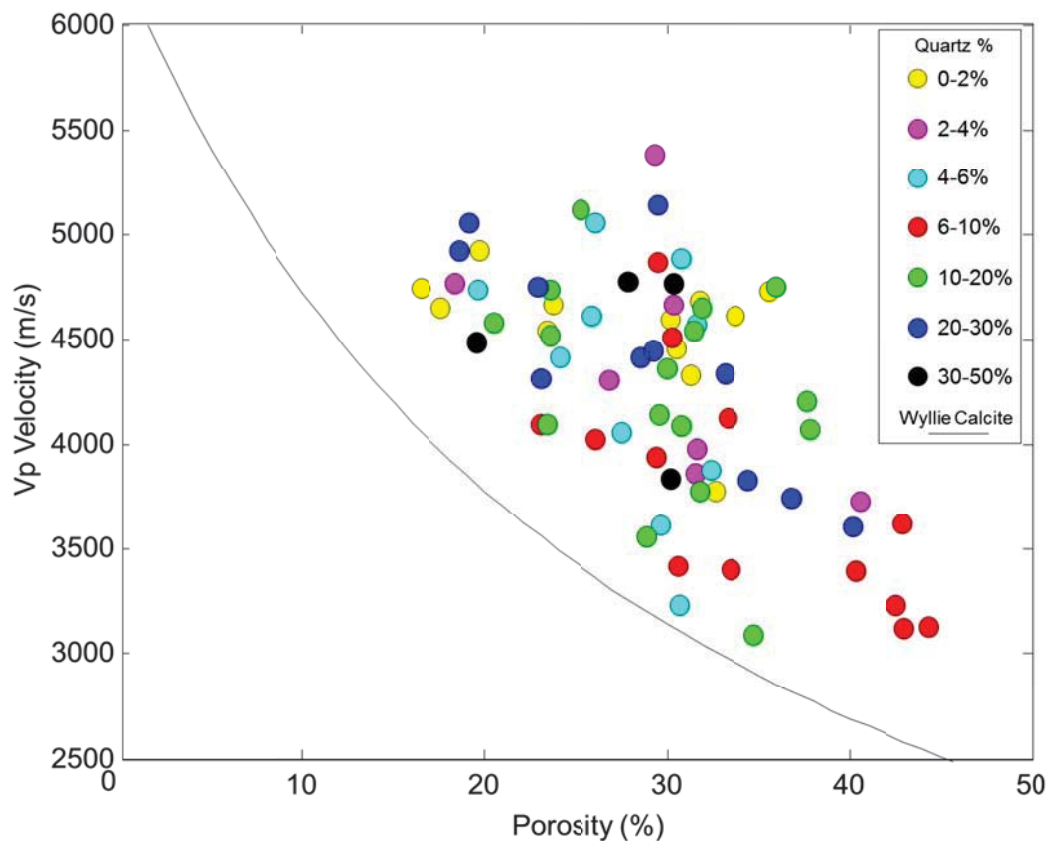


Figure 4.21: Velocity versus porosity with different quartz percentages in color. There is not a clear trend with quartz percentages in the cross-plot.

Figure 4.22 shows the DIA parameters for pore structure of Hamelin Pool stromatolites and pavements with velocities superimposed in color and ranges of different quartz percentages are indicated with different markers. There is not a clear trend between pore structures and quartz percentages. However, samples with less amount of quartz tend to have simpler and bigger pores relative to the samples containing more quartz.

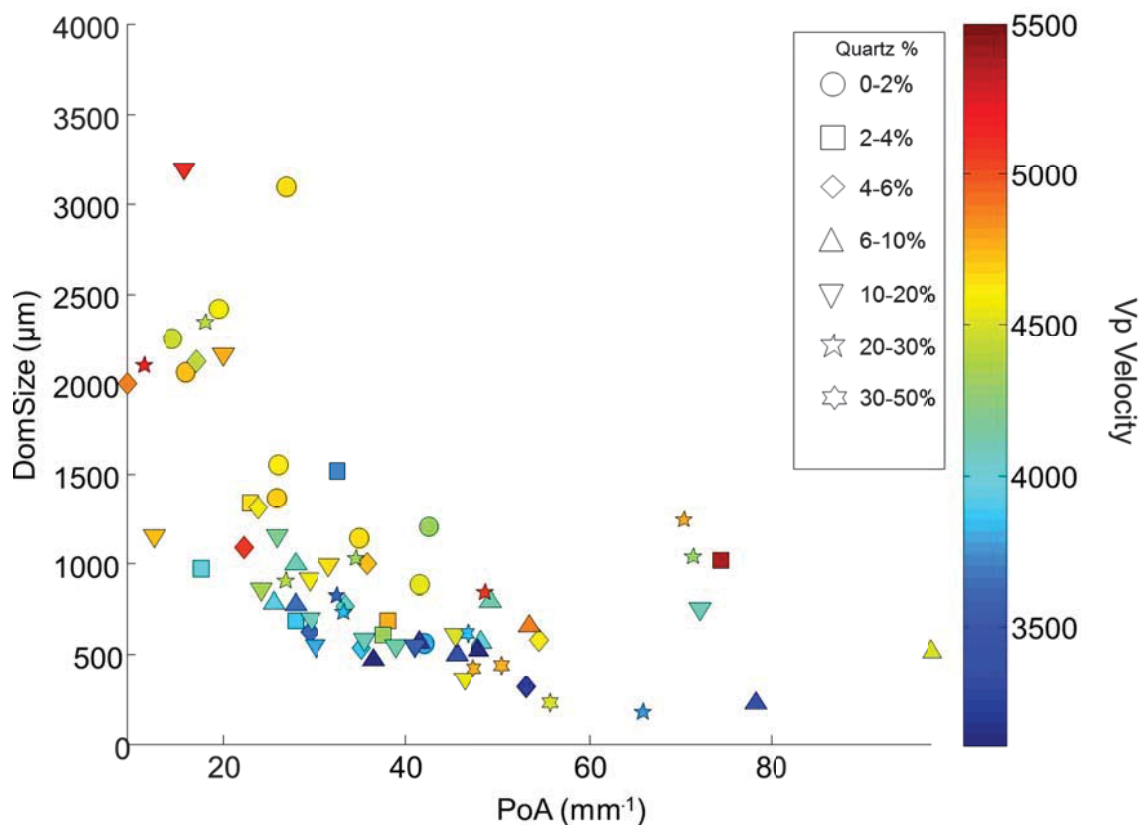


Figure 4.22: DomSize versus PaA with velocities in color bar and quartz percentages with different marker types. There is not a clear relationship but samples with less quartz percentages tend to have bigger pores and simpler pore structures.

In Hamelin Pool windblown quartz is admixed to the sediments and the stromatolites. This admixture is likely to have an influence on physical properties.

For example, quartz content in the excess of 7% influences the acoustic velocity of carbonates (Kenter et al. 2002).

Three different scenarios are observed in the Hamelin Pool data set. First, samples consisting of similar compressional acoustic velocities and porosities but with different amount of quartz percentages are present (Figure 4.23 and 4.24). The other controlling factors such as saturation, fluid type and pressure are the same for each specimen, thus they are not regarded as effective controlling factors. Because quartz lowers the velocity in carbonates (Kenter et al., 2002), the sample with more quartz is expected to have a slower velocity. Yet in these samples the velocity is similar, indicating that other factors compensate for the lowering effect of quartz. What is different in these samples is the pore geometry (Figure 4.22 and 4.23, bottom). Two samples are displayed to illustrate the difference. In samples with high quartz content (19.03%) the DomSize is larger than in the sample with equal velocity but less quartz (1.7%) (Figure 4.22). In the other sample, the sample with the higher quartz content has a smaller PoA, indicating a less complicated pore structure (Figure 4.23 bottom). As shown above, samples with large simple pores are faster than samples with small, complicated pores (Figure 4.13). Obviously the velocity increasing effect of the pore geometry compensates for the velocity lowering effect of the quartz admixture in both samples.

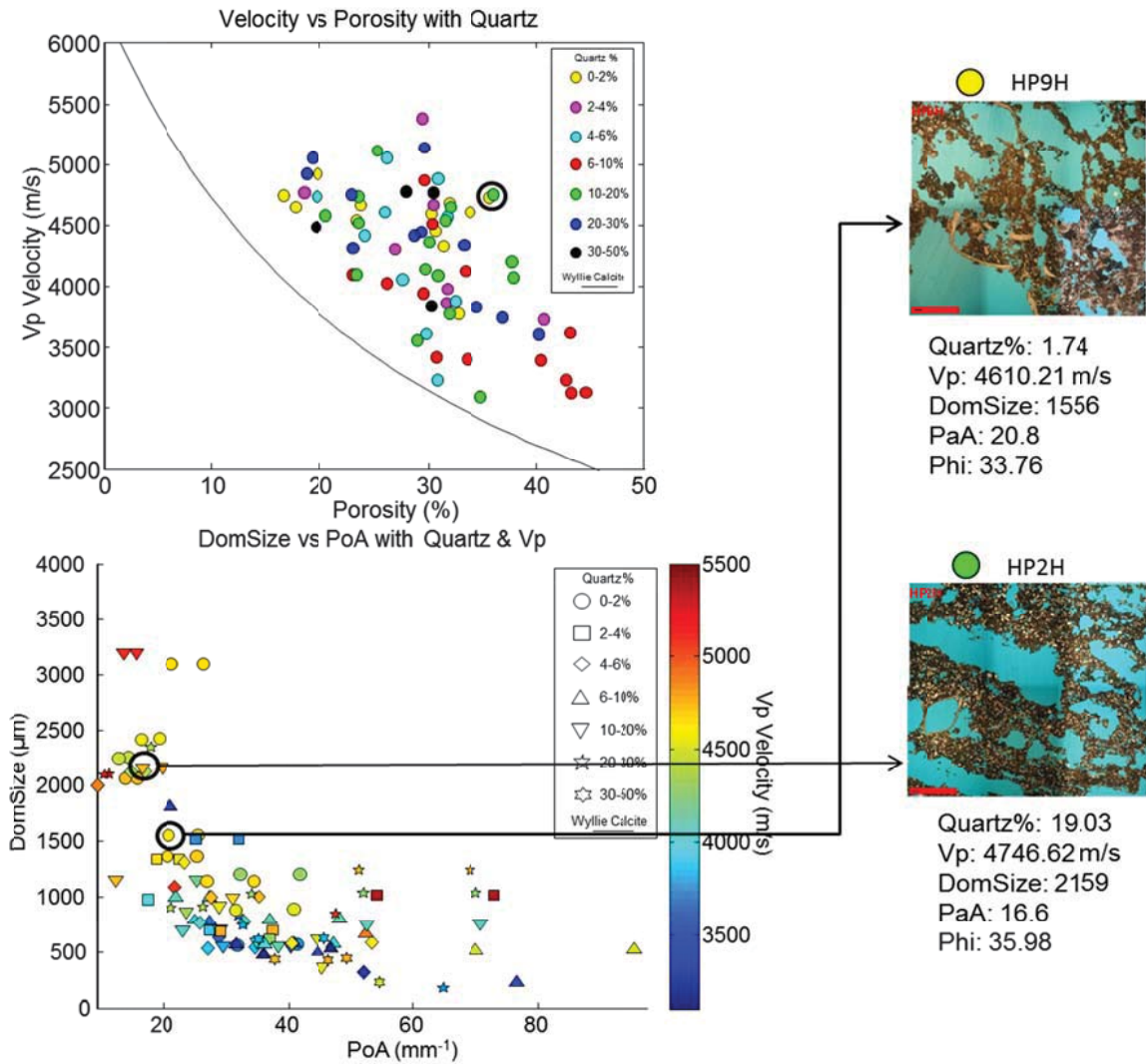


Figure 4.23: Correlation of quartz by using pore structure parameters over velocity and porosity data. The samples that have similar velocities and porosity are selected to compare. The sample with higher amount of quartz (top figure) which is expected to have slower ultrasonic velocity shows larger DomSize and lower PoA (bottom figure) which explains the similar velocities.

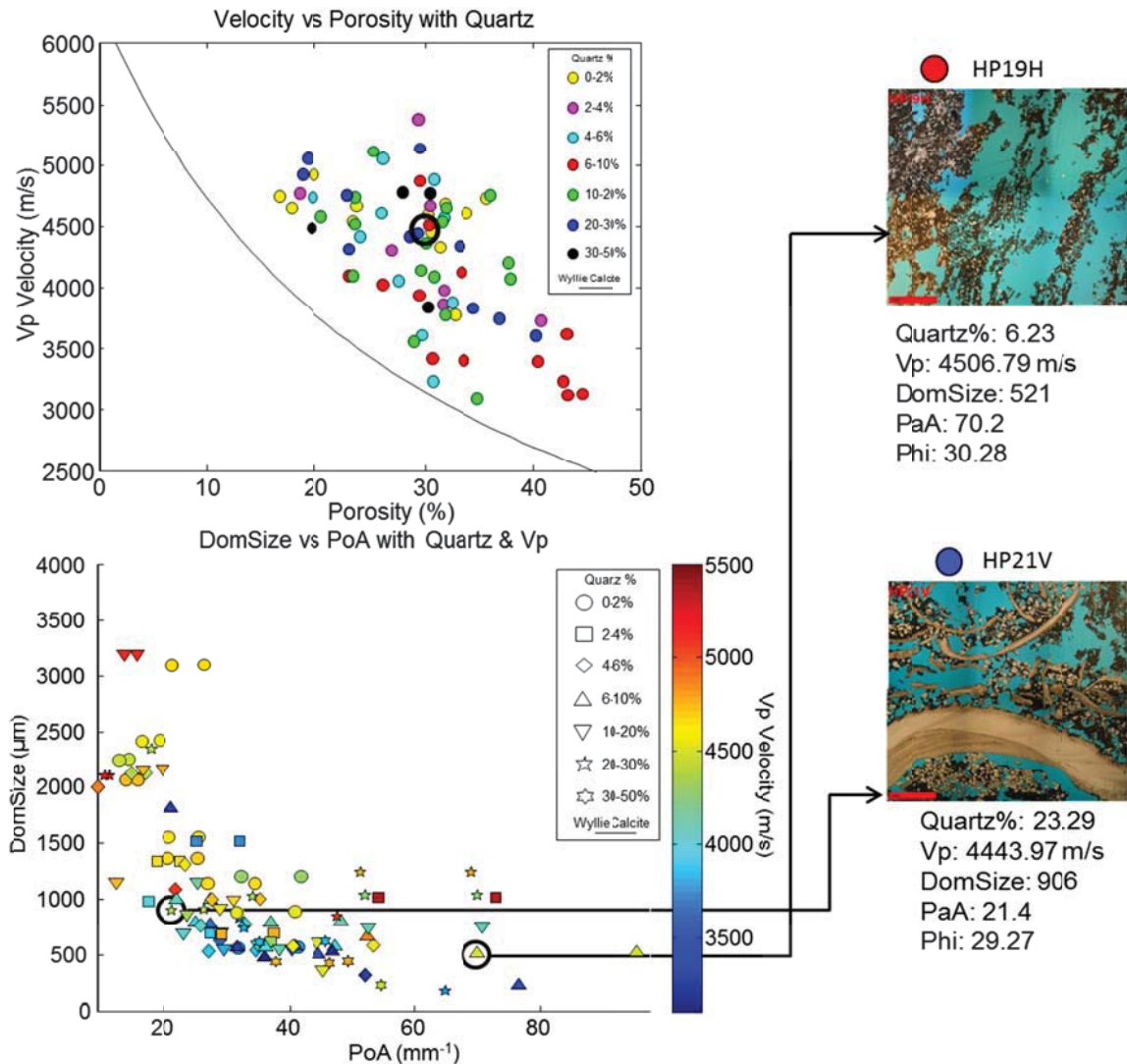


Figure 4.24: Correlation of quartz by using pore structure parameters over velocity and porosity data. The samples that have similar velocities and porosity are selected to compare. The sample with higher amount of quartz which is expected to have slower ultrasonic velocity shows larger (top figure) DomSize and lower PoA which (bottom figure) explains the similar velocities.

In the second subsample data set two samples have similar porosity and quartz contents but different velocity. In these samples, the velocity variation occurs by the various pore geometry of the samples (Figure 4.25 and Figure 4.26). For instance, the sample with 3770.72 m/s compressional velocity has a similar quartz percentage and porosity with the other sample that has a

compressional velocity of 4674.95 m/s which is expected to have less quartz content. However, this sample with 1.54% quartz has a larger DomSize and lower PoA relative to the other sample. Therefore, the velocity difference in with similar porosity and quartz content can be explained by the variation of the pore geometry.

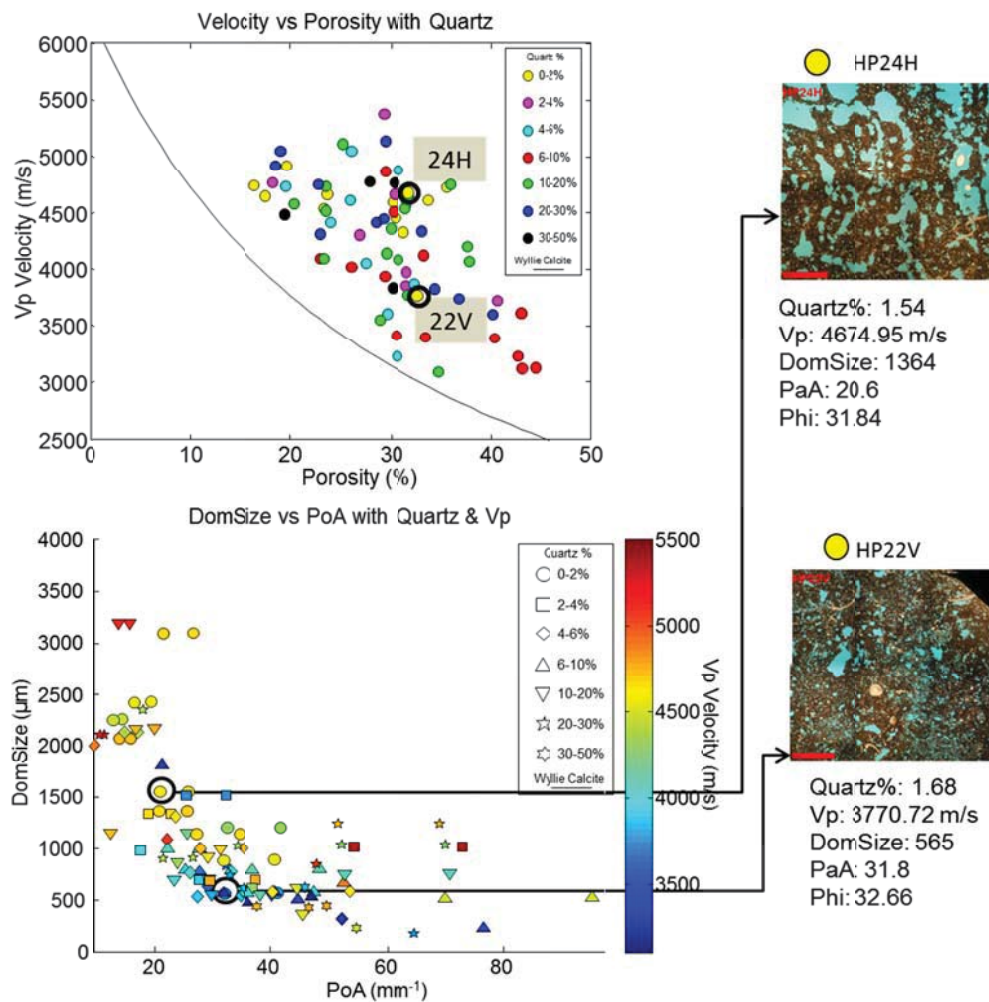


Figure 4.25: Correlation of quartz by using pore structure parameters over velocity and porosity data. The samples that have similar quartz percentages and porosity but different velocities were picked. The sample with higher ultrasonic velocity (top figure) which is expected to have lower quartz content shows larger DomSize and lower PoA (bottom figure) which explains the velocity deviation.

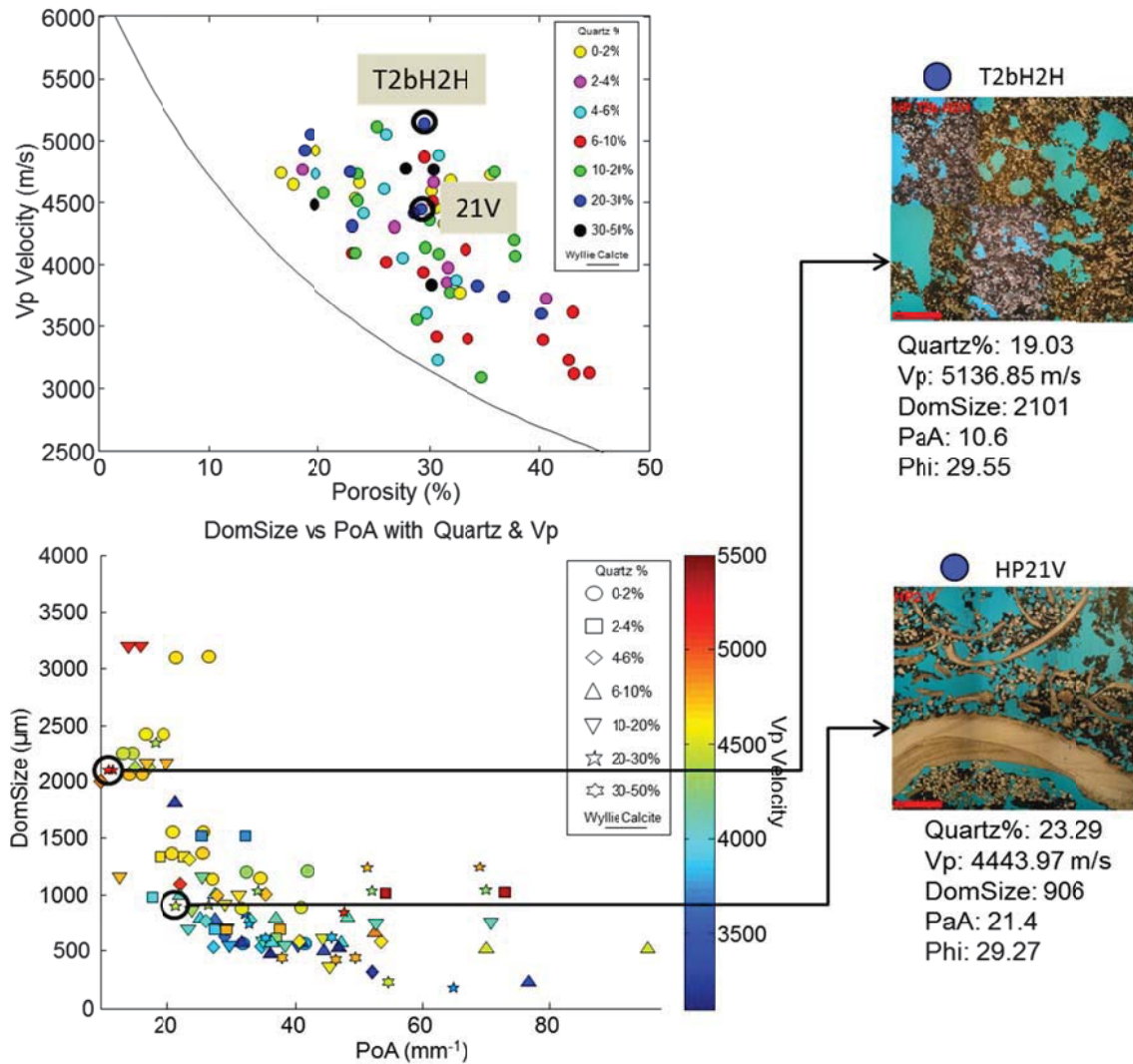


Figure 4.26: Correlation of quartz by using pore structure parameters over velocity and porosity data. The samples that have similar quartz percentages and porosity but different velocities were picked. The sample with higher ultrasonic velocity (top figure) which is expected to have lower quartz content shows larger DomSize and lower PoA (bottom figure) which explains the velocity deviation.

In the third scenario samples with similar pore structure and similar amount of porosity shows a clear decreasing gradient in velocities with respect to quartz content. In Figure 4.27, the circled samples have similar porosity (on the left) and similar pore structures (on the right). Since the other controlling factors on velocity such as saturation, fluid type and pressures are the same for all

samples, quartz content is attributed as the only controlling effect on velocities. The average gradient is -10.89 with a range from -11.86 to -8.005. The standard deviation is 1.671. For example by using the average slope between the lines, 10% quartz causes 108.9 m/s decrease in velocity values.

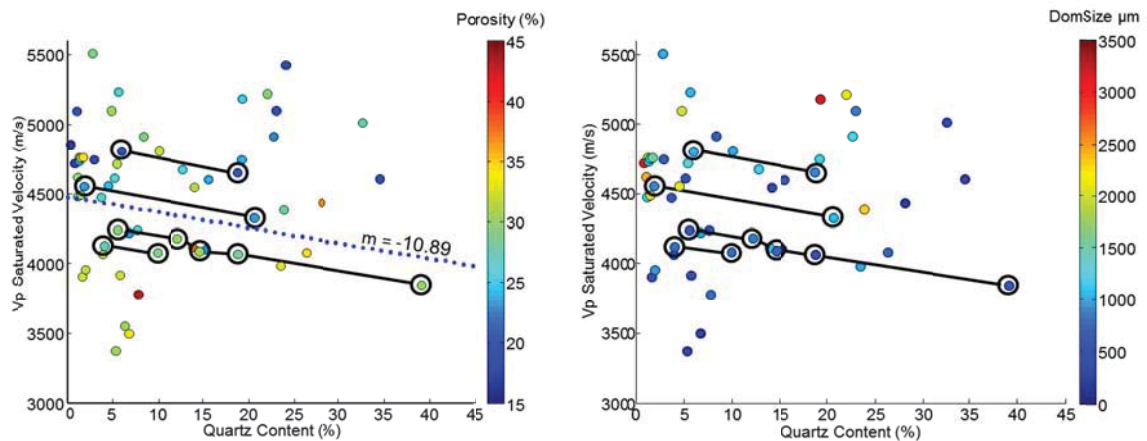


Figure 4.27: Velocity versus quartz content with similar porosity and DomSize. Quartz content is the controlling effect on ultrasonic velocities.

4.3.6. Summary

Hamelin Pools stromatolites and pavements are dominated by simple pores with variable pore sizes. There is no significant anisotropy and both vertical and horizontal core plugs show very similar petrophysical properties. The stromatolites forming in this restrictive area show a porosity range from 16% to 46%, while the porosity of pavements ranges from 18% to 44%. Hamelin Pool stromatolite permeability ranges from 570 mD to 9000 mD, while pavements range from 7 mD to 5140 mD. These values are almost a magnitude higher those of the reference data set. This indicates that permeability in Hamelin Pool samples is independent of porosity. Neither porosity nor permeability show a

clear trend with water depth. A weak trend of decreasing porosity can be observed with increasing distance from shore.

Ultrasonic velocity measurements of Hamelin Pool stromatolites and pavements are all higher than the Wyllie time-average equation for calcite would predict. These samples show a large variation of velocity at any given porosity. They also show a large range of porosity at any given velocity. V_p/V_s ratios of Hamelin Pool stromatolites and pavements range from 1.5 to 1.9. The low values of V_p/V_s ratio are due to the presence of high amount of quartz. The velocity ranges from 3903 m/s to 5504 m/s in stromatolites while it ranges from 3369 m/s to 5424 m/s in pavements. Horizontal core plugs show relatively faster ultrasonic velocities. Shear moduli of Hamelin Pool stromatolites and pavements change with fluid interaction causing shear strengthening and shear weakening.

The large proportion of quartz found in some of our samples during mineralogical determination experiments can be explained but the fact that stromatolites trap and bind sediments present in their close environment, and that large amounts of quartz are present in the eastern shore of Hamelin Pool originating from the nearby Peron Sandstone.

Lastly, ultrasonic velocities show a clear decrease with amount of quartz. However, this correlation between quartz content with ultrasonic velocities can only be observed when comparing samples of similar pore geometry. Otherwise, that effect of pore geometry on velocity overpowers the effect of the quartz grains.

4.3.7. Implications for Fluid Substitution and Seismic Inversion

The Hamelin Pool data reveal that stromatolites and pavements have large velocity variations at any given porosity. This becomes important when seismic inversion is attempted. Most seismic inversion techniques involve a single relationship between porosity and acoustic impedance. As shown by Eberli et al. (2003) and confirmed by the data in the present study, carbonates show a high variability of velocity at any given porosity, and implicitly, a high variability of porosity values for a given velocity. Hence, the results of a seismic inversion, assuming a single relationship between porosity and velocity, carry a high degree of uncertainty.

Hamelin Pool stromatolites and pavements show both shear weakening and shear strengthening during interaction with brine. Gassmann's fluid substitution equations allow us to predict from a velocity measured on a rock containing a known fluid the hypothetical velocity of this rock if it would contain a different fluid. This method is often used to generate synthetic seismic gathers for a given rock formation with a variety of different pore fluids. These sets of gathers can then be used by an interpreter for comparison with the observed response of amplitude variation with offset on actual measured seismic data. The studied microbialites from Hamelin Pool with their strong shear weakening and strengthening violate the assumption of constant shear moduli during saturation changes. This finding corroborates results by Baechle et al. (2009) on carbonates.

4.4. Electrical Resistivity

4.4.1. Background

Electrical resistivity is measured routinely in downhole logs because it allows for calculation of the Formation Factor `F` and the cementation factor `m` of the reservoirs through the Archie's equation, $F = \phi^{-m}$ (where ϕ is porosity). The cementation factor, m , is further used to calculate hydrocarbon/water saturation.

$$S_w = [\phi^{-m} * (R_w / R_t)]^{(1/n)} \quad (6)$$

Where; S_w = Water saturation, R_t = Measured formation resistivity, R_w = Resistivity of brine, Φ = Porosity, m = Cementation Factor and, n = Saturation exponent.

If an `m` value of 2, for example, predicts a 70% of hydrocarbon saturation in a given reservoir, increasing the m value from 2 to 3 or 4 may reduce the predicted hydrocarbon saturations (Focke and Munn, 1987; Lucia, 1999).

Laboratory studies of resistivity are not often performed, especially for carbonates. Verwer et al. (2010) used seventy-one carbonate plugs including eleven Bahamian stromatolites in a comprehensive resistivity study in carbonates (Figure 4.28). In his data set `m` was varying between 1.72 and 4.16. It is well known that large variation of `m` is characteristic in carbonates and makes saturation estimates in carbonates difficult. In the same data set, the cementation factor of the Bahamian stromatolites displayed only a narrow range from 2.1 to

2.6, which would make saturation prediction more accurate (Focke and Munn, 1987; Lucia, 1999).

$$F = \phi^{-m}$$

Where,

$$F = R_o / R_w$$

ϕ = porosity

F = formation resistivity factor

R_o = resistivity of fully saturated rock (100% saturation)

R_w = resistivity of pore fluid

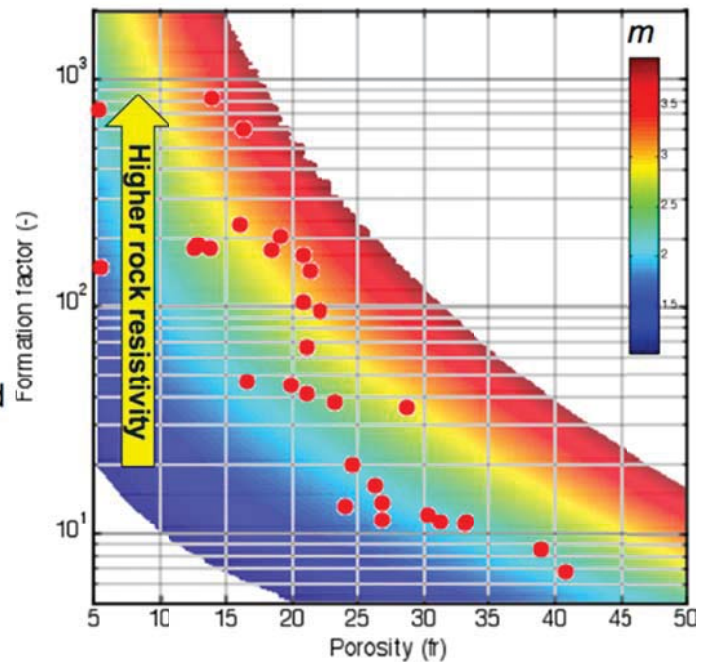


Figure 4.28: Formation factor 'F' versus Porosity with the color coding of the cementation factor 'm'. An increase formation factor increases the resistivity in these carbonates (Verwer et al., 2011).

Verwer et al. (2011) document a relationship between pore structure parameters and cementation factor 'm' (Figure 4.29). Samples with small dominant pore sizes and high perimeter over area are dominated by pore structures more complex than samples with large pore sizes and low perimeter over area. Grainstones with large pores tend to have large DomSize and low PoA values, and the opposite is true for rocks with a large amount of microporosity, small DomSize and high PoA. Rocks that have vuggy or moldic porosity have high electrical resistivity because they often contain insufficiently connected pore structures. Similarly, it is also observed that rocks with large and

simple pores tend to give high resistivity values. However, rocks consisting of large amount of microporosity with small and complex pores are the less resistant in respect to the others since the high amount of pores and connections between pores reduce the electrical resistivity (Verwer et al., 2011). The cross-plot in Figure 4.19 shows that there is a clear trend relating pore structure to Cementation Factor. Increase in DomSize and decrease in PoA shows increasing Cementation Factors.

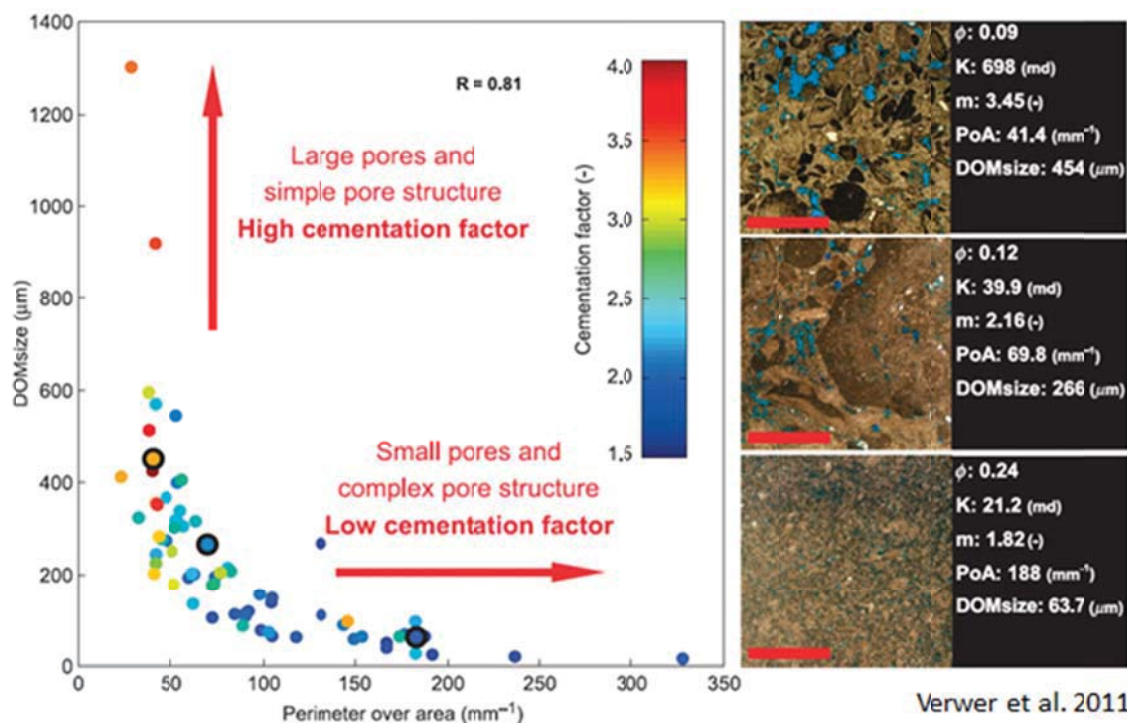


Figure 4.29: Pore structure parameters (Perimeter over area versus Dominant pore size) with cementation factor in color. The selected data points are shown with their corresponding thin sections on the right (adopted from Verwer et al., 2011).

4.4.2. Resistivity of Hamelin Pool Stromatolites and Pavements

Electrical resistivity was measured on 64 Hamelin Pool stromatolites and pavements plugs. The Cementation Factor of stromatolite samples ranges from

2.0 to 3.71 while “m” in the pavement samples ranges from 2.0 to 3.1 (Figure 4.30). The Formation Factor of Hamelin Pool pavements ranges from 9.7 to 321.1 while the pavements show a range from 8.8 to 114.3.

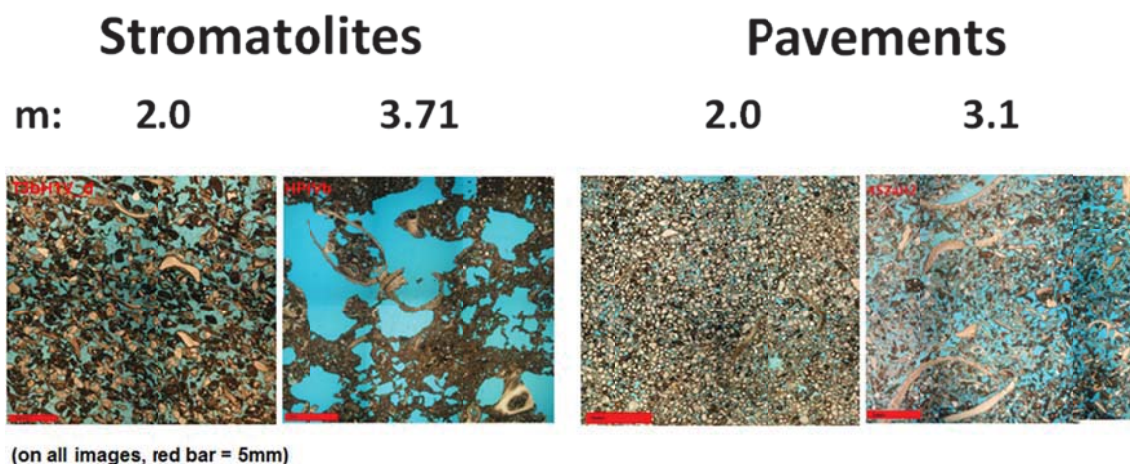


Figure 4.30: The maximum and minimum cementation factor values of stromatolites (on the left) and pavements (on the right) with their corresponding thin sections.

Comparing the samples from Hamelin Pool to Verwer et al.’s (2011) resistivity diagram, Hamelin Pool stromatolites and pavements have lower electrical resistivity values than the reference data (Figure 4.31). There is no significant anisotropy between vertically and horizontally drilled core plugs. Water saturation calculations with Archie’s equation with the known ranges of those microbialites might contribute to make more precise hydrocarbon-water predictions when comparing to the other carbonates.

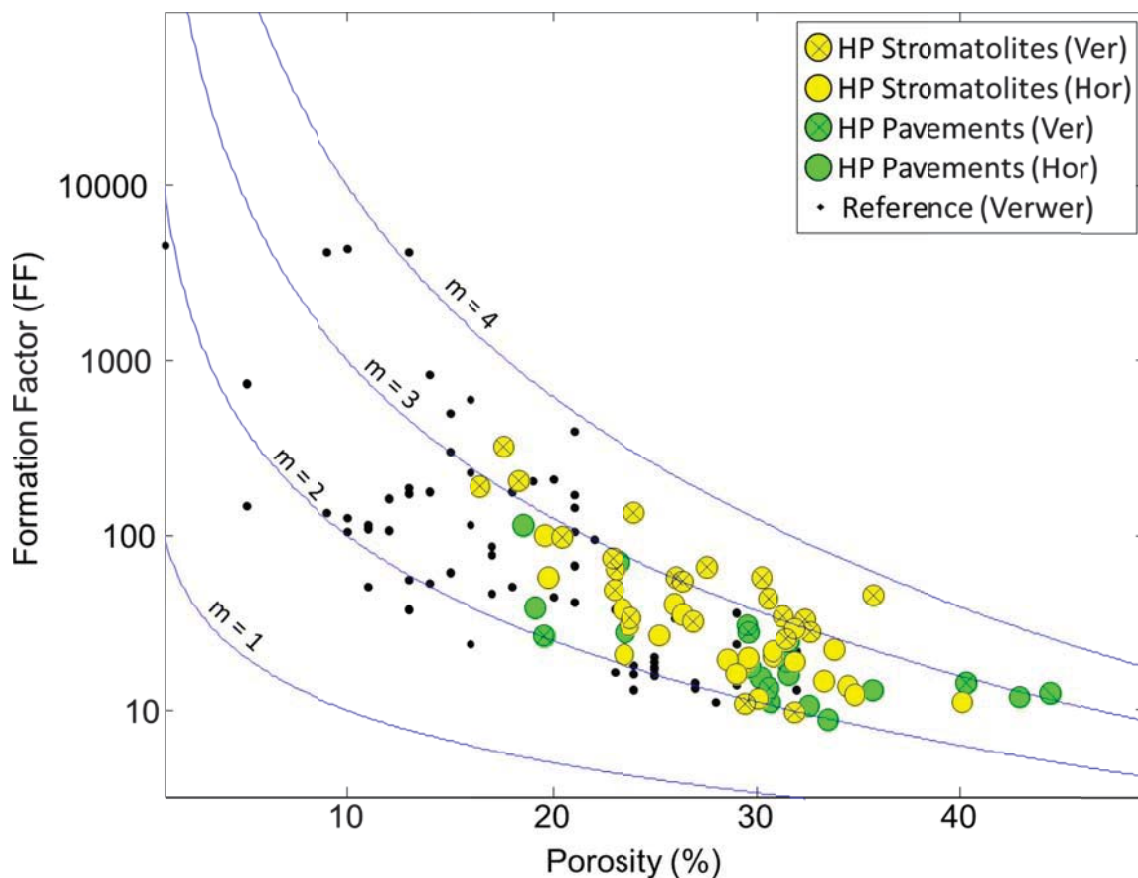


Figure 4.31: Formation factor versus porosity of Hamelin Pool stromatolites and pavements with the cementation factor 'm' values.

In order to test the relationship of cementation factor with pore structure the DIA parameters are color-coded with "m" (Figure 4.32). The following trend is discernable. Samples with large DomSize and small PoA values tend to have higher Cementation Factor, while samples with small and complex pore network have low Cementation Factors.

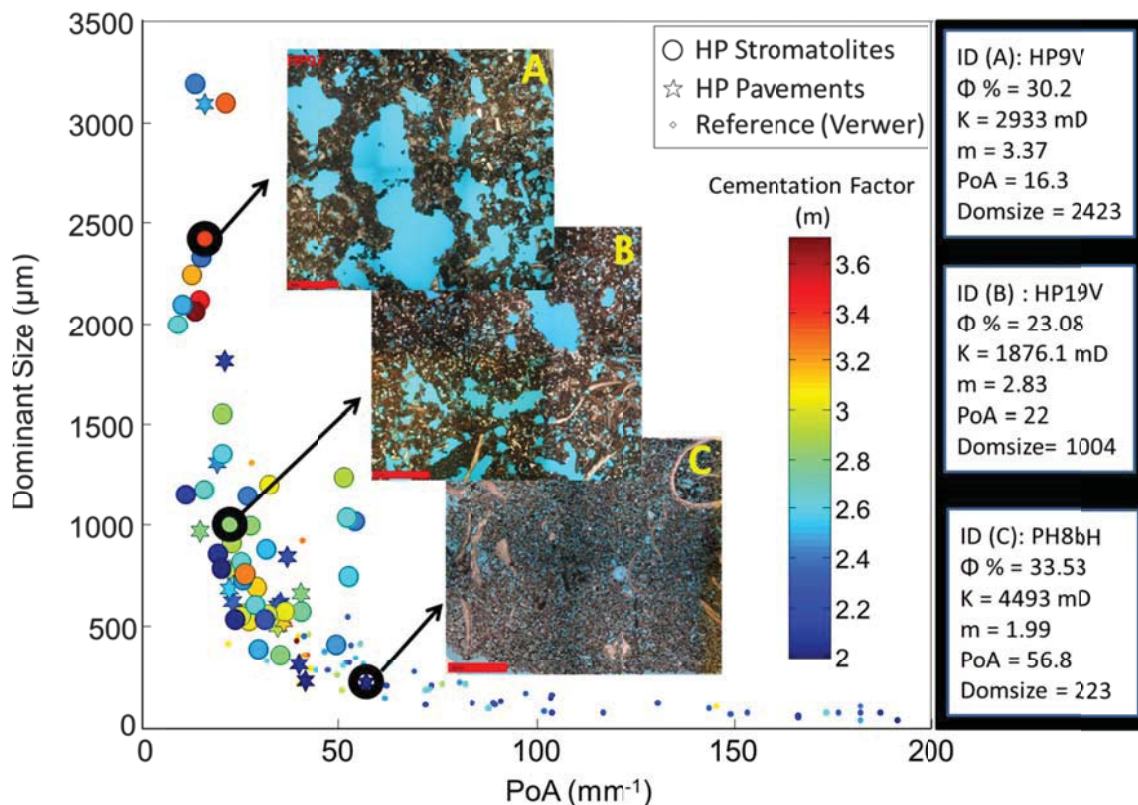


Figure 4.32: DIA parameters PoA versus $DominantSize$ with cementation factor in color. The selected data points are shown with their corresponding thin sections and the physical properties on the right.

For permeability the connectivity of the pores is the most important property for the fluid flow through rocks. Thus, the pore structure has a controlling effect on permeability in carbonates (Lucia, 1995; Weger et al., 2009). Verwer et al., (2011) shows that samples with high permeability values have large, simple pores with a high Cementation Factor (Figure 4.33). High values of cementation factor are also displayed in low permeable rocks with moldic porosities since the pores display poor connection. Overall, decrease in permeability shows a slight trend with decreasing Cementation Factors.

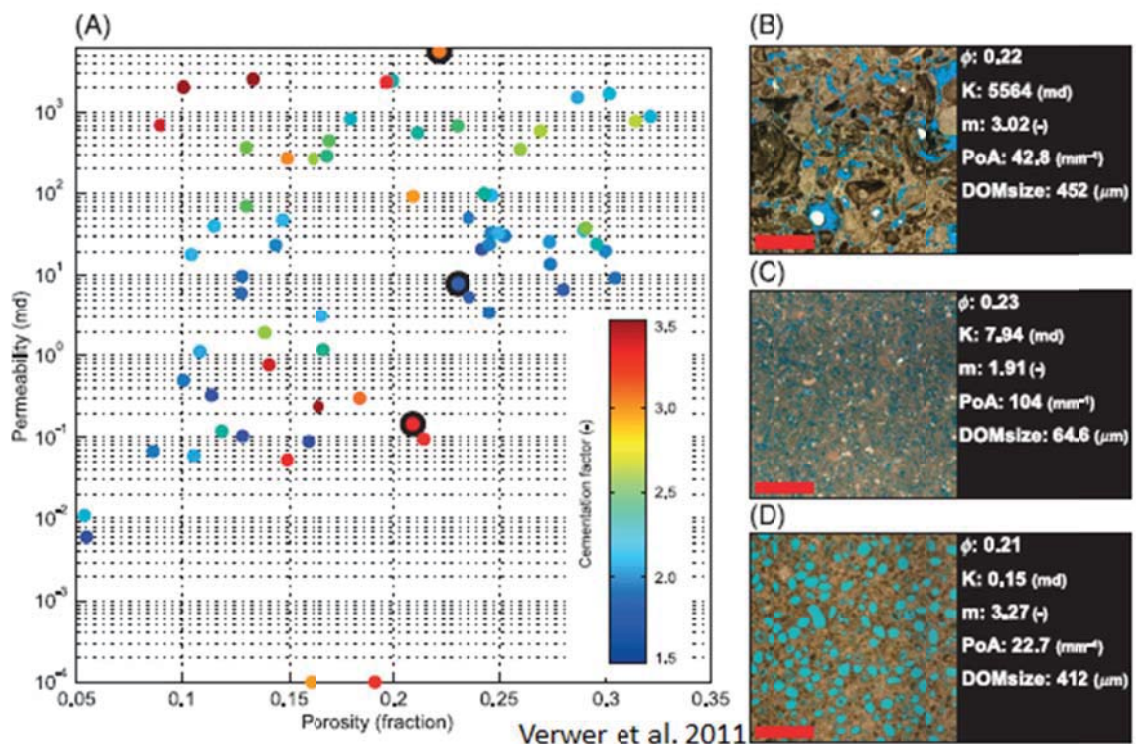


Figure 4.33: This cross-plot shows permeability versus porosity with cementation factor in color. The trend of decreasing cementation factor with increasing permeability is observed in samples with similar porosity but different pore types and DIA parameters (from Verwer et al., 2011)

In order to investigate the relationship between permeability and Cementation Factor in stromatolites and pavements from Hamelin Pool, Cementation Factors are superimposed in color on the permeability versus porosity cross-plot (Figure 4.34). Our microbialite samples display a trend of decreasing permeability with increasing “m”. For example, in stromatolites the sample with the lowest cementation factor of 1.96 has 8139 mD permeability while the sample with the highest cementation factor of 3.61 has 2900 mD permeability. Similarly, in pavements the sample with the lowest cementation factor of 1.99 has 4493 mD permeability while the sample with the highest cementation factor of 3.12 has

4420 mD permeability. The pavement sample with the lowest amount of permeability of 7.46 mD has a cementation factor of 2.93. The microbilitates of the Hamelin Pool show the opposite relationship to what Verwer et al. (2011) found. The rocks that Verwer et al. (2011) used had almost a magnitude lower permeability values, which might be the reason of this reverse relationship.

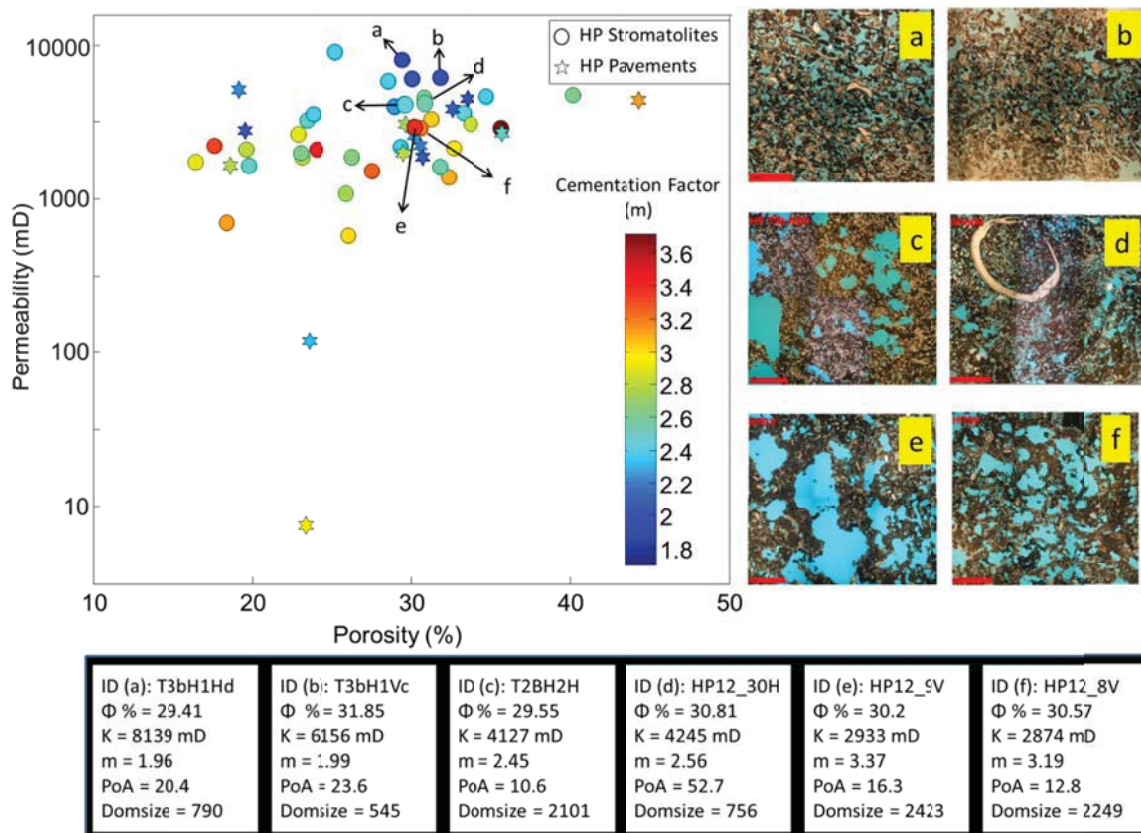


Figure 4.34: This cross-plot shows permeability versus porosity with cementation factor in color. Both stromatolites and pavements display a trend of decreasing permeability with increasing “m”. Besides, pore structure becomes simpler with big pores with decreasing permeability.

If the samples are color coded according to their micro and mesofabrics and displayed in a cross-plot of formation factor and porosity, no trend is

observed (Figure 4.35). Thus, it can be concluded that defined micro and mesofabrics do not correlate to electrical resistivity.

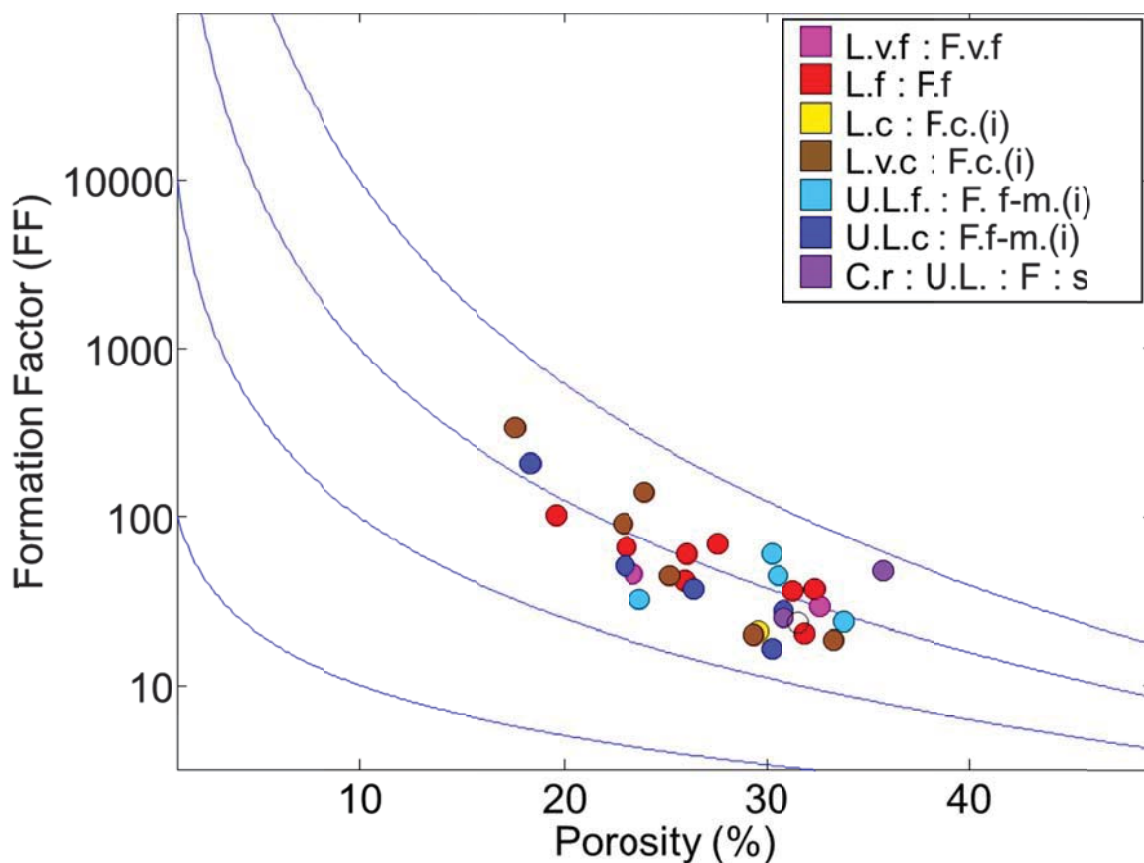


Figure 4.35: Formation factor versus porosity of Hamelin Pool stromatolites and pavements in respect to meso/microfabric classification (L: laminated, F: fenestrae, U: unlaminated, C: crust, S: serpulid, i: irregular, f: fine, v.f: very fine, f-m: fine to medium, c: coarse).

4.4.3. Summary

Sixty-four electrical resistivity measurements show that Hamelin Pool stromatolites and pavements have relatively low resistivity values with respect to the reference carbonate data (Figure 4.31). The cementation factors range from 2.0 to 3.71 in stromatolites and from 2.0 to 3.1 in pavements. The formation

factors display a range from 9.7 to 321.1 in stromatolites while the pavements show a range from 8.8 to 114.3. The samples do not show significant resistivity anisotropy. Cementation factors do correlate to pore structure. Samples with simple and big pores show high cementation factors while samples with more complex and smaller pores display low cementation factors (Figure 4.32). In both stromatolites and pavements, increasing permeability decreases the cementation factors (Figure 4.34). No trend is observed between internal meso/microfabric classification and resistivity values (Figure 4.35).

CHAPTER 5. DISCUSSION AND COMPARISON

5.1. Background

In this chapter, the porosity, permeability, digital image analysis (DIA), ultrasonic velocity, electrical resistivity measurements of Hamelin Pool stromatolites and pavements are compared to data from other microbialites. These data are 14 samples from the modern open marine stromatolites from Exuma Sound, Bahamas (about at the point Pl.1) and 11 samples from hardgrounds in the Tongue of The Ocean (Figure 5.1).

5.1.1. Background of Bahamian Stromatolites

Bahamian high-relief stromatolites form in Exuma Sound, in a high-energy environment under normal sea-water salinity. These Bahamian stromatolites were first described by Dravis (1983). Later, "giant" subtidal stromatolites near Lee Stocking Island, Exuma Cays, Bahamas were discovered by Dill et al. (1986) (Figure 5.2). Many other locations with stromatolites have been discovered in the Exuma Cays, Bahamas since (Figure 5.1) (Reid and Browne, 1991; Reid et al., 1995).

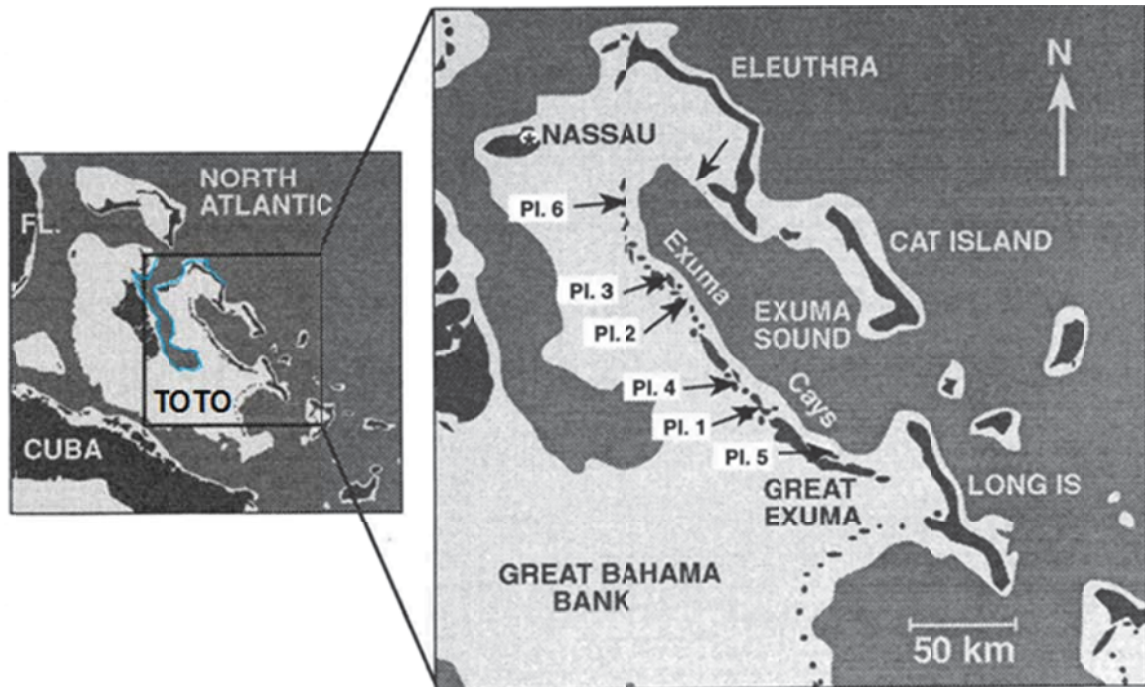


Figure 5.1: Distribution of stromatolites in Exuma Cays, Bahamas. The arrows having numbers point the locations where stromatolites form and the arrow on the northeast margin of Exuma Sound is the place where Dravis (1983) first recognized the stromatolites, adapted and from Reid (1995).

Some of the Exuma Cays' stromatolites are located in the intertidal zone, while most of Bahamian stromatolites are forming in subtidal zones such as tidal channels and sandy embayments (Dravis, 1983; Griffin, 1988; Dill, 1991; Browne, 1993; Reid et al., 1995; MacIntyre et al., 1996)



Figure 5.2: “Giant” stromatolites in Exuma Sound, Bahamas (Dill et al., 1986).

5.1.2. Tongue of The Ocean Hardgrounds

Tongue of The Ocean (TOTO), is a deep oceanic embayment in the Bahamas which separates Andros Island from New Providence. The bottom water depths range from 850 meters to 3500 meters (Schalk 1946; Hurley and Shepard, 1964; Shepard and Dill, 1966). In the southern part of TOTO, where the samples were collected, giant submarine dunes form all along the (Dill et al., 1989). In this area, the common components of sediments are ooid sands, *Halimeda* plates and pelleted muds (Crevello and Schlager, 1979). The sediments in TOTO and Exumas are undergoing submarine cementation, thus forming the subtidal marine hardgrounds. (Shinn and Ginsburg, 1964; Taft et al., 1968; Shinn, 1983).

In this study, the hardground samples were collected from the southern margin of TOTO.



Figure 5.3: The map of Bahamas and Tongue of The Ocean. The hardground samples were collected from the south margin of TOTO where giant subtidal dunes form (Adapted from Google Earth).

5.2. Pore Structure of the Bahamian Microbialites

Stromatolites and pavements of Hamelin Pool are dominated by simple pore structures and a large variety of pore sizes whereas the Bahamian stromatolites show overall more complex pore structures. In Figure 5.4 the DIA parameters of Hamelin Pool and the Bahamas are plotted for comparison. For of Hamelin Pool stromatolites, PoA ranges from 9.3 mm^{-1} to 70 mm^{-1} and for pavements it ranges from 15 mm^{-1} to 57 mm^{-1} . In the Bahamian stromatolites, PoA more complex geometries indicated by higher values of PoA ranging from 32 mm^{-1} to 82 mm^{-1} while TOTO hardgrounds range from 18 mm^{-1} to 31 mm^{-1} , demonstrating overall simpler pores than Hamelin Pool pavements.

With respect to pore size, Hamelin Pool stromatolite DomSize's ranges from 175 μm to 3193 μm for while pavements only range from 140 μm to 3093 μm . The Bahamian samples are dominated by much smaller pores indicated by DomSize values ranging from 180 μm to 448 μm for stromatolites and from 453 μm to 963 μm for TOTO hardground samples.

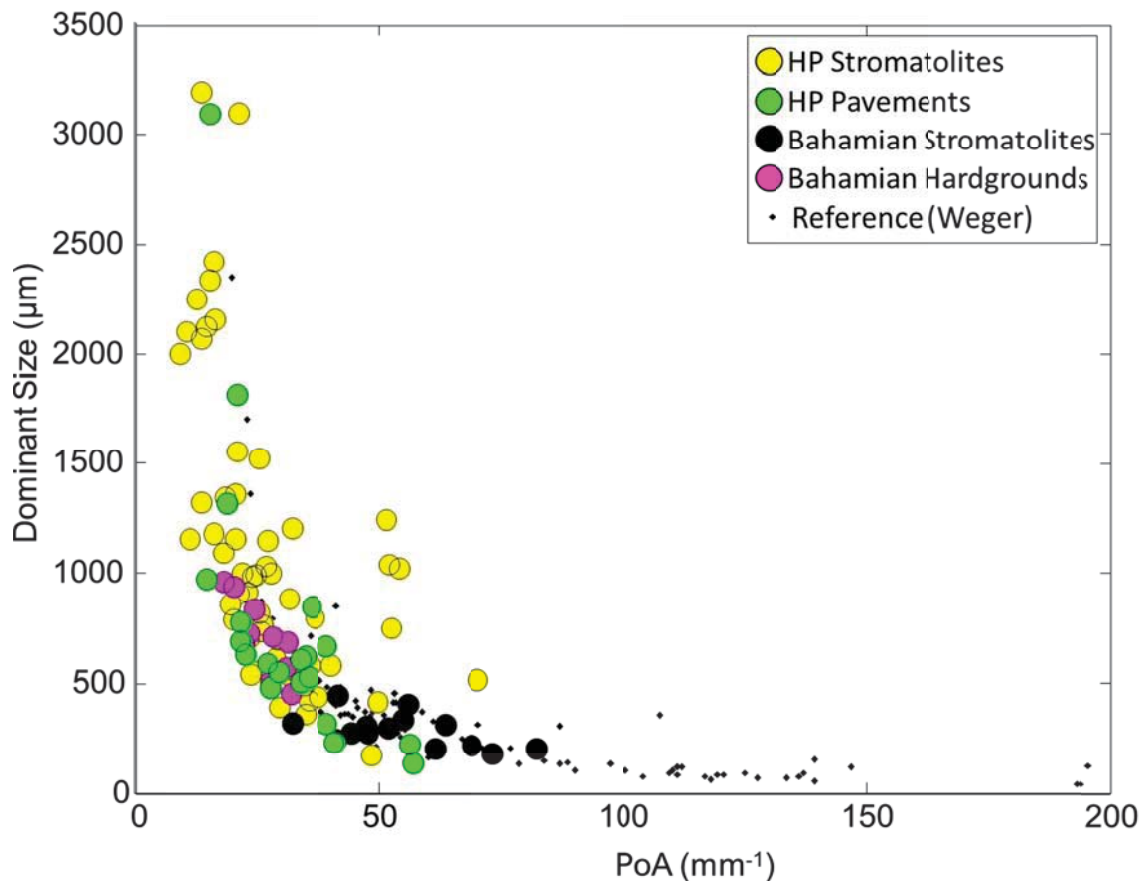


Figure 5.4: Pore structure comparison between Hamelin Pool stromatolites, pavements, Bahamian stromatolites and hardgrounds. Hamelin Pool stromatolites and pavements have simple pores with variable sizes. However, Bahamian stromatolites display more complex structures while the hardgrounds have a narrow range of both PoA and DomSize.

5.3. Porosity and Permeability

Bahamian stromatolites and pavements have a porosity range from 13% to 41% while their permeability values range from 70 mD to 1700 mD. The Hamelin Pool stromatolites and pavements range from 7 mD to 9000 mD. Both data sets have high permeability and a large range of porosity but Hamelin Pool stromatolites and pavements have a wider porosity range and much higher values of permeability than both Bahamian stromatolites and hardgrounds (Figure 5.5). Moreover, in comparison to the reference data both data sets have remarkably high and relatively consistent permeability. The porosities in stromatolites, pavements, and hardgrounds cover a large range of porosity compared to the reference data.

The data from Weger et al. 2009 shows that small values of DomSize and high values of PoA result in lower permeability values. A slight trend of increasing permeability with increasing DomSize is observed in Hamelin Pool stromatolites and pavements (Figure 5.6, left). In the Bahamian stromatolites and hardgrounds slightly higher values of permeability are seen in samples with increased DomSize and decreased PoA (Figure 5.6, right).

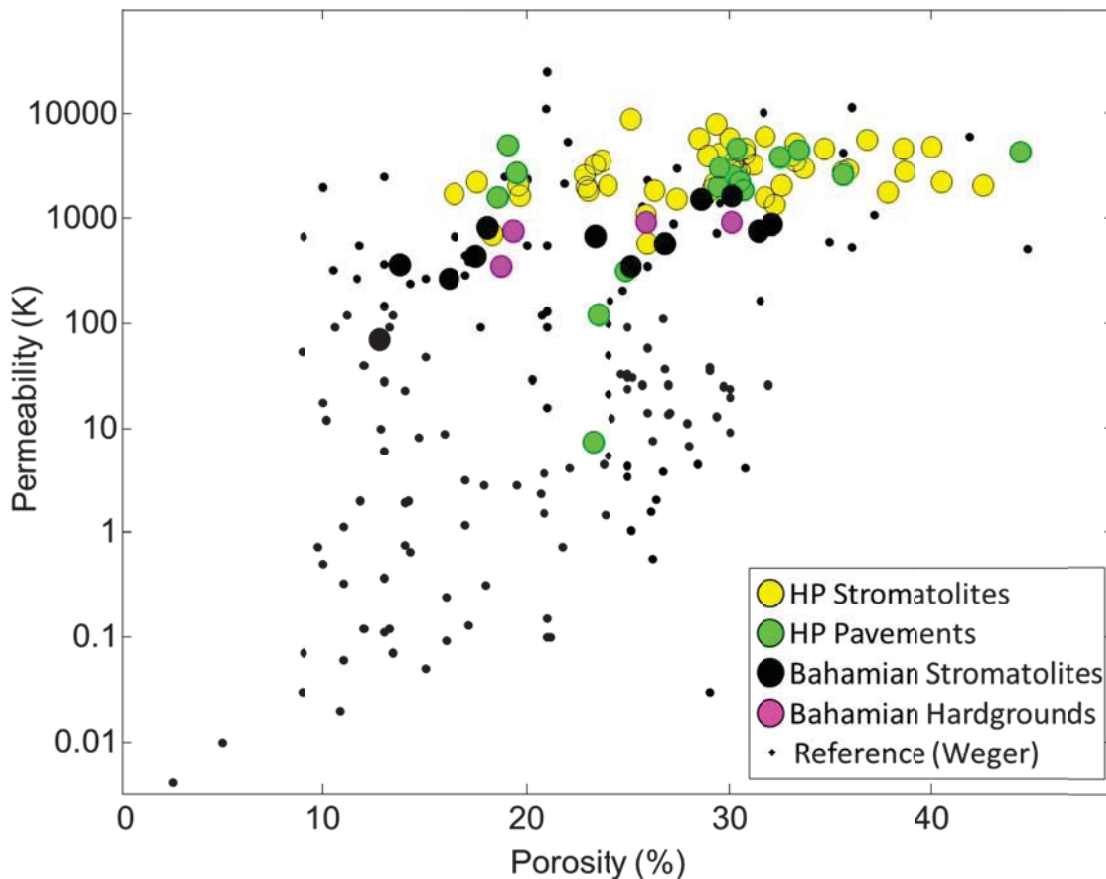


Figure 5.5: Permeability and porosity comparison between Hamelin Pool stromatolites, pavements, Bahamian stromatolites and hardgrounds.

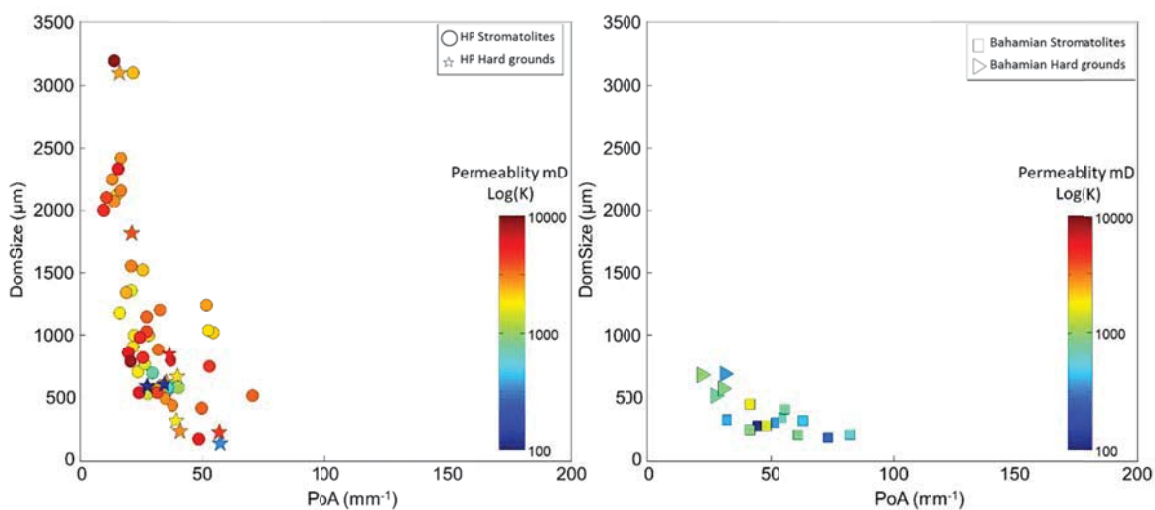


Figure 5.6: Pore structure and permeability comparison between Hamelin Pool stromatolites, pavements (left) and Bahamian stromatolites and hardgrounds (right).

Based on Lucia's (2003) limestone rock-fabric relationships, permeability in non-vuggy carbonates is related to interparticle porosity, grain size and sorting. The permeability results in Figure 5.5 and Figure 5.6 show that Hamelin Pool stromatolites develop a large range of porosity and very high values of permeability. Thin section images (Figure 2.3) show that the micritic cemented Hamelin Pool stromatolites are mostly *bindstone* with varying amount of fenestrae depending on their mat types. The pavements are poorly sorted *floatstone* with large amount of coquina (grains larger than 2 mm). On the other hand, Bahamian stromatolites have ooid grains with micritic cements and they are classified as *oid grainstones*. The grain sizes of Bahamian stromatolites are smaller than Hamelin Pool stromatolites and better sorted (Figure 5.7). Hence, the reason for the different permeability and porosity ranges in samples from Hamelin Pool and the Bahamas can be related to varying amounts of fenestrae, different sediment types, and different grain size and sorting.

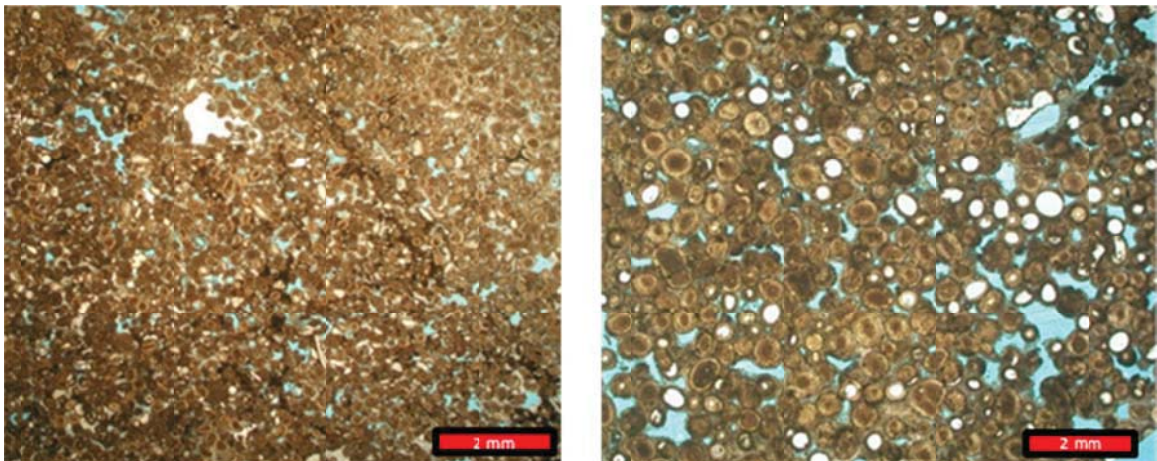


Figure 5.7: Individual thin section images of Bahamian Stromatolite (left) and hardground (right). The grains are cemented by micritic cements and they are classified as ooid grainstones with respect to Dunham (1962).

5.4. Ultrasonic Velocity

The comparison between the Hamelin Pool samples and Bahamian yield some differences but also similarities. The compressional velocity of saturated Hamelin Pool stromatolites and pavements ranges from 3903 m/s to 5504 m/s at the confining pressure of 20 MPa. At the same pressure, the saturated Bahamian hardground core plugs show a velocity range from 3266 m/s to 4986 m/s. At the pressure of 20 MPa, the compressional velocity of the saturated Bahamian stromatolites ranges from 4407 m/s to 5407 m/s (Figure 5.8).

Compressional and shear velocities increase with increasing confining pressures (Kern et al. 2001; Ji et al., 2007). This increase, however, is very small in both Hamelin Pool and Bahamian microbialites. Pavements and hardgrounds show overall lower velocity values than the stromatolite samples but increasing confining pressure does not have a great effect on ultrasonic velocities in both data sets (Figure 5.6). The minimal increase of velocity during pressurisation indicates that that the stromatolites, pavements and hardgrounds from Hamelin Pool and Bahamas are very pressure resistant.

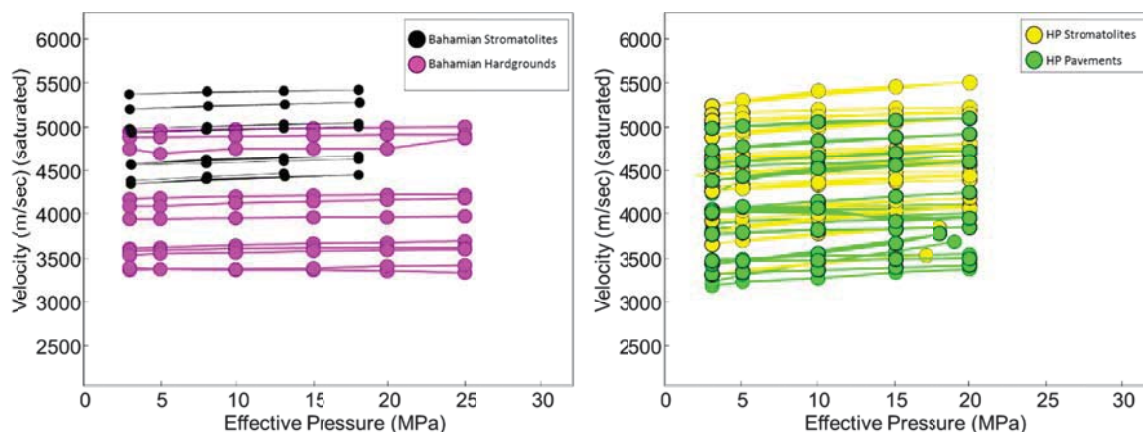


Figure 5.8: Compressional velocities versus effective pressure of Hamelin Pool stromatolites, pavements (on the left), Bahamian stromatolites and hardgrounds (on the right).

Carbonates have a large range of V_p and V_s at any given porosity due to highly variable pore structure (Anselmetti and Eberli, 1997). Carbonate mineralogy (e.g. the difference between dolomite and calcite) is not the cause of these large ranges (Anselmetti and Eberli 1997). The stromatolites and pavements from Hamelin Pool display similar velocity-porosity trends with large velocity variation at a given porosity. For example, in Hamelin Pool samples, acoustic velocity at 29% porosity ranges from 3611 m/s to 5384 m/s. Likewise, at a velocity of 4048 m/s the porosity ranges from 23% to 46%. However, the Bahamian stromatolites display an unusual narrow range of velocity for carbonate samples at any given porosity. Bahamian hardgrounds show a fairly narrow range with a decrease of velocity with increasing porosity (Figure 5.9). All samples plot high above the Wyllie time average trend line. If used for porosity estimation, the Wyllie time average equation underestimates porosity substantially for all of the measured microbialites. This high variability and non-conformance with Wyllie's equation complicates porosity estimation from

acoustic impedance. If the Wyllie's time average equation is used to calculate porosity from acoustic impedance, the resulting porosity will always be too low. Thus, seismic inversion in microbialites carries very high uncertainty. Unfortunately, in most seismic inversion workflows, pore geometry, which is responsible for most of the variations in velocity, is difficult to incorporate (Anselmetti and Eberli, 1993).

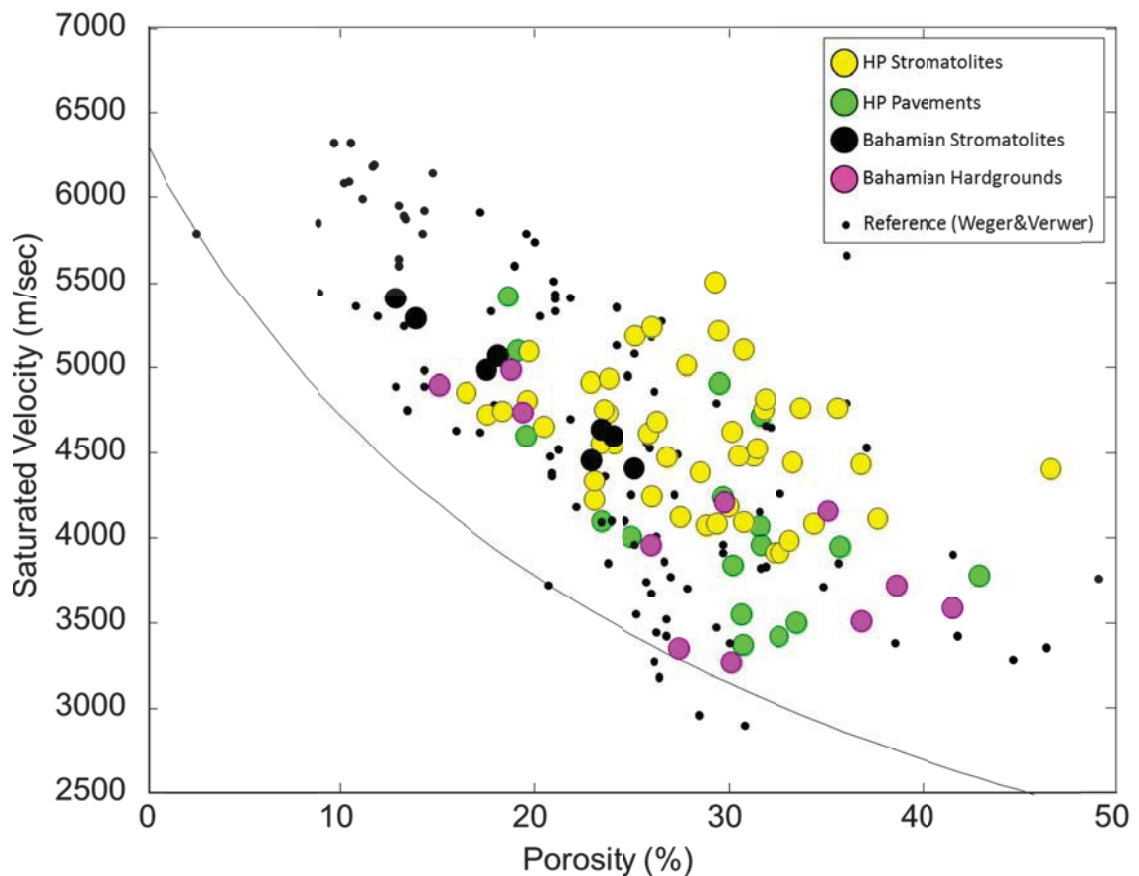


Figure 5.9: Saturated compressional velocities versus Porosity with Wyllie "time-average" for calcite.

PoA (perimeter over area) and DomSize (dominant pore size) are two of the 37 DIA parameters we used to quantify internal pore geometry. PoA measures the complexity of the overall pore structure of an entire thin section.

High PoA values result from more complex pore networks. DomSize measures the size fraction of individual pores that dominate the porosity in a thin section. The higher DomSize values mean that a thin section is dominated by larger pores. Weger et al. (2009) documented how samples with simple (low PoA) and large (high DomSize) pores (given they have similar mineralogy) have higher acoustic velocity than samples with complex (high PoA) and small (low DomSize) pores. Hamelin Pool stromatolites and pavements follow this trend of increasing velocities with decreasing complexity (Figure 5.10). Overall, neither the Bahamian nor the Hamelin pool sample sets contain samples with high complexity composed of really small pores. Within their range, Bahamian stromatolites and hardgrounds only display very weak trend. The Bahamian stromatolites have some more complex pores than the Hamelin Pool stromatolites. However, the main difference lies in their pore sizes, but velocity correlates only poorly to pore structure.

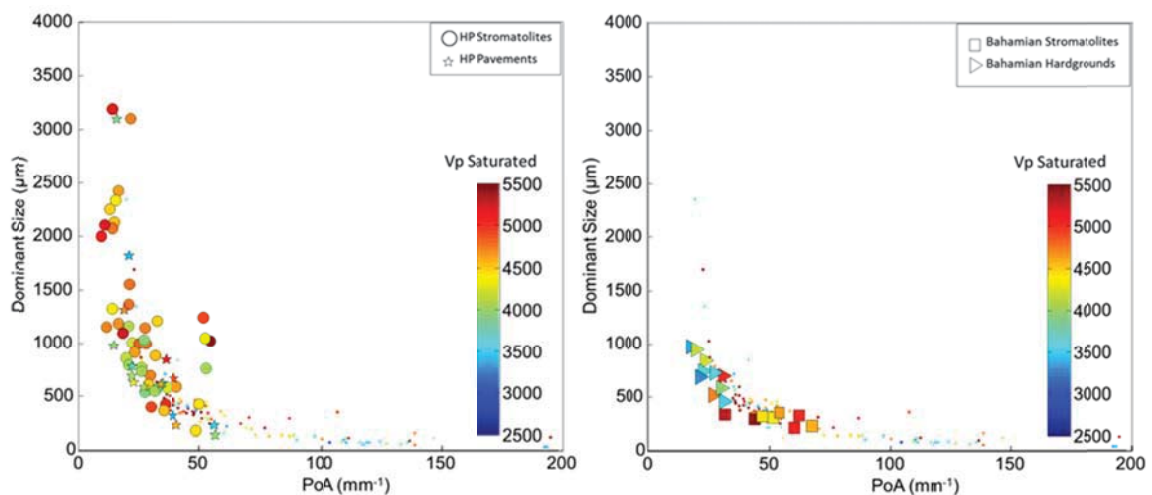


Figure 5.10: Pore structure with superimposed velocities in color from Hamelin Pool (on the left) and Bahamas (on the right).

5.5. Electrical Resistivity

Electrical resistivity is an important tool to determine water saturation in reservoirs. The formation factor 'F' of the rocks is acquired with the electrical resistivity measurements. Archie's equation $F = \phi^{-m}$ (where ϕ is porosity) provides a correlation between porosity, formation factor and Cementation Factor 'm'. Archie's second equation uses Cementation Factor as input for water saturation estimation in reservoirs. Since 'm' usually has to be assumed or estimated during this process of water saturation calculation, Focke and Munn (1987) and Lucia (1999) emphasize the importance of accurate assumptions with respect to 'm'. A large range of 'm', adds a large uncertainty to water saturation estimation.

Verwer et al. (2011) used seventy-one carbonate plugs including eleven Bahamian stromatolites to make an electrical resistivity assessment. The Cementation Factor 'm' of the entire data set of carbonate samples ranged from 1.72 to 4.16. The Cementation Factor of the Bahamian stromatolites shows only a narrow range from 2.1 to 2.6 (Verwer et al., 2010). The Cementation Factor of Hamelin Pool stromatolites ranges from 2 to 3.71 and from 2 to 3.1 in pavements. Figure 5.11 show that stromatolites, pavements, and hardgrounds from the Bahamas and Hamelin Pool are low resistant rocks. However, Hamelin Pool stromatolites have a larger range of Cementation Factors.

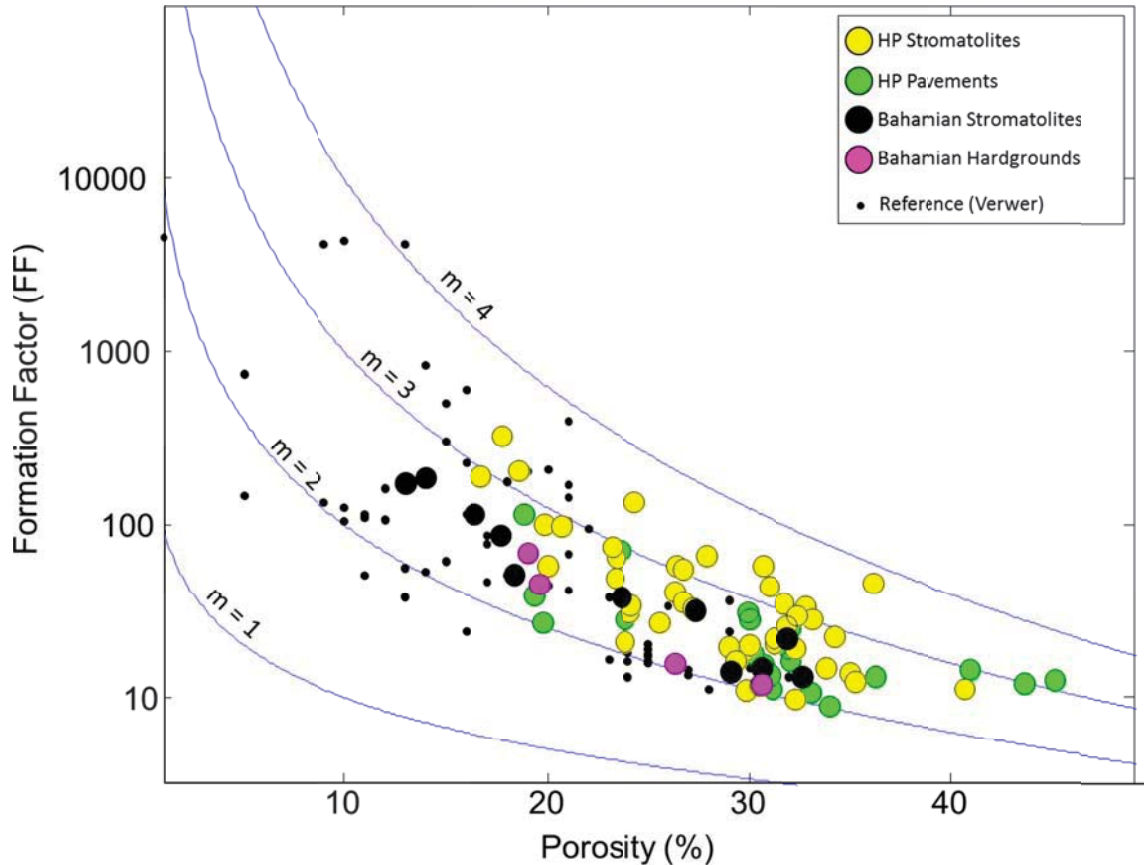


Figure 5.11: Formation factor versus porosity of Bahamian stromatolites, Hamelin Pool stromatolites and pavements with the cementation factor 'm' values.

A relationship between pore structure parameters and Cementation Factor was found by Verwer et al. (2011). Samples with microporosity and complex structures (small DomSize and high PoA values) display overall low resistivity. When PoA values become lower and DomSize values become bigger, the cementation factors increase. Verwer et al. (2011) postulated that the reason behind this is that samples with complex structures and micropores have better connectivity and conductivity due to a larger number of connecting pore throats. On the contrary, samples with simple pores tend to have high resistivity values due to lower connectivity (Verwer et al., 2011). The samples from Hamelin Pool

show an overall trend of increasing cementation factor with simpler and bigger pores, whereas samples with smaller and more complex structures show decreasing cementation factor. The Hamelian stromatolites and hardgrounds do not display a clear trend, however, they fit the reference data set (Figure 5.12).

Generally samples with high permeability and high cementation factor are consisting of simple, big pores (Verwer et al., 2011). The Hamelin Pool stromatolites and pavements show the opposite relationship. Samples with small “m” tend to have higher permeability than samples with larger “m” (Figure 4.34). A similar relationship between cementation factor and permeability is seen in samples from the Bahamas (Figure 5.13). However, all samples from Verwer et al. (2011) had substantially lower permeability values (over a magnitude).

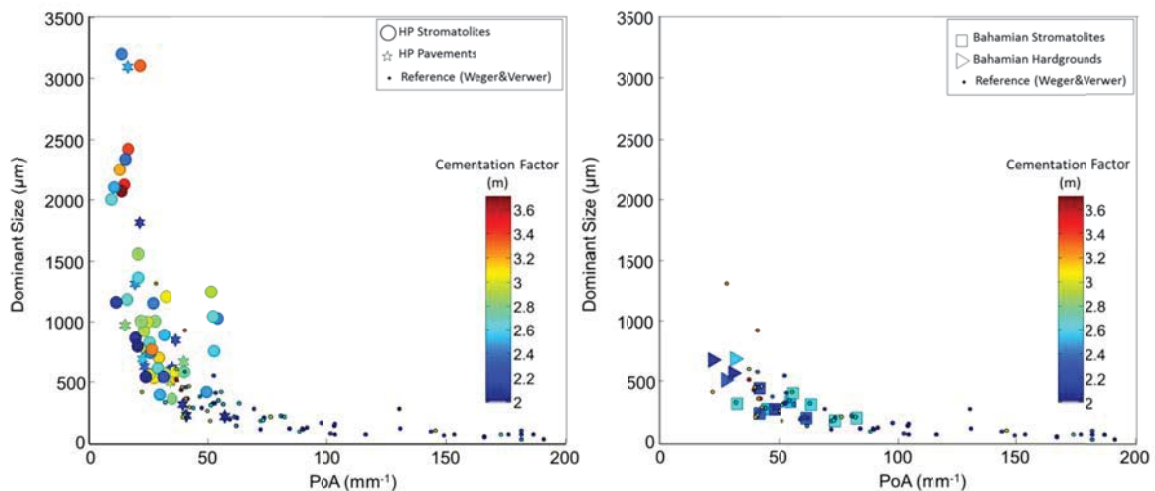


Figure 5.12: Pore structure parameters (Perimeter over area versus Dominant pore size) with cementation factor in color. Modified from Verwer et al. (2011).

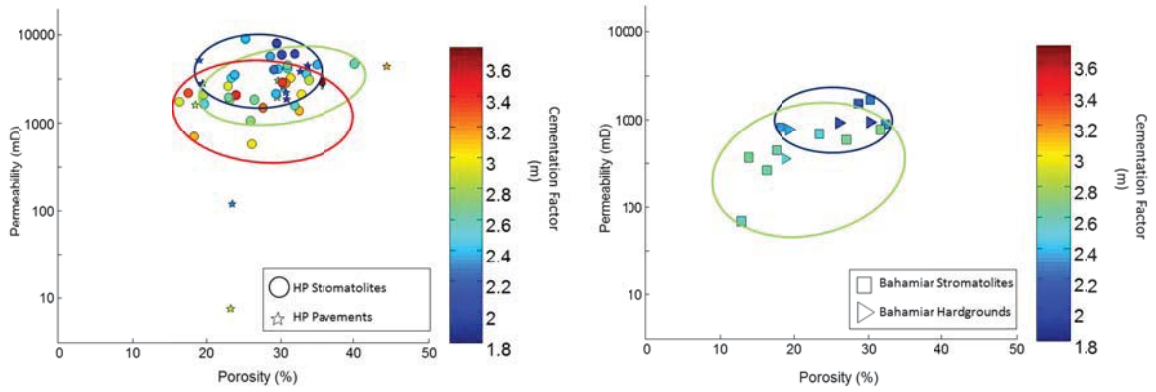


Figure 5.13: Cross-plot of permeability versus porosity with superimposed cementation factors) of Hamelin Pool samples (on the left) and Bahamian samples (on the right). Modified from Verwer et al. (2011).

CHAPTER 6. CONCLUSIONS

In this study, petrophysical properties of Hamelin Pool stromatolites and associated facies (pavements) were analyzed by interrelating porosity, permeability, sonic velocity, resistivity and pore geometry derived from Digital Image Analysis (DIA).

For the 84 core plugs that were used in this study, Digital Image Analysis results show that stromatolites generally have simple and large pore structures and impressively high permeabilities. Permeability values of the Hamelin Pool stromatolites and pavements range from 8 mD to 9000 mD, while porosity shows a large variation ranging from 16% to 46%. Due to the high porosity and permeability of stromatolites and pavements they have the potential to be reservoir facies.

Ultrasonic velocity is generally high with large scatter at any given porosity. For example, at 29% porosity, velocity ranges from 3611 m/s to 5384 m/s. Similarly at a velocity of 4403 m/s the porosity ranges from 23% to 46%. The large range of porosities at a given velocity makes porosity estimates from seismic inversion a challenge. Digital image analysis indicates that the main control on the variations is pore network complexity and pore size. More complex pore systems containing larger pores produce higher velocities at equal porosity. Compressional velocities measured under saturated conditions are up to 686m/s higher than in dry conditions. In contrast, shear velocities show both a decrease (up to 578 m/s) and an increase (up to 597 m/s) in shear velocity (V_s) with saturation. These changes in V_s indicate that the shear modulus of stromatolites

changes with saturation and result in both shear weakening and shear strengthening and thus violating the assumption by Gassmann. Just as the large range of porosities at a given velocity adds uncertainty to porosity estimation from seismic inversion, the shear moduli changes and the resultant shear strengthening and weakening add uncertainties to AVO analysis in microbialite strata.

The percent quartz in each specimen was related to velocities while considering internal pore geometry. The effect of quartz percentage variability on ultrasonic velocities in stromatolite samples, can be observed only when comparing samples of similar internal geometry, since geometry has an effect on velocity more substantially than mineral variability.

The Cementation Factor “m” (from Archie’s equation, $F = \phi^{-m}$) determined from electrical resistivity varies from 2.0 to 3.7 in stromatolites and from 2.0 to 3.1 in pavements. These relatively narrow range of Cementation Factors with respect to the other carbonates provide more precise hydrocarbon-water saturation estimation in microbial facies.

The internal fabrics of the Hamelin Pool stromatolites are related with the petrophysical properties. Porosity, permeability, acoustic velocity and resistivity do not show a correlation with different meso or microfabrics.

The comparison between the samples from Hamelin Pool and Bahamas showed that Bahamian hardgrounds have slightly more complex pore structure with small pores than Hamelin Pool pavements. Both data sets have high permeability and porosity. The grain sizes of Bahamian stromatolites are smaller

than Hamelin Pool stromatolites and better sorted. Thus their permeability is slightly lower than Hamelin Pool samples. The minimal increase of velocity during pressurisation indicates that the stromatolites, pavements and hardgrounds from Hamelin Pool and Bahamas are very pressure resistant. The stromatolites and pavements from Hamelin Pool display similar velocity-porosity trends with large velocity variation at a given porosity. Bahamian stromatolites show an unusual narrow range of velocity for carbonate samples at any given porosity. Bahamian hardgrounds show a fairly narrow range with a decrease of velocity with increasing porosity. Electrical resistivity measurements show that stromatolites, pavements, and hardgrounds from the Bahamas and Hamelin Pool are low resistant rocks. However, Hamelin Pool stromatolites have a larger range of Cementation Factors.

References

- Adekanle, A., and Enikanselu, P. A., 2013, Porosity prediction from seismic inversion properties over 'XLD' field, Niger Delta, American Journal of Scientific and Industrial Research, pp. 31-35.
- Allwood AC, Walter MR, Kamber BS, Marshal CP, Burch IW 2006, Stromatolite reef from the early archean era of Australia. Nature, 441, 714–718.
- Altermann, W., and Kazmierczak, J. 2003, Archean Microfossils: A reappraisal of early life on Earth. Research in Microbiology, 154, 611 – 617.
- Angeleri, G., and R. Carpi, 1982, Porosity prediction from seismic data: Geophysical Prospecting, 30, 580–607, doi: 10.1111/j.1365-2478.1982.tb01328.x.
- Anselmetti, F. S., and G. P. Eberli, 1993, Controls on sonic velocity in carbonates: Pure and Applied Geophysics, 141, 287-323.
- Anselmetti, F. S., Eberli, G. P., 1997, Sonic velocity in carbonate sediments and rocks. In: Marfurt, F.J., Palaz, A. (Eds.), Carbonate Seismology: Society of Exploration Geologists, Geophysical Developments Series 6, pp. 53-74.
- Anselmetti, F. S., G. A. von Salis, K. J. Cunningham, and G. P. Eberli, 1997, Acoustic properties of Neogene carbonates and siliciclastics from the subsurface of the Florida Keys; implications for seismic reflectivity: Marine Geology, 144, 9-31.
- Archie, G. E., 1952, Classification of carbonate reservoir rocks and petrophysical considerations: Bulletin of the American Association of Petroleum Geologists, v. 36, p. 278-298.
- Archilha, L.N, Misságia, M.R., Ceia, M.A.R., Neto, I.A.L., 2012, Petrophysical, mineralogical and elastic property characterization of Halocene carbonates from Salgada lagoon, Brazil. 13th International Congress of the Brazilian Geophysical Society held in Rio de Janeiro, Brazil, August 26-29, 2013.
- Awramik, S.M. and Margulis, L., 1974, Definition of stromatolite: Stromatolite Newsletter, 2, p. 5 (unpublished).

- Awramik, S.M., and Grey, K., 2005, Stromatolites: Biogenicity, biosignatures, and bioconfusion, in Hoover, R.B., Levin, G.V., Rozanov, A.Y., and Gladstone, G.R., eds., *Proceedings of the SPIE (International Society for Optics and Photonics), Astrobiology and Planetary Missions: SPIE abstracts*, v. 5906, p. 59060P-1–59060P-2, doi: 10.1117/12.625556.
- aechle, G.T., Eberli, G.P., Weger, R.J., and Massaferro, J.L., 2009, Changes in dynamic shear moduli of carbonate rocks with fluid substitution. *Geophysics*, v. 74/3 P, E135–E147.
- Bauld, J., 1984, Microbial mats in marginal marine environments: Shark Bay, Western Australia, and Spencer Gulf, South Australia. In: *Microbial mats: stromatolites*, R.W. Castenholz, Y. Cohen and H.O. Halvorson (eds.): New York, Alan R., Liss Inc., p. 39-58.
- Braaksma, H., Kenter J.A.M., Proust J.N., Dijkmans V., van Hoek T., Mahieux, G. and Drijkoningen G.G., 2003, Controls on acoustic properties of Upper Jurassic siliciclastic rocks (Boulonnais, northern France). *Geophysics* 68, 58–69.
- Braithwaite, C.J.R., Zedef, V., 1996, Hydromagnesite stromatolites and Sediments in an alkaline lake, Salda Gölü, Turkey. *Journal of Sedimentary Research*, Vol. 66, No. 5, 991-1002.
- Brie A., Johnson D.L. and Nurmi R.D. 1985, Effect of spherical pores on sonic and resistivity measurements. 26th Annual Logging Symposium, SPWLA, 1 Paper W.
- Brownie, K.M., 1993, Lamination in recent Bahamian subtidal stromatolites: origin and lithification. (unpublished) Ph.D. thesis, University of Miami, 296 p., Coral Gables, F1.
- Burling, M. C., Ivey, G. N., and Pattiaratchi, C. B., 1999, Convectively driven exchange in a shallow coastal embayment. *Continental Shelf Research* 19, 1599–1616. doi:10.1016/S0278-4343(99)00034-5.
- Burne, R.V., and Moore, L.S., 1987. Microbialites: Organosedimentary deposits of benthic microbial communities. *Palaios*, 2, 241-245.
- Burne, R.V., Johnson, K. 2012, Sea-level variation and the zonation of microbialites in Hamelin Pool, Shark Bay, Western Australia. *Marine and Freshwater Research*, Vol. 63, 994-1004.

- Butcher, B.P., Van de Graaff, W.J.E., Hocking, R.M., 1984, Explanatory notes on the Shark Bay-Edel geological sheet. Western Australia Geological Survey, pp. 1-21.
- Choquette, P. W., and L. C. Pray, 1970, Geologic nomenclature and classification of porosity in sedimentary carbonates: The American Association of Petroleum Geologists Bulletin, v. 54, p. 207-244.
- Crevello, P .D. and Schlager, W., 1979, Carbonate debris sheets and turbidites, Exuma Sound, Bahamas: Jour. Sed. Pet., v. 50, p. 1121-1148.
- Davies, G.R., 1970a, Carbonate bank sedimentation, eastern Shark Bay, Western Australia, -in Logan and others, carbonate sedimentation and environments, Shark Bay, Western Australia: Amer. Assoc. Petrol. Geol. Mem. 13, pp. 85-168.
- Dill, R. F., Grotzinger, J. P. & Read, J. F., 1991, A comparison of elongated, subtidal stromatolites in high-energy bays of the Exuma Islands, Bahamas, to Paleozoic and Precambrian forms.
- Dill, R. F., Kendall, C. G. and Shinn, E. S., 1989, IGC Field Trip T 373:Giant subtidal stromatolites and related sedimentary features, Lee Stocking Island, Exumas, American Geophysical Union, Washington, D. C.. doi: 10.1002/9781118667224.ch1.
- Dill, R.F., Shinn, E.A., Jones, A.T., Kelly, K., & Steinen, R.P., 1986, Giant subtidal stromatolites forming in normal salinity water. - Nature, 324, 55-58.
- Dravis, J.J., 1983, Hardened subtidal stromatolites, Bahamas. Science, 219, 385-386.
- Dunham, R. J., 1962, Classification of carbonate rocks according to depositional texture: Memoir, American Association of Petroleum Geologists, 108-121 p.
- Dupraz, C., Visscher, P.T., 2005, Microbial lithification in marine stromatolites and hypersaline mats. TRENDS in Microbiology, Vol. 13, No. 9, 429-438.
- Eberli, G.P., Baechle, G.T., Anselmetti, F.S. and Incze, M.L., 2003, Factors controlling elastic properties in carbonate sediments and rocks: The Leading Edge, v. 22, p. 654-660.

- Eberli, P.G., Verwer, K. Weger, R.J., Porta, G.D., 2012, The role of microbial activity on petrophysical properties. AAPG Hedberg Conference June 4-8, 2012 – Houston, TX.
- Embry, A. F., and J. E. Klovan, 1971, A Late Devonian reef tract on Northeastern Banks Island, N.W.T: Canadian Petroleum Geology Bulletin, v. 19, p. 730-781.
- Fabricius, I.L., Baechle, G. T., Eberli, G. P., 2010, Elastic moduli of dry and water-saturated carbonates-effect of depositional texture porosity and permeability. Geophysics, vol. 75/ 3, p. N65–N78, doi: 10.1190/1.3374690.
- Feldman, M., 1995, Controls on stromatolite formation: a comparative study of modern stromatolites from the Bahamas with Messian examples from southeast Spain. - Ph.D. Thesis, Swiss Federal Institute of Technology, 128 p., Ziarich.
- Fischer, AG 1965, Fossils, early life, and atmospheric history: Proceedings of the National Academy of Sciences, v. 53, p 1205– 1215.
- Focke, J.W., Munn, D., 1987, Cementation exponents in Middle Eastern carbonate reservoirs. Society of Petroleum Engineers SPE-13735-PA p. 155 – 167.
- Folk, R. L., 1959, Practical petrographic classification of limestones: Bulletin of the American Association of Petroleum Geologists, v. 43, p. 1-38. Folk, R. L., 1962, Spectral subdivision of limestone types.
- Gassmann, F., 1951, Über die elastizität poröser medien: Vierteljahresschrift der Naturforschenden Gesellschaft in Zürich, 96p.
- Gischler, E., Gibson, M., and Oschmann, W., 2008, "Giant Holocene freshwater microbialites, Laguna Bacalar, Quintana Roo, Mexico". Sedimentology 55 (5): 1293–130.
- Golubic, S., 1985, Microbial mats and modern stromatolites in Shark Bay, Western Australia. In: Planetary Ecology, D.E. Cardwell, J.A. Brierley, and C.L. Brierley (eds.), van Nostrand Rienhold Co., New York, p.3-16.
- Griffin, K.M., 1988, Sedimentology and paleontology of thrombolites and stromatolites of the Upper Cambrian Nopah Formation and their modern analog on Lee Stocking Island, Bahamas. - Unpubl. M. A. thesis, University of California, 117 p, Santa Barbara, Ca.

- Grotzinger, J.P., Knoll, A.H., 1999, Stromatolites in Precambrian carbonates: Evolutionary mileposts or environmental dipsticks. *Annu. Rev. Earth Plant. Sci.* v. 27, p. 313-58.
- Hoffman, PF 1976, Stromatolite morphogenesis in Shark Bay, Western Australia, in *Stromatolites (Developments in Sedimentology, v. 20)* edited by MR Walter: Elsevier, Amsterdam, The Netherlands, p. 261– 271.
- Hofmann H.J., Grey K., Hickman A.H., Thorpe R.I., 1999, Origin of 3.45 Ga Coniform stromatolites in the Warrawoona Group, Western Australia. *GSA bulletin* 111, 1256–1262.
- Hofmann, H.J., 1969b, Stromatolites from the Proterozoic Animikie and Sibley Groups. *Geological Survey of Canada Paper* 68 - 69.
- Hurley, R.H., and Shepard, F.P., 1964, Submarine canyons in the Bahamas. (Abst) *Program Geol. Soc. Am., Ann. Mtg. Miami*, p. 99.
- Jahnert, J.R. and Collins L.B., 2012, Characteristics, distribution and morphogenesis of subtidal microbial systems in Shark Bay, Australia. *V* 303–306, pp 115–136 *Marine Geology*.
- Jahnert, R.J., and Collins, L.B., 2011, Significance of subtidal microbial deposits in Shark Bay, Australia, *Marine Geology*, v. 285, p. 106-111.
- Jahnert, R.J., Collins, L.B., 2013, Controls on microbial activity and tidal flat evolution in Shark Bay, Western Australia. *Sedimentology*, Vol. 60, No. 4, 1071-1099.
- Jahnert, R.J., Paula, O., Collins, L.B., Strobach, E., Pevzner, R., 2012, Evolution of a coquina barrier in Shark Bay, Australia by GPR imaging: Architecture of a Holocene reservoir analog, *Sedimentary Geology* 281, 59–74.
- James, N.P., 1984, Shallowing-upward sequences in carbonates, in Walker, R.G., ed., *Facies Models: Geological Association of Canada, Geoscience Canada, Reprint Series 1*, p. 213–228.
- Ji, S., Wang, Q., Marcotte, D., Salisbury, M. H., and Xu, bZ., 2007, P-wave velocities, anisotropy and hysteresis in ultrahigh-pressure metamorphic rocks as a function of confining pressure: *Journal of Geophysical Research*, 112, B09204.

- Jixin, D., Genyang, T., and Ping, Y., 2015, Microtextural, seismic rock physical properties and modeling of Longmaxi Formation shale. 3rd International Workshop on Rock Physics, Perth, Western Australia.
- Judd, A.G., Hovland, M., 2007, Seabed fluid flow: The impact on geology, biology and the marine environment. Cambridge University Press, New York. 308 pp.
- Kalkowsky, E., 1908, Oolith und Stromatolith im norddeutschen Buntsandstein. Z. Deutschen Geologischen Gesellschaft, Vol. 60, 68-125, pls 4-1.
- Keng, E.Y.H., 1969, Air and helium pycnometer, Powder Technology, 3, No. 3, 179-180, 1969.
- Kenter, J.A.M., Anselmetti, F.S., Kramer, P.A., Westphal, H. and Vandamme, M.G.M., 2002, Acoustic properties of "young" carbonate rocks, ODP Leg 166 and Boreholes Clino and Unda, Western Great Bahama Bank: Journal of Sedimentary Research, v. 72, p. 129-137.
- Kern, H., Popp, T., Gorbatshevich, F., Zharikov, A., Lobanov, K. V., and Smirnov, Y. P., 2001, Pressure and temperature dependence of V_p and V_s in rocks from the super deep well and from surface analogues at Kola and the nature of velocity anisotropy: Tectonophysics, 338, 113–134.
- King, M.S., 1966, Wave velocities in rocks as a function of changes in overburden pressure and pore fluid saturants: Geophysics, v. 31, p. 50-73.
- Klement, K. W., 1967, Practical classification of reefs and banks, bioherms and biostromes: Am. Assoc. Petroleum Geologists Bull., v. 51, p. 167-168.
- Krumbein, W.E., 1983, Stomatolites - the challenge of a term in space and time. Precambrian Research, 20, 493 - 531.
- Kumar, D., 2006, A tutorial on Gassmann Fluid Substitution: Formulation, algorithm and matlab code. Geohorizons 11, 4-12.
- Logan, B.W. and Cebulski, D.E., 1970, Sedimentary environments of Shark Bay, Western Australia: Book; M 13: Carbonate Sedimentation and Environments, Shark Bay, Western Australia, A040.

- Logan, B.W. and Read, F.J., Davies., G.R, 1970, History of carbonate sedimentation, Quaternary epoch, Shark Bay, Western Australia; M 13: Carbonate Sedimentation and Environments, Shark Bay, Western Australia, 38-84.
- Logan, B.W., 1961, Cryptozoon and associated stromatolites from the Recent, Shark Bay, Western Australia: Jour. Geol. 69, p.517-533.
- Logan, B.W., Ginsburg R.N., 1964, Classification and environmental significance of algal stromatolites. The Journal of Geology, Vol. 72, No. 1, pp. 68-83.
- Lucia F.J. 1995, Rock-fabric/petrophysical classification of carbonate pore space for reservoir characterization. American Association of Petroleum Geologists Bulletin 79, 1275–1300.
- Lucia, F. J., 1999, Carbonate reservoir characterization: An Integrated Approach 2nd edition Book, p.94.
- Lucia, F. J., 2003, Estimating permeability in carbonates using the Rock-Fabric Method. American Geological Institute and American Association of Petroleum Geologists.
- Macintyre, I.G., Reid, R.P. and Steneck, R.S., 1996, Growth history of stromatolites in a Holocene fringing reef, Stocking Island, Bahamas. J. Sedim. Res., 66, 231±242.
- Monty, CLV 1965, Recent algal stromatolites in the Windward Lagoon, Andros Island, Bahamas: Annales de la Société Géologique de Belgique, v. 90, p. 585–624.
- Neto, I.A.L., Misságia, M.R., Ceia, M.A.R., Archilha, L.N., 2013, Application of effective elastic media models for pore system evaluation of Albian grainstone carbonates from Campos Basin, Brazil, presented 13th International Congress of the Brazilian Geophysical Society held in Rio de Janeiro, Brazil.
- Noffke, N. and S. M. Awramik, 2013, Stromatolites and MISS – differences between relatives, GSA Today, 23(9):4-9.
- Ohen, A.H., and Kersey, G. D., 1993, Permeability; AAPG Methods in Exploration Series; No. 9: Biomarkers for Geologists, AAPG (1991), p212.

- Pendrel, J., "Seismic Inversion, 2006, A Critical Tool in Reservoir Characterization", *Scandinavian Oil-Gas Magazine*, No. 5/6, p. 19-22.
- Pickett, G.R., 1963, Acoustic character logs and their applications in formation evaluation: *Journal Petroleum Technology*, v. 15, p. 659-667.
- Playford, P.E., 1980a, Environmental controls on the morphology of modern stromatolites at Hamelin Pool, Western Australia. *Western Australia Geological Survey Annual Report (for 1979)*, 73-77.
- Playford, P.E., 1990, Geology of the Shark Bay area, Western Australia. In: P.F. Berry, S.D. Bradshaw and B.R. Wilson (Editors), *Research in Shark Bay*, Western Australia Museum, Perth, pp.13-31.
- Playford, P.E., Cockbain, 1976, A. E., Berry, P. F., Roberts, Anthony P., Haines, P.W., Brooke, B., *Geological Survey of Western Australia, The geology of Shark Bay*, Geological Survey of Western Australia: Bulletin 146 p.246.
- Playford, P.E., Cockbain, A.E., Berry, P.F., Roberts, A.P., Haines, P.W., Brooke, B.P. 2013, *The geology of Shark Bay*. Geological Survey of Western Australia: Bulletin 146, Geological Survey of Western Australia.
- Rasmussen, K.A., Macintyre, I.G. and Prufert, L., 1993, "Modern stromatolite reefs fringing a brackish coastline, Chetumal Bay, Belize". *Geology* 21(3): 199–202.
- Reid, R.P. & Browne, K.M., 1991, Intertidal stromatolites in a fringing Holocene reef complex in the Bahamas. *Geology*, 19, 15-18.
- Reid, R.P., James N.P., Macintyre I.G., Dupraz C.P., Burne R.V., 2003, Shark Bay stromatolites: Microfabrics and reinterpretation of origins. *Facies* 49:45–53.
- Reid, R.P., Macintyre, I.G., Browne, K.M., Steneck, R.S., and Miller, T., 1995, Modern marine stromatolites in Exuma Cays, Bahamas: Uncommonly common: *Facies*, v.33, p. 1-18.
- Reid, R.P., Visscher, P.T., Decho, A.W., Stolz, J.F., Bebout, B.M., Dupraz, C., Macintyre, I.G., Paerl, H.W., Pinckney, J., Prufert-Bebout, L., Steppe, T.F., DesMarais, D.J., 2000, The role of microbes in accretion, lamination and early lithification of modern marine stromatolites. *Nature* 406, p. 989-992.

- Sadeghi, H., and Khosravi, F., 2003, A study of the effect of wave velocity on solubility of limestone and chalk. *Deformation Characteristics of Geomaterials*, pg.409.
- Schalk, M., 1946, Submarine topography off Eleuthera Island, Bahamas. (abst.), *Bull. Geol. Soc. Amer.*, v. 57, p.12-28.
- Scholle, P. A., and Ulmer-Scholle, D. S., 2003, A color guide to the petrography of carbonate rocks: AAPG Memoir 77, 474 p.
- Schopf, J.W., 1983, editor, *Earth's earliest biosphere*, Princeton University Press, Princeton, NJ.
- Seabrook, B., and Boadu, F. K., 2002, Relating electrical response and petrophysical properties of sands subjected to stress changes: *Journal of Environmental and Engineering Geophysics*, 7: 88-99.
- Shepard, F.P., and Dill, R.F., 1966, *Submarine canyons and other sea valleys*. Rand McNally Co., Chicago, 381 p.
- Shinn, E. A., and Ginsburg, R.N., 1964, Formation of Recent dolomite in Florida and the Bahamas. (abs.), *Bull. Am. Assoc. Petrol. Geologists*, v. 45, p. 547.
- Shinn, E.A., 1983, Tidal flats in Scholle, Bebout, and Moore, eds. *Carbonate Depositional Environments*, Am. Assoc. Petrol. Geologists Memoir 33, p. 171-210.
- Smith, M. Tad, Carl H. Sondergeld, and Chandra S. Rai, 2003, Gassmann fluid substitutions: A tutorial: *Geophysics*, 68, 430-440.
- Taft, W. H., Arrington, F., Haimoritz, A., MacDonald, C., and Woolheater, C., 1968, Lithification of modern carbonate sediments at Yellow Bank, Bahamas. *Bull. Mar. Sci. Gulf Caribbean*, v. 18, p. 762-828.
- Tatham, R.H., and Stoffa, P.L., 1976, Vp/Vs – A potential hydrocarbon indicator: *Geophysics*, v. 41, p. 837-849.
- Tatham, R.H., 1982, Vp/Vs and lithology: *Geophysics*, v. 47, p. 336-344.

- Todd, T. W., 1966, Petrogenetic classification of carbonate rocks: *Journal of sedimentary Research*, v. 36, p. 317-340.
- Toksoz, M.N., Johnston, D.H., and Timur, A., 1979, Attenuation of seismic waves in dry and saturated rocks: 1. Laboratory measurements: *Geophysics*, 44, 681-690.
- Verwer, K., Eberli, G.P., Baechle, G. T., and Weger R. J, 2010, Effect of carbonate pore structure on dynamic shear moduli. *Geophysics*, v. 75/1, P. E1–E8. doi:10.1190/1.3280225.
- Verwer, K., Eberli, G.P., Weger, R.J., 2011, Effect of pore structure on electrical resistivity in carbonates: *AAPG Bulletin* v.95, p. 175-190.
- Walter, M. A., 1972, Stromatolites and the biostratigraphy of the Australian Precambrian and Cambrian. *Special Papers in Palaeontology*, 11, paleontological Association London, 190 pp.
- Walter, M. R., Buick, R. and Dunlop, J. S. R. 1980, Stromatolites 3400-3500 Myr old from the North Pole area, Western Australia. *Nature*, 284, 443-445.
- Wang, Z., 1997, Seismic properties of carbonate rocks. *Carbonate Seismology; Geophysical Developments* No. 6, P.29-52.
- Weger R., J., Eberli, G., P., Baechle, G. T., Massaferro, J., L., and Sun, Y., F., 2009, Quantification of pore structure and its effect on sonic velocity and permeability in carbonates. *AAPG Bulletin*, v. 93/10, p. 1-21.
- Wyllie, M.R., Gregory, A.R. and Gardner, G.H.F., 1956, Elastic wave velocities in heterogeneous and porous media: *Geophysics*, v. 21/1, p. 41-70.

APPENDIX 1. Data used in this petrophysical reseach

Name	Orientation	Latitude	Longitude	Vpdry (m/s)	Vsdry (m/s)	VPVSdry
H1	H	-26.382441	114.163551	5111.4	2776.08	1.84
H2	V	-26.383471	114.163612	4737.94	2847.09	1.66
H3	H	-26.383501	114.163651	4921.02	2782.89	1.77
H4	V	-26.383501	114.163651	4647.95	2718.55	1.71
H5	H	-26.319987	114.232635	3226.5	1922.07	1.68
H6	V	-26.319987	114.232635	3873.87	2355.35	1.64
H7	H	-26.319898	114.232502	4074.01	2619.12	1.56
H8	V	-26.319898	114.232502	4052.26	2499.09	1.62
H9	H	-26.31978	114.232033	4610.36	2609.11	1.77
H10	V	-26.31978	114.232033	4023.74	2534.57	1.59
H11	H	-26.319692	114.231832	4731.3	2785.87	1.7
H12	H	-26.319589	114.231656	4506.79	2397.65	1.88
H13	V	-26.319589	114.231656	4093.4	2393.63	1.71
H14	H	-26.319553	114.231465	4425.18	2936.96	1.51
H15	V	-26.319553	114.231465	4410.05	2490.73	1.77
H16	V	-26.3716824	114.0018627	4443.97	2499.48	1.78
H17	H	-26.419316	114.142816	4536.68	2505.6	1.81
H18	V	-26.419316	114.142816	3770.72	2184.51	1.73
H19	V	-26.419161	114.142827	3724.4	2082.79	1.79
H20	H	-26.418803	114.142633	4674.95	2683.34	1.74
H21	V	-26.418803	114.142633	4325.49	2622.69	1.65
H22	H	-26.38282	114.16142	5383.57	2919.28	1.84
H23	V	-26.38282	114.16142	4660	2709.3	1.72
H24	H	-26.3714838	114.0019447	0	0	0
H25	V	-26.3715987	114.0019055	4129.01	2459.24	1.68
H26	H	-26.051872	113.909106	4746.62	2790.48	1.7
H27	H	-26.3716285	114.001797	4085.99	2518.18	1.62
H28	V	-26.3716285	114.001797	4311.78	2580.3	1.67
H29	H	-26.1550224	113.9499175	4767.76	2864.72	1.66
H30	V	-26.1550224	113.9499175	4749.28	3026.39	1.57
H31	H	-26.1549978	113.9491693	4877.53	2859.26	1.71
H32	V	-26.1549978	113.9491693	4721.97	2701.04	1.75
H33	H	-26.265252	114.215232	4666.47	2724.67	1.71
H34	V	-26.265252	114.215232	4455.38	2570.78	1.73

Name	Orientation	Latitude	Longitude	Vpdry (m/s)	Vsdry (m/s)	VPVSdry
H35	H	-26.265875	114.215824	4610.21	2643.3	1.74
H36	V	-26.265875	114.215824	4594.39	2633.08	1.74
H37	H	26.1549978	113.9491693	5136.85	3115.48	1.65
H38	V	0	0	4761.71	2680.56	1.78
H39	V	-26.1645	113.94333	4045.22	2215.54	1.83
H40	H	-26.33718	113.972824	4735.06	2864.69	1.65
H41	V	-26.337358	113.97258	4575	2985.29	1.53
H42	V	-26.337519	113.97255	4768.76	2712.71	1.76
H43	H	-26.09505	113.90788	3829.33	2378.48	1.61
H44	V	-26.09505	113.90788	4535.88	2646.85	1.71
H45	V	-26.26542	114.21709	4204.98	2420	1.74
H46	H	-26.386554	114.154458	5055.93	3324.59	1.52
H47	V	-26.386554	114.154458	4300.92	2452.87	1.75
H48	H	-26.268	114.2163	4644.97	2549.31	1.82
H49	V	-26.3379	113.9724	4821.42	2566.72	1.88
H50	V	0	0	5000.9	2885.62	1.73
H51	V	-26.24524	113.97041	3939.08	2291.24	1.72
H52	H	-26.172	113.939	4414.72	2596.07	1.7
H53	H	-26.172	113.939	3600.2	2242.32	1.61
H54	H	-26.172	113.939	3744.17	2486.92	1.51
H55	V	-26.172	113.939	4334.92	2668.39	1.62
H56	V	-26.172	113.939	3287.55	2151.43	1.53
H57	H	-26.074	114.23182	4015.33	2645.15	1.52
H58	H	-26.24524	113.97041	3556.44	2035.79	1.75
H59	H	-26.24524	113.97041	3089.05	1943.97	1.59
H60	H	-26.24524	113.97041	4355.48	2536.59	1.72
H61	V	-26.24524	113.97041	3776.42	2183.07	1.73
H62	H	0	0	4008.8	2367.55	1.69
P1	V	0	0	4557.6	2592.48	1.76
P2	H	0	0	3250.41	1991.01	1.63
P3	H	0	0	3840.47	2542.7	1.51
P4	H	0	0	3120.01	1876.59	1.66
P5	H	0	0	3620.64	2130.41	1.7
P6	V	0	0	3389.05	2000.87	1.69
P7	H	0	0	3610.99	2133.98	1.69
P8	V	0	0	3859.19	2256.5	1.71
P9	H	0	0	4570.86	2946.25	1.55
P10	V	0	0	3978.87	2356.51	1.69
P11	H	0	0	5051.02	2835.93	1.78
P12	H	0	0	4916.56	2846.95	1.73

Name	Orientation	Latitude	Longitude	Vpdry (m/s)	Vsdry (m/s)	VPVSdry
P13	V	0	0	3230.42	1837.08	1.76
P14	V	0	0	3749.03	2282.24	1.64
P15	H	0	0	3401.69	2119.38	1.61
P16	V	0	0	3413.37	2023.29	1.69
P17	V	0	0	4487.36	2735.38	1.64
P18	H	0	0	4861.96	2671.95	1.82
P19	V	0	0	4093.29	2289.07	1.79
P20	H	0	0	4518.79	2395.24	1.89
P21	V	0	0	4143.56	2379.97	1.74
P22	V	0	0	3123.78	1615.89	1.93

APPENDIX 2. Data used in this petrophysical reseach

Name	Vpwet (m/s)	Vswet (m/s)	VPVSwet	m	FF	PoA mm-1	DOMsize μ m
H1	5182.83	0	0	2.39	26.61	13.7	3193
H2	4851.47	2947.94	1.65	2.91	191.7	0	0
H3	5094.67	2780.63	1.83	2.49	56.71	0	0
H4	4717.97	2595.97	1.82	3.32	321.1	21.3	3099
H5	0	0	0	0.00	0	31.5	571
H6	3911.58	2401.66	1.63	3.10	33.1	27.1	535
H7	0	0	0	0.00	0	23.2	703
H8	4122.29	2743.32	1.5	3.25	65.8	25.9	769
H9	4609.96	2510.87	1.84	2.74	40.44	40.5	583
H10	4238.38	2686	1.58	3.01	57.35	36.2	579
H11	4802.18	2672.22	1.8	2.82	99.02	27.6	998
H12	0	0	0	0.00	0	70.2	521
H13	4218.08	2358.9	1.79	2.83	63.78	22	1004
H14	4439.75	2840.82	1.56	2.45	14.78	49.8	420
H15	4550.32	2465.49	1.85	3.44	134.8	14.7	2125
H16	0	0	0	0.00	0	21.4	906
H17	4549.83	2397.59	1.9	2.50	37.74	31.5	884
H18	3903.38	2067.46	1.89	2.98	28.14	31.8	565
H19	0	0	0	0.00	0	25.3	1522
H20	4753.56	2706.01	1.76	2.58	19.1	20.6	1364
H21	4475.35	2724.59	1.64	3.05	34.71	32.2	1208
H22	5504.72	2946.18	1.87	2.37	18.37	54.3	1023
H23	0	0	0	0.00	0	18.7	1342
H24	4674.88	2631.13	1.78	2.67	35.06	16.2	1184
H25	0	0	0	0.00	0	36.9	800
H26	0	0	0	0.00	0	16.6	2159
H27	4089.97	2429.54	1.68	2.56	20.3	52.7	756
H28	4324.99	2382.93	1.81	2.64	48.23	52.3	1041
H29	0	0	0	0.00	0	37.7	437
H30	4911	0	0	2.91	73.44	51.6	1244
H31	5096.75	2798.2	1.82	2.62	21.74	9.3	2000
H32	4760.78	2542.99	1.87	3.71	45.86	13.8	2066
H33	4730.68	2654.9	1.78	2.39	31.02	27	1146
H34	4483.96	-2742.47	-1.64	3.19	43.82	12.8	2249
H35	4759.64	2608.75	1.82	2.85	22.05	20.8	1556
H36	4615.91	2502.84	1.84	3.37	56.81	16.3	2423

Name	Vpwet (m/s)	Vswet (m/s)	VPVSwet	m	FF	PoA mm-1	DOMsize μ m
H37	5215.88	3196.04	1.63	2.45	19.92	10.6	2101
H38	4743.03	-2732.68	-1.74	3.14	202.3	29.1	694
H39	4403.82	2546.37	1.73	0.00	0	13.8	1320
H40	4745.44	2926.83	1.621358261	2.09	20.55	11.4	1155
H41	4651.77	0	0	2.89	97.99	23.1	915
H42	5008.13	2645.91	1.89	0.00	0	35.6	425
H43	4076.6	2513.7	1.62	2.45	13.58	25.8	735
H44	4518.5	2736.89	1.650961493	2.80	25.38	34.9	361
H45	4112.72	2261.39	1.82	0.00	0	20.6	1157
H46	5230.03	2727.06	1.92	0.00	0	18.2	1092
H47	4471.38	2470.01	1.81	2.64	31.97	28.7	613
H48	4808.41	2885.61	1.67	2.95	29.02	24.7	993
H49	4926.71	2602.74	1.89	2.45	33.76	29.5	396
H50	0	0	0	3.00	54.06	25.3	554
H51	4075.3	2250.52	1.81	1.96	10.99	20.4	790
H52	4383.87	2493.59	1.76	2.36	19.32	15.4	2335
H53	0	0	0	2.63	11.05	25.3	820
H54	4430.22	2546.33	1.74	0.00	0	48.5	175
H55	3979.04	2145.68	1.85	0.00	0	26.7	1032
H56	0	0	0	0.00	0	24.1	985
H57	0	0	0	0.00	0	34.5	496
H58	4063.89	2073.3	1.96	2.25	16.2	31.1	544
H59	0	0	0	2.37	12.18	0	0
H60	4178.91	2258.25	1.85	2.03	11.53	19.5	860
H61	0	0	0	1.99	9.786	23.6	545
H62	3951.51	2418.51	1.63	2.49	12.99	15.9	3093
P1	0	0	0	0.00	0	0	0
P2	3415.21	1878.41	1.82	2.10	10.56	21.2	1810
P3	3841.36	2450.35	1.57	2.29	15.52	35.1	623
P4	0	0	0	0.00	0	28.1	479
P5	3773.9	2269.29	1.66	2.94	12.02	22.1	778
P6	0	0	0	2.94	14.36	34.3	504
P7	4240.08	2261.58	1.87	2.36	17.52	23.1	624
P8	4065.52	2267.76	1.79	2.54	18.81	22.1	686
P9	4714.95	2946.67	1.6	2.42	16.23	19.2	1314
P10	3954.86	2090.43	1.89	2.80	25.18	15	974
P11	5096.91	3293.7	1.55	2.21	38.51	36.5	844
P12	5424.44	3419.36	1.59	2.82	114.3	0	0

Name	Vpwet (m/s)	Vswet (m/s)	VPVSwet	m	FF	PoA mm-1	DOMsize μm
P13	3369.68	1800.08	1.87	2.05	11.21	39.6	316
P14	4004.52	2116.29	1.89	0.00	0	57.4	140
P15	3493.65	2025.18	1.73	1.99	8.812	56.8	223
P16	3545.28	2100.88	1.69	2.19	13.44	0	0
P17	4602.31	2630.6	1.75	2.02	26.83	41.3	227
P18	4908.8	3225.11	1.52	2.80	30.52	39.8	666
P19	4100.62	2222.41	1.85	2.93	70.62	27.4	588
P20	4595.99	2885.03	1.59	2.30	28.07	34.2	608
P21	0	0	0	2.74	28.15	29.7	548
P22	0	0	0	3.12	12.53	35.9	527

APPENDIX 3. Data used in this petrophysical reseach

Name	K (mD)	Phi (%)	Quartz_ %	% HMC	% Aragonite	Fabric - Color
H1	8990.65	25.27	19.34	NaN	NaN	brown
H2	1747.1	16.46	0.40	NaN	NaN	brown
H3	1654.25	19.74	1.03	NaN	NaN	brown
H4	2241.21	17.59	0.87	NaN	NaN	brown
H5	2101.11	42.65	8.57	8.23	83.20	red
H6	1392.56	32.38	5.77	NaN	NaN	red
H7	1809.51	37.9	11.15	8.88	79.96	red
H8	1519.84	27.53	4.05	NaN	NaN	red
H9	1086.7	25.96	5.15	NaN	NaN	red
H10	577.69	26.09	7.64	4.62	87.74	red
H11	2113.86	19.62	5.96	NaN	NaN	red
H12	3405.12	30.28	6.24	NaN	NaN	red
H13	1876.13	23.08	6.74	NaN	NaN	red
H14	3620.2	33.32	0.00	NaN	NaN	brown
H15	2113.24	24.03	4.53	NaN	NaN	brown
H16	1922.86	29.27	23.29	NaN	NaN	pink
H17	3272.02	23.39	0.00	NaN	NaN	pink
H18	2128.43	32.66	1.69	NaN	NaN	pink
H19	2274.11	40.59	2.15	3.91	93.94	pink
H20	1613.51	31.84	1.55	NaN	NaN	red
H21	3298.4	31.27	1.23	NaN	NaN	red
H22	2183.95	29.31	2.78	27.22	70.00	brown
H23	2502.98	30.37	3.14	55.21	41.65	brown
H24	1886.22	26.37	12.80	NaN	NaN	blue
H25	5367.9	33.33	9.81	NaN	NaN	blue
H26	2978.72	35.98	19.03	3.24	77.73	brown
H27	4245.32	30.81	14.59	NaN	NaN	blue
H28	1990.49	23	20.64	NaN	NaN	blue
H29	2956	30.4	42.97	2.28	54.75	brown
H30	2646.08	22.89	22.70	NaN	NaN	brown
H31	4612.37	30.82	4.81	NaN	NaN	purple
H32	2900.17	35.67	1.31	NaN	NaN	purple
H33	3588.62	23.75	1.32	NaN	NaN	lt. blue
H34	2874.43	30.57	1.54	NaN	NaN	lt. blue
H35	3076.67	33.76	1.75	NaN	NaN	lt. blue
H36	2933.85	30.2	1.17	NaN	NaN	lt. blue

Name	K (mD)	Phi (%)	Quartz_%	% HMC	% Aragonite	Fabric - Color
H37	4127.82	29.55	22.07	1.56	76.37	yellow
H38	702.4	18.39	2.97	3.88	93.14	NaN
H39	0	46.65	0.00	NaN	NaN	NaN
H40	0	23.54	19.26	NaN	NaN	NaN
H41	0	20.46	18.77	NaN	NaN	NaN
H42	0	27.90	32.71	NaN	NaN	NaN
H43	0	34.47	26.33	NaN	NaN	NaN
H44	0	31.49	14.07	NaN	NaN	NaN
H45	0	37.69	13.86	NaN	NaN	NaN
H46	0	26.09	5.62	NaN	NaN	NaN
H47	0	26.88	3.72	NaN	NaN	NaN
H48	0	31.91	10.05	NaN	NaN	NaN
H49	0	23.84	0.00	NaN	NaN	NaN
H50	0	26.43	0.00	NaN	NaN	NaN
H51	8139	29.41	9.92	NaN	NaN	NaN
H52	5824	28.57	23.82	NaN	NaN	NaN
H53	4795	40.13	26.97	NaN	NaN	NaN
H54	5760	36.88	28.09	NaN	NaN	NaN
H55	4056	33.16	23.50	NaN	NaN	NaN
H56	4720	38.63	0.00	NaN	NaN	NaN
H57	2876	38.73	0.00	NaN	NaN	NaN
H58	4041	28.96	18.84	NaN	NaN	NaN
H59	4702	34.76	10.07	NaN	NaN	NaN
H60	6028	30.06	12.17	NaN	NaN	NaN
H61	6156	31.85	13.61	NaN	NaN	NaN
H62	2674	35.72	0.00	NaN	NaN	NaN
P1	4745	30.38	0.00	NaN	NaN	NaN
P2	3831	32.6	0.00	NaN	NaN	NaN
P3	2573.92	30.23	39.17	NaN	NaN	NaN
P4	0	43.1	6.41	NaN	NaN	NaN
P5	0	42.95	0.00	NaN	NaN	NaN
P6	0	40.37	7.81	NaN	NaN	NaN
P7	0	29.72	5.55	NaN	NaN	NaN
P8	0	31.56	3.95	NaN	NaN	NaN
P9	0	31.65	5.45	NaN	NaN	NaN
P10	0	31.63	2.04	NaN	NaN	NaN
P11	5142	19.14	23.02	NaN	NaN	NaN

P12	1627	18.60	24.05	NaN	NaN	NaN
Name	K (mD)	Phi (%)	Quartz_ %	% HMC	% Aragonite	Fabric - Color
P13	1885	30.75	5.35	NaN	NaN	NaN
P14	317	24.98	0.00	NaN	NaN	NaN
P15	4493	33.53	6.75	NaN	NaN	NaN
P16	2232	30.60	6.30	NaN	NaN	NaN
P17	2791	19.56	34.59	NaN	NaN	NaN
P18	1978	29.53	8.33	NaN	NaN	NaN
P19	7.46	23.34	15.31	NaN	NaN	NaN
P20	120	23.53	15.59	NaN	NaN	NaN
P21	3047	29.62	14.91	NaN	NaN	NaN
P22	4420	44.44	7.91	NaN	NaN	NaN